NMR STRATEGIES TO INVESTIGATE MARINE CARBON CYCLING

by

NICOLE R. HOLDERMAN

(Under the Direction of Arthur S. Edison)

ABSTRACT

Here, we present considerations and strategies for the use of nuclear magnetic resonance (NMR) spectroscopy to investigate metabolic flux in marine microorganisms. Phytoplankton perform half the carbon fixation and oxygen generation on Earth. A substantial fraction of fixed carbon becomes part of a metabolite pool of small molecules known as dissolved organic matter (DOM), which are taken up by marine bacteria proximate to phytoplankton. Little is known about the metabolite-mediated, structured interactions occurring between phytoplankton and associated marine bacteria, in part due to challenges of studying high-salt solutions on various analytical platforms. NMR spectroscopy analysis is problematic due to the high-salt content of both natural seawater and culture media for marine microbes, which degrades the performance of the radio frequency coil, reduces the efficiency of some pulse sequences, limits signal-to-noise, and prolongs experimental time. We first describe a method to reproducibly extract low molecular weight DOM from small-volume, high-salt cultures as a promising tool for elucidating metabolic flux and genetic screening between marine microorganisms. Next, we describe the utility of the method at elucidating differential flux between several clades of marine bacteria cocultured with phytoplankton. We end with our latest work observing real-time metabolic flux using continuous *in vivo* metabolism by NMR (CIVM-NMR). This method shows promise for future investigations into substrate

utilization by marine bacteria and could aid in better understanding the metabolic flux crucial to sustaining life as we know it.

INDEX WORDS: NMR spectroscopy; dissolved organic matter; carbon flux; high-salt extraction; extraction methods; *Thalassiosira pseudonana*; *Ruegeria pomeroyi*; *Stenotrophomonas*; *Polaribacter*; CIVM-NMR; *in vivo* metabolism; substrate utilization

NMR STRATEGIES TO INVESTIGATE MARINE CARBON CYCLING

by

NICOLE R. HOLDERMAN

BS & BA, Indiana University, 2012

MS, Lincoln Memorial University, 2016

A Dissertation Submitted to the Graduate Faculty of The University of Georgia in Partial Fulfillment of the Requirements for the Degree

DOCTOR OF PHILOSOPHY

ATHENS, GEORGIA

2023

NMR STRATEGIES TO INVESTIGATE MARINE CARBON CYCLING

by

NICOLE R. HOLDERMAN

Major Professor:	Arthur S. Edison
Committee:	Michael Adams
	I. Jonathan Amster
	Diana Downs
	Mary Ann Moran

Electronic Version Approved:

Ron Walcott
Vice Provost for Graduate Education and Dean of the Graduate School
The University of Georgia
August 2023

DEDICATION

For Aiden—You are the reason that made my reason stronger, the strength that made my strength greater, and the greatest joy of my life.

ACKNOWLEDGEMENTS

I would like to extend my deepest gratitude to Art Edison. To say he made this achievement possible is an understatement, and no amount of thanks would ever be enough. His patience has been unending as I navigated graduate school with my son, Aiden, and he has never ceased being my biggest supporter despite any challenges that arose. Art creates a healthy, challenging atmosphere for graduate students to learn their craft. Every step along the way students are met with respect and encouragement while learning to think like scientists, and despite how impossibly busy he is, Art always makes time to meet with his students. Those conversations have been an incredible source of strength and inspiration for me throughout these years and something I'll always be grateful for. The environment in Art's lab has been the absolute best I could have asked for as a doctoral student.

My sincere gratitude to Mary Ann Moran for always being willing to answer questions and for her unfailing positivity in meetings. Thank you to her research professional Christa Smith for seemingly countless cell cultures and questions answered.

Many thanks to the rest of my committee—Diana Downs, Michael Adams, and Jon Amster—for their helpful suggestions and motivating discussion.

I'd like to acknowledge John Glushka for his patience in training me how to use NMR instrumentation at the CCRC and for being a source of great ideas and suggestions.

Special thanks to Professor Brian Cummings who helped me realize motherhood and pursuing my PhD did not have to be at odds. During my UGA interview he was the first academic

to tell me being a mother in a PhD program was a strength and to seek labs that shared the same views. This conversation convinced me to come to UGA, and I will always be grateful for it.

I'd like to recognize Zac Wood for telling me early in my career that we can learn anything if we work hard enough and for his support during the most trying times.

My sincerest gratitude to Brianna Buchalski for years of weekly phone calls, laughs, and comradery that saw us both through graduate school; Janice Elliot for her indefatigable inspiration; Anna Smith for a lifetime of sisterhood; and Christopher Cotgrove for years of support and partnership.

I am profoundly grateful to my parents Ray and Karen Holderman who demonstrated the value of hard work and perseverance every day of my life. I'd also be remiss in not mentioning my mom's many trips from Indiana to help with Aiden when I needed it most. She is the reason I was able to attend conferences, job interviews, and prepare for important talks, and I'm so grateful for her support.

TABLE OF CONTENTS

Page

LIST OF TABLES

Page

LIST OF FIGURES

Page

CHAPTER 1

BACKGROUND

Marine environments and carbon cycling

Phytoplankton are photosynthetic microorganisms that generate 50% of the oxygen on Earth and contribute nearly half of the turnover in the global carbon cycle. Half of the carbon fixed by phytoplankton joins the marine food web or sinks to the deep ocean while the other half becomes part of a pool of small molecules known as dissolved organic matter (DOM).[1,2] DOM is an assemblage of greater than 100,000 organic metabolites[3] that play vital roles in global carbon, nitrogen, sulfur, and phosphorus cycles; metabolism of nutrients and xenobiotics; and marine biodiversity.[4,5] Loosely associated marine bacteria quickly scavenge (within minutes to days) DOM and transform labile DOM as part of the microbial loop, cycling nutrients back into all trophic layers of the marine food web and contributing a crucial step in elemental cycling.[1,6] The microhabitat including phytoplankton, released DOM, and associated bacteria is known as the phycosphere.[7,8]

Phytoplankton densities do not exist in a steady state and instead vary temporally and/or in the presence of specific nutrients. Temporary, concentrated increases in phytoplankton abundance are known as blooms, which most commonly occur when exposure to sunlight is increased during the spring months or when levels of nitrogen, phosphorus, iron, and silicate produce favorable conditions. The bloom can last weeks to months and is followed by population collapse caused by nutrient constraints, viral attack, or consumption by other organisms.[1] DOM can therefore be secreted directly by actively photosynthesizing phytoplankton or through cell death and lysis of

declining phytoplankton populations. A majority of secreted DOM is labile and may be a chemoattractant for loosely associated heterotrophic marine bacteria from Alphaproteobacteria, Flavobacteriia, or Gammaproteobacteria classes.[1,8-10] These bacteria typically grow in direct proportion to phytoplankton density and can utilize chemotaxis for motility or attach directly to phytoplankton cells.[11]

The distinction between bacterial interactions as mutualistic or pathogenic is a fine one, often varying with regards to timing of the bloom and bacterial species identity. Microbial populations within the bacterial loop can contribute metabolites including essential vitamins and nutrients that support phytoplankton growth, and some bacteria may act as probionts, protecting phytoplankton from pathogens.[2] Conversely, previously mutualistic bacteria can become pathogenic towards phytoplankton to outcompete for scarce nutrients in the final stages of a bloom.[1]

There are five major types of phytoplankton—cyanobacteria, dinoflagellates, green algae, coccolithophores, and diatoms. The focus of this thesis, diatoms, are covered in a porous silica shell and move on ocean currents.[11] Intricate interactions between diatoms and heterotrophic bacteria are the result of hundreds of millions of years of evolution, with bacterial genes being acquired and incorporated into diatoms throughout that period. We have only begun to realize the dynamism of reactivity, metabolic turnover, and chemical transformation occurring between these microorganisms. Characterizing metabolites released by phytoplankton and transformed by bacteria is a crucial step toward enhancing our understanding of these processes.

Marine exometabolome

The phycosphere metabolome consists of the entire repertoire of metabolites produced by affiliated microorganisms and can be divided further into the endometabolome and

exometabolome. Metabolites associated with the endometabolome are contained within cells, while the exometabolome represents metabolites excreted from cells.[12] The advantage of analyzing the latter is the ability to profile secreted metabolites acting as currencies in ocean carbon flux.[13] A majority of the marine microorganismal exometabolome has yet to be elucidated, and knowledge has previously been limited to analytical methods that require desalting, altering, or targeting specific groups of metabolites.[14-17] This owes to the high salt content required for culturing marine microorganisms or present within field samples and the inhibitory effect salt has on direct analysis by mass spectrometry (MS) and NMR instruments.[18] Both platforms experience signal interference from high salt samples—MS from ionization suppression or aberrant enhancement[16] and NMR from affecting the tuning and response of the probe[18,19]—so salt elimination or inhibition is necessary.

Another challenge is the steady state concentration of DOM, which lies in the picomolar to nanomolar range.[17] Thus, sample concentration is required to reach detectable metabolite levels for NMR analysis, unfortunately further concentrating the salt. This step is typically followed by membrane-based or solid phase extraction (SPE) to remove salts from the solution, but SPE does not effectively work for the majority of DOM, which is between 250-550 Da.[18] Studies employing SPE retain an estimated 43-62% of DOM at the exclusion of many compounds important to central metabolism.[14] Another challenge of detecting LMW (low molecular weight, < 1 kDa) metabolites from seawater media is that the smallest and most polar metabolites behave like salt. They are often difficult to separate from the high-salt media background, particularly at such low concentrations.

Chapter 2 describes a novel method developed by Holderman et al. to extract such LMW metabolites from the coculture exudates of bacteria *Ruegeria pomeroyi* and diatom *Thalassiosira*

pseudonana, two marine microorganisms commonly shown in ecological association.[20] *T. pseudonana* was chosen as a model system because the diatom class of phytoplankton contributes approximately 20-25% of net primary production globally and 40% of marine primary production.[1,11,21] *R. pomeroyi* is an Alphaproteobacteria and was the first published genome from the *Roseobacter* clade, which is among the most plentiful and ecologically significant clades of marine bacteria.[2,22] *Roseobacters* are prevalent throughout the world's oceans from polar to equatorial regions and are the predominate members of phytoplankton-associated bacteria.[22]

These bacteria are also significant contributors to global climate regulation. Alphaproteobacteria (including the *Roseobacter* species) and a few Gammaproteobacteria are responsible for breaking down dimethylsulfoniopropionate (DMSP), one of the most abundant metabolites (from nanomolar in surface waters to micromolar during blooms) released by phytoplankton.[23] DMSP catabolism is crucial to the global sulfur cycle as a precursor of dimethylsulfide (DMS), the principal contributor of naturally occurring sulfur to the atmosphere. DMS is oxidized (to products such as sulfate, sulfur dioxide, and methanesulfonic acid) and released into the atmosphere as a crucial regulator of climate.[24,25] The particles significantly impact the amount of solar radiation reaching earth by directly scattering solar energy and functioning as cloud condensation nuclei upon which water droplets condense in the initial stages of cloud formation.[25,26] Given the respective importance of diatoms and *Roseobacters*, *T. pseudonana* and *R. pomeroyi* were ideal model organisms for this research.

[The following indented paragraphs are an unmodified excerpt from my contribution to "NMR: Unique Strengths that Enhance Modern Metabolomics Research" published in *Analytical Chemistry* by the Edison Lab in 2021.]

R. pomeroyi + *T. pseudonana* cocultures demonstrate bacterial upregulation of several genes linked to the transport and catabolism of dihydroxypropanesulfonate (DHPS), a small metabolite rich in carbon and sulfur.[20] *T. pseudonana* releases large quantities of DHPS, a concentrated source of DOM, which *R. pomeroyi* is able to consume as a sole carbon source. Three amplified genes (*hpsK*, *hpsL*, and *hpsM*) were hypothesized to form a tripartite ATP-independent periplasmic (TRAP) transporter for import of DHPS into the cytoplasm.[20]

To verify that DHPS was significant to *R. pomeroyi* carbon exchange, methods were developed (Chapter 2) for extracting and analyzing ^{13}C-labeled spent media from *R. pomeroyi* + *T. pseudonana* cocultures via NMR using lyophilization, reconstitution in DMSO-d_6, and analysis in a 1.7 mm cryogenic probe at 800 MHz. The smaller diameter probe enhances mass sensitivity and minimizes loss due to salt. The group developed an *R. pomeroyi* transporter mutant (*ΔhpsKLM*) in which the putative transporter genes were knocked out to determine whether DHPS was significant to carbon exchange in an *R. pomeroyi* + *T. pseudonana* coculture. ^{13}C-HSQC (heteronuclear single quantum coherence spectroscopy) was used to analyze extracted spent media from axenic *T. pseudonana*, *R. pomeroyi* + *T. pseudonana*, and *ΔhpsKLM* + *T. pseudonana* coculture pairs. ^{13}C-labeled DHPS was absent in wild-type samples, indicating the metabolite was taken up by *R. pomeroyi*. ^{13}C-labeled DHPS was present in both the axenic *T. pseudonana* and the *ΔhpsKLM* coculture import mutant of DHPS.

The extraction method was later applied (Chapter 3) to expand knowledge of metabolic interactions between ocean microbes across a range of bacterial taxa commonly associated with phytoplankton. Spent media from axenic *T. pseudonana* and coculture pairs of *T. pseudonana* with marine bacteria *R. pomeroyi*, *Stenotrophomonas sp.*, and *Polaribacter sp.* were investigated via 2D ^{1}H-^{13}C-HSQC. The 2D helped by reducing overlap and also took advantage of the uniform ^{13}C labeling of the cocultures. These analyses of extracted spent media demonstrated that metabolic interactions between phytoplankton and marine bacteria generate niche-specific fingerprints that differentiate cocultures, revealing differential patterns of uptake and enhancement of certain DOM species between coculture groups versus axenic *T. pseudonana*.[27]

Chapter 4 wraps up with an exploration of continuous *in vivo* metabolism by NMR (CIVM-NMR), a technique developed by the Edison lab and optimized for *R. pomeroyi* in this work.[28] CIVM-NMR uses high-resolution magic angle spinning (HR-MAS) NMR and enables real-time observation of dynamic metabolic activities within live cells. Several substrates were spiked into a culture of live *R. pomeroyi* cells and followed with consecutive NMR experiments over the course of hours and at a ~6-minute temporal resolution. These substrates included DMSP, acetate, and glucose. While several aspects of metabolic flux can often be observed in more complex systems such as human leukemia cells and the model organism *Neurospora crassa*, a filamentous fungus, we were ultimately limited in the detection of many lower abundance compounds. This chapter is therefore largely exploratory and represents an area of promise in future works.

Implications of research

Ultimately, the goal of this work is to begin addressing a critical need to enhance our understanding of dynamic exchanges between two microorganisms vital to elemental cycling and climate regulation. Anthropogenic drivers of climate change are affecting the chemical, phenotypic, and species composition of seawater, thus increasing the amount of atmospheric CO_2 absorbed by the ocean. This process is decreasing ocean pH and available oxygen while increasing water temperature at an energetic cost to some marine microbes.[29] In the past century, ocean water temperature has increased 1-5˚C[30] and acidity has increased by 30%.[31] These numbers are expected to increase by 1-10˚C[30] and 60-90% greater acidity[31] depending on location by the year 2100.

Warmer, more acidic waters generally cause a decrease in phytoplankton size and acceleration of growth rates, which results in an overall reduction in net carbon flux.[32-34] In the past 50 years, water temperatures in the Antarctic Peninsula have increased at five times the rate of the global average, which has led to a 12% reduction in total phytoplankton, carbon turnover, and photosynthetic output.[35] Thus, we face an urgent need to understand metabolic exchange between phytoplankton and bacteria in order to closely monitor anthropogenic effects on these essential marine microorganisms.

We have begun to address that need in this work through the use of NMR as a tool to elucidate some of these unseen processes. First, we developed a robust method of extraction that mitigates the effects of salt within spent media samples for NMR. This method also helped identify DMSO-d_6 as a solvent of particular interest in the study of high-salt biofluids, opening up a new avenue of research within our lab. Further, we were able to use this method to compare differential uptake of DOM between co-cultures of *T. pseudonana* and marine bacteria from ecologically important clades. Lastly, we have been able to optimize the CIVM-NMR protocol for use in *R.*

pomeroyi to begin the work of peering into the black box of marine bacterial metabolism in real-time. This work is a step toward better understanding the dynamic exchanges foundational to supporting all life on Earth.

CHAPTER 2

DISSOLVED ORGANIC METABOLITE EXTRACTION FROM HIGH SALT MEDIA[1]

Chapter 2 was originally published in NMR in Biomedicine and has been reproduced with permission. It is reproduced as written. Nicole R. Holderman* performed the method development on the samples with help from John Glushka and under the advisement of Arthur S. Edison. Method development would not have been possible without the expertise of Frank X. Ferrer-Gonzalez* who provided the coculture and axenic samples under the advisement of Mary Ann Moran. The paper was written by Nicole R. Holderman in close collaboration with John Glushka and Arthur S. Edison with input from all authors.

*Co-first author

[1] Holderman NR, Ferrer-González FX, Glushka J, Moran MA, Edison AS (2023) Dissolved organic metabolite extraction from high-salt media. *NMR Biomed.* **36(4):** e4797. [Published] Reprinted here with permission of publisher.

ABSTRACT

We describe considerations and strategies for developing a nuclear magnetic resonance (NMR) sample preparation method to extract low molecular weight metabolites from high-salt spent media in a model coculture system of phytoplankton and marine bacteria. Phytoplankton perform half the carbon fixation and oxygen generation on Earth. A substantial fraction of fixed carbon becomes part of a metabolite pool of small molecules known as dissolved organic matter (DOM), which are taken up by marine bacteria proximate to phytoplankton. There is an urgent need to elucidate these metabolic exchanges due to widespread anthropogenic transformations on the chemical, phenotypic, and species composition of seawater. These changes are increasing water temperature and the amount of CO_2 absorbed by the ocean at energetic costs to marine microorganisms. Little is known about the metabolite-mediated, structured interactions occurring between phytoplankton and associated marine bacteria, in part because of challenges in studying high-salt solutions on various analytical platforms. NMR analysis is problematic due to the high-salt content of both natural seawater and culture media for marine microbes. High-salt concentration degrades the performance of the radio frequency coil, reduces the efficiency of some pulse sequences, limits signal-to-noise, and prolongs experimental time. The method described herein can reproducibly extract low molecular weight DOM from small-volume, high-salt cultures. It is a promising tool for elucidating metabolic flux between marine microorganisms and facilitates genetic screens of mutant microorganisms.

KEYWORDS: bacteria, carbon cycling, dissolved organic matter, extraction, high-salt, microbial ecology, NMR, phytoplankton

Abbreviations used:

CBA1, cobalamin acquisition protein; DHPS, 2,3-dihydroxypropane 1-sulfonate; DMSO-d_6, deuterated dimethyl sulfoxide; DOM, dissolved organic matter; HMW, high molecular weight; HSQC, heteronuclear single quantum coherence spectroscopy; LMW, low molecular weight; MS, mass spectrometry; ppm, parts per million; RF, radio frequency; RT, room temperature; SPE, solid phase extraction; S/N, signal-to-noise; TRAP, tripartite ATP-independent periplasmic (transporter).

1 | INTRODUCTION

1.1 | Microorganisms and the marine carbon cycle

Phytoplankton are indispensable contributors to the biogeochemical cycles that support all life on Earth. Through photosynthesis, phytoplankton perform half of all carbon fixation (Figure 1A).[35] A major fraction goes on to become part of the largest pool of active carbon on Earth known as dissolved organic matter (DOM), which can include carbohydrates, lipids, nitrogenous compounds, organic acids, and growth factors.[18,36] This collection of up to hundreds of thousands of organic metabolites plays vital roles in global carbon, nitrogen, sulfur, and phosphorus cycles; nutrient and xenobiotic catabolism; and ecological diversity.[20,37,38]

Marine bacteria in the surface ocean scavenge, transform, and decompose DOM as part of the microbial loop (Figure 1A).[4,39] Although ocean microorganisms would be physically distant from each other if evenly spaced in seawater (with a density of 10^4 to 10^6 cells per mL), phytoplankton and marine bacteria form concentrated spatial networks that maximize their interactions (Figure 1A).[9,11,40] These unique exchanges between phytoplankton and bacteria influence the physiology and ecology of one another. The variety of DOM released by phytoplankton informs the community structure of bacteria, while the taxonomic identity and abundance of bacteria inform the concentration and variety of DOM released by phytoplankton.[9,39]

Eukaryotic diatoms represent a particularly vital taxon of phytoplankton, generating 40% of all photosynthetic output from the ocean.[11,41] Diatoms and marine bacteria share specific associations with interactions tracing back on an evolutionary timescale greater than 200 million years. There is strong evidence that hundreds of bacterial genes were incorporated into diatoms over that time.[42]

Further substantiation of ecological relationships is the bacterial production of essential vitamins required by diatoms.[43] Much research has centered on cobalamin (vitamin B_{12}), which is required by organisms lacking the cobalamin-independent methionine synthase gene.[11,44] One such example is the provision of B_{12} to the diatom *Thalassiosira pseudonana* by the marine bacterium *Ruegeria pomeroyi*, representatives of two microbial taxa commonly found in close ecological association (Figure 1B). Vitamin B_{12} is an essential exogenous nutrient for *T. pseudonana*, which exhibits poor growth rates as an axenic culture in B_{12}-null media.[20] Addition of *R. pomeroyi* to the culture causes upregulation of the cobalamin acquisition protein (*CBA1*) gene that allows *T. pseudonana* to take up and utilize the form of B_{12} produced by *R. pomeroyi*. As a result, growth rates recover to that of axenic phytoplankton grown in B_{12}-enriched media. [20]

Concurrently, in coculture with *T. pseudonana*, *R. pomeroyi* upregulates several genes linked to the transport and catabolism of the DOM substrate 2,3-dihydroxypropane 1-sulfonate (DHPS) (structure shown in Figure 1B). *Thalassiosira pseudonana* exudes large amounts of DHPS, which *R. pomeroyi* is able to use as a sole carbon source. Three of the upregulated genes (*hpsKLM*) were experimentally annotated as components of a tripartite ATP-independent periplasmic (TRAP) transporter for the import of DHPS from the extracellular environment into the cytoplasm of *R. pomeroyi* (Figure 1B). [20 45]

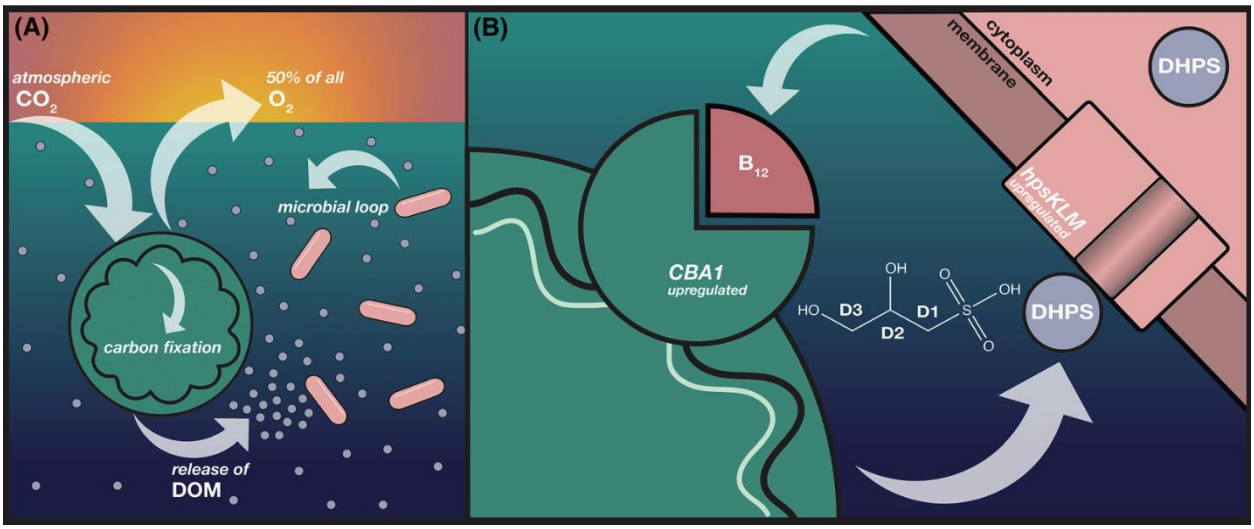

FIGURE 1 Phytoplankton and marine bacteria interact specifically, playing a pivotal role in global oxygen production and carbon flux. (A) Atmospheric CO_2 is absorbed by the ocean and taken up by phytoplankton, which performs photosynthesis to yield O_2 and fixed carbon. Approximately half of the fixed carbon is released as DOM, which is scavenged by marine bacteria within the microbial loop. (B) In a model coculture, *Thalassiosira pseudonana* and *Ruegeria pomeroyi* upregulate transcription of CBA1 and hpsKLM genes, respectively. *T. pseudonana* (teal) upregulates the CBA1 gene to enhance uptake of *R. pomeroyi*-produced vitamin B_{12}. Simultaneously, *R. pomeroyi* (pink, upper right) upregulates hpsKLM genes, which encode for a transporter to uptake DHPS into the cytoplasm of the cell. DHPS, 2,3-dihydroxypropane 1-sulfonate; DOM, dissolved organic matter

We obtained bulk quantities of ^{13}C-labeled spent medium from axenic *T. pseudonana* and cocultures of *T. pseudonana* grown with either wild-type *R. pomeroyi* or a transporter knockout mutant (*ΔhpsKLM*). We developed and utilized a method of exometabolome footprint analysis to extract low molecular weight (LMW) metabolites contained within the high-salt spent media of marine microorganisms. Exudate is advantageous because it provides a snapshot of metabolites potentially participating in flux. ^{13}C-DHPS was used as an indicator of extraction efficacy because it is a known metabolite that we could monitor via nuclear magnetic resonance (NMR) spectroscopy.

We used the method to confirm the presence of ^{13}C-DHPS in ^{13}C-labeled spent media containing exudate from *T. pseudonana* cocultured with the transporter knockout mutant *ΔhpsKLM*. The metabolite footprint of the mutant coculture was compared with *T. pseudonana*

cocultured with wild-type *R. pomeroyi* with the rationale that ^{13}C-DHPS should be present in the transporter knockout mutant due to an inability of the bacteria to uptake ^{13}C-DHPS. Conversely, absence of ^{13}C-DHPS was predicted in the wild-type cocultures, which possessed a functional transporter for the molecule.

We then applied this method to further investigate the exometabolome of spent media from cocultures of *T. pseudonana* and representative marine bacteria from several taxa to explore differential uptake of LMW DOM by members of several bacterial clades. These data are available in Ferrer-González et al. (Chapter 3).[27]

To our knowledge, this is the first method for extracting LMW metabolites from high-salt spent media for NMR analysis. In the results of this paper, we will describe our optimization process for these analyses, as well as the strengths and limitations of the method for other applications. For clarity, the material is organized into three sections based on spent media preparation strategies: D_2O reconstitution, methanol (MeOH) extraction, and deuterated dimethyl sulfoxide (DMSO-d_6) extraction. We conclude by describing our optimized method of lyophilization, mechanical homogenization, and extraction in DMSO-d_6.

2 | EXPERIMENTAL

2.1 | Cell culturing and isotope-labeling method

Axenic *T. pseudonana* diatom cultures were acclimated for 7 days in 150 mL of Paul Harrison Saltwater Medium prepared with 0.47% $NaH^{13}CO_3$ (Cambridge Isotope Laboratories, Inc.; ^{13}C, 99%) in 75 cm^2 vented tissue culture flasks (Falcon; 353, 110). Experimental diatom cultures were transferred from the acclimated flasks and bacteria (*R. pomeroyi* wild type or *ΔhpsKLM*) were inoculated in the experimental replicates at 10^6 bacteria mL^{-1} and allowed to grow at 18 ºC for 8 h. Samples were then taken using a 0.2-µm Teflon filter membrane to separate diatom

and bacterial cells from spent media, which was then stored in 50 mL Falcon tubes and flash-frozen at 80 ºC. Further details of the cell culture protocol are available in Ferrer-González et al.[27]

2.2 | Extraction and preparation procedures

2.2.1 | D_2O reconstitution

Coculture extract was prepared by SpeedVac drying or rotary evaporating 50 mL of spent media and dissolving into 10 mL of D_2O. This suspension was centrifuged for 15 min at 22 ºC at 5000 x g. The supernatant (600 µL) was transferred to a 5-mm NMR tube.

2.2.2 | MeOH extraction

Coculture extract was prepared by rotary evaporating 50 ml of spent media and dissolving solutes into 10 mL of MeOH. This suspension was centrifuged for 15 min at 22 ºC at 5000 x g. The supernatant was rotary evaporated again and resuspended in 1 mL of D_2O with 5 µM deuterated sodium trimethylsilylpropanesulfonate (DSS-d_6, Cambridge Isotope Laboratories, Inc.). This suspension was placed into a 1.7 mL Eppendorf tube and centrifuged for 15 min at room temperature (RT) at 5000 x g. The supernatant (600 µL) was transferred to a 5-mm NMR tube.

2.2.3 | DMSO-d_6 extraction

25 and 15 mL starting material

Coculture extracts were prepared by lyophilizing 25 or 15 mL of spent media in 50 mL conical tubes. The resulting solid salt and DOM mixture was then manually homogenized with a metal spatula. The dry material was extracted with 1.5 or 1 mL of DMSO-d_6 (Cambridge Isotope Laboratories, Inc.), respectively, containing 50 µM DSS-d_6. Tubes were centrifuged for 10 min at 22 ºC at 5000 x g. The supernatant was extracted into 1.7 mL Eppendorf tubes and centrifuged for 15 min at RT at 5000 x g. The final supernatant (550 µL) was transferred to 5-mm NMR tubes.

5 mL starting material

Coculture extracts were prepared by lyophilizing 5 mL of spent media in 15 mL conical tubes. The resulting solid salt and DOM mixture was then homogenized (MP Biomedicals FastPrep-96) to a fine powder through three 30 s cycles at 1800 rpm using 5 x 3.5-mm glass beads. The dry material was extracted with 200 µL of DMSO-d_6 containing 50 µM DSS-d_6 by further homogenizing with three 30 s cycles at 1800 rpm. Tubes were centrifuged for 10 min at 22 ºC at 5000 x g. The supernatant was extracted into 1.7 mL Eppendorf tubes and centrifuged for 15 min at RT at 5000 x g. The final supernatant (40 µL) was transferred to 1.7-mm NMR tubes.

2.3 | NMR analysis

2.3.1 | 800-MHz Bruker NEO sample storage

Samples were kept in a refrigerated sample changer (SampleJet) followed by temperature equilibration at 300 K for 5 min within the NMR probe head immediately prior to analysis.

2.3.2 | Experimental parameters

The utilized NMR experiments are summarized in Table1.

2.3.3 | Spectral processing

^{1}H-^{13}C-HSQC spectra were processed in MNOVA by applying a squared cosine apodization, 4K zero-filling, and Fourier transformation. Transformed spectra were auto-phased, baseline-corrected, and referenced along f1 and f2 to DSS-d_6.

2.4 | Extraction efficiency

We made a 70 mM stock solution of DHPS in D_2O + 1 mM DSS and added the same concentration of DHPS to 3 mL of blank saltwater media. The 3 mL DHPS solution was split into three parts, flash-frozen, lyophilized, and extracted with 600 µL of DMSO-d_6 with 1 mM DSS.

Measurements were collected on the 1.7-mm probe on the 800-MHz Bruker NEO spectrometer and the percentage recovery was calculated.

Sample preparation	NMR solvent	NMR method*	NMR B_0 (MHz)**	SW (ppm)	Center (ppm)	Acquisition time (ms)
50 mL SpeedVac	D_2O	1D carbon	600	236	100	700
Unmodified	10% D_2O	2D HSQC	900	14 x 90	4.7, 45	164, 2.3
50 mL rotovap	D_2O	2D HSQC	900	14 x 90	4.7, 45	120, 6.3
25 mL rotovap, MeOH extract	D_2O	2D HSQC	900	14 x 90	4.7, 45	200, 6.3
25 mL lyophilized DMSO-d_6 extract	DMSO-d_6	2D HSQC	900	12 x 90	2.5, 45	230, 3.15
15 mL lyophilized DMSO-d_6 extract	DMSO-d_6	2D HSQC	900	12 x 90	2.5, 45	230, 3.15
5 mL lyophilized DMSO-d_6 extract	DMSO-d_6	2D HSQC	800	13 x 90	3.7, 45	200, 3.5

TABLE 1. NMR experiment parameters
Abbreviations: DMSO-d_6, deuterated dimethyl sulfoxide; HSQC, heteronuclear single quantum coherence spectroscopy; MeOH, methanol; NMR, nuclear magnetic resonance; ppm, parts per million; SW, spectral window.
*indicates that standard Bruker pulse sequences were used: 1D proton-presat or noesypr1d, 1D carbon-zgpg, 2D HSQC- hsqcetgpsisp2.2.
**indicates the associated probes: 600-MHz–5-mm DCH probe; 800-MHz–1.7-mm TCI; 900-MHz–5-mm TXO.
***parameters for ^{1}H and ^{13}C, respectively.

2.5 | DHPS concentration

Spent media from a 5 mL culture of axenic *T. pseudonana* were extracted with DMSO-d_6 as described above, yielding 200 µL of extract. A 40 µL aliquot of unaltered extract was measured on the 1.7-mm probe on the Bruker NEO 800-MHz spectrometer. A 1% addition of 70 mM DHPS stock solution was added to the remaining 160 µL of extract, and a 40 µL aliquot of this initial titration was measured on the 1.7-mm probe. A second 1% addition of 70 mM DHPS stock was added to the remaining 120 µL of sample, and a 40 µL aliquot was taken for measurement on the 1.7-mm probe. A final addition of 1% 70 mM DHPS stock was added to the remaining 80 µL, and 40 µL was removed and measured on the 1.7-mm probe. The integral values of peak D1 were

recorded in each spectrum, and values from the titrated samples were incorporated into a titration curve with accompanying trendline (ADD fig). The equation for this line was utilized to calculate the amount of endogenous DHPS present in the axenic sample.

3 | RESULTS

Here, we discuss the challenges, strategies undertaken (Scheme1), and outcomes of each attempt to develop a method for extracting LMW metabolites from high-salt spent media. The large salt concentration of spent media required for successful culturing of marine microorganisms presents numerous technical challenges to NMR. It is well established that high-salt solutions affect the tuning and response of the probe, leading to poor signal response and prolonged experimental acquisition times.[18,19] It also limits the use of more demanding NMR experiments that rely on multiple radio frequency (RF) pulses or high-power decoupling.

3.1 | Limitations of existing extraction methods

Most sample preparation for the chemical analysis of marine cultures has utilized solid phase extraction (SPE), diafiltration, and/or C18 silica columns to desalt spent media and extract DOM.[46-49] These techniques typically have an approximate 1-kDa cutoff that excludes most LMW DOM.[14] A principal challenge for the elucidation of dissolved metabolites is retaining small, polar, ionic DOM while separating it from the more than 20 inorganic salts present in the medium at a total concentration of 34 grams per kilogram! Additionally, the concentration of individual components of DOM in the culture medium and ocean is in the picomolar to micromolar range[18] and is often scavenged within minutes by bacteria.[50] Therefore, samples must be concentrated to reach detectable levels for ^{1}H NMR; this unfortunately increases the salt concentration as well.

3.2 | Approach to method development

The key goals were as follows:

•To develop a practical and reproducible high-throughput method to analyze and compare a large quantity of samples.

•To extract as many small, polar compounds as possible while minimizing both salt concentration and sample modification.

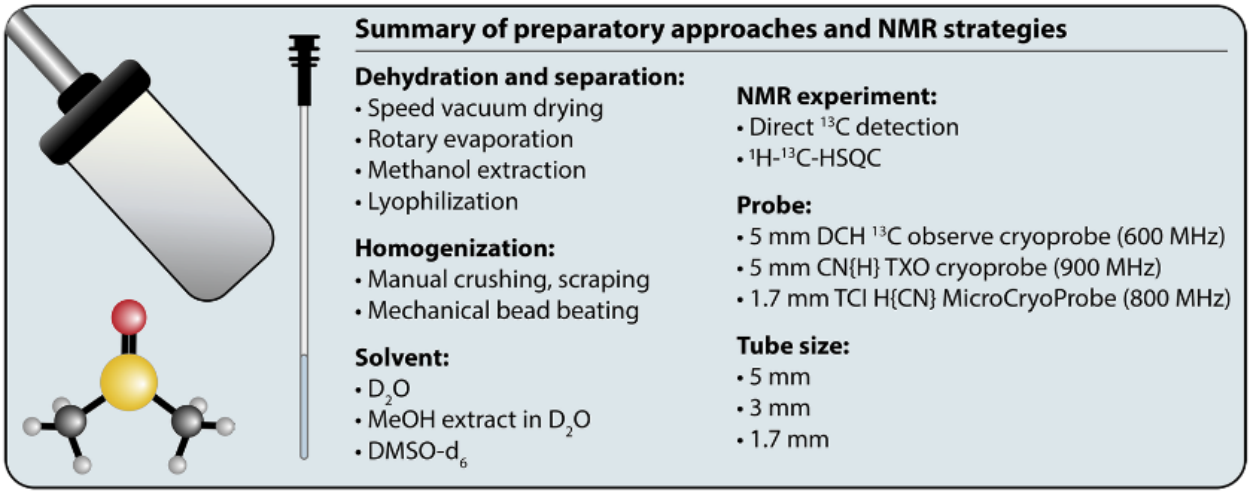

SCHEME 1 Strategies to isolate DOM from high-salt spent media. Several methods of dehydration, separation, homogenization, and solvent selection were employed. NMR experiment choice, probe type, and tube diameter were also evaluated.

The results are organized into three subsections that describe the combination of dehydration, homogenization, and NMR techniques employed with each of the following extraction solvents:

•Subsection 3.4: D2O

•Subsection 3.5: MeOH

•Subsection 3.7: DMSO-d6.

3.3 | NMR analysis: Nuclei observed, probe type, and tube size

To develop a practical and sensitive NMR method that would enable analyses of many samples—for differing biological conditions as well as replicates—we considered the advantages of both ^{13}C detection and small-volume cryoprobes. The ^{13}C nucleus is less sensitive than ^{1}H by several orders of magnitude due to possessing a smaller gyromagnetic ratio and a natural abundance of only 1.1%.[51] However, isotopic labeling with ^{13}C increases the percentage of ^{13}C nuclei for detection by enhancing the effective ^{13}C concentration of the metabolites being actively synthesized.[51] Axenic *T. pseudonana* and cocultures with *R. pomeroyi* were thus cultured using media labeled with $NaH^{13}CO_3$. We capitalized on the unique assets of several NMR magnet strengths, probes, and experiments to analyze the extracted spent media. These include 600-, 800-, and 900-MHz spectrometers, specialty cryoprobes, ^{13}C observe direct-detection and two-dimensional (2D)^{1}H-^{13}C-HSQC. We describe these and other key strategies of sample drying, homogenization, and solvent choice below.

3.4 | D_2O

In an effort to modify the sample as little as possible, our investigation began by utilizing a simple drying method combined with D_2O reconstitution.

3.4.1 | SpeedVac drying and D_2O reconstitution

The process of sample drying can exert a powerful influence over the metabolite profiles determined by NMR.[52] SpeedVac drying involves the concentration of a sample by using a centrifugal vacuum evaporator.[52] This is a high throughput method of sample drying that can be performed with temperature control in some instruments. Salt is concentrated to the point of saturation, so the sample is unsuitable for later analysis in some NMR probes. Initially, to maintain as much material as possible, we simply added D_2O as an extraction solvent for its strong polarity

and ability to solubilize a range of molecules. Although this only slightly diluted the salt concentration, we exploited the ^{13}C enrichment in our cultures and attempted to detect ^{13}C directly with a high-sensitivity carbon cryoprobe.

3.4.2 | Direct-detection ^{13}C-NMR and ^{1}H-^{13}C-HSQC

We utilized a Bruker NEO 600-MHz NMR spectrometer equipped with a 5-mm DCH ^{13}C observe cryoprobe to perform direct ^{13}C detection on spent media concentrated to saturation with a SpeedVac and reconstituted in D_2O. Cryoprobes have greater sensitivity than RT probes, and the DCH probe is optimized for the detection of ^{13}C nuclei.[53] Because of the lower frequency, this probe is less susceptible to interference from high-salt concentrations compared with ^{1}H-optimized cryoprobes at the same field strength, which can suffer dramatic signal-to-noise (S/N) losses as sample conductivity increases.[54]

After 16 h of acquisition, this experiment allowed us to discern several differences between axenic *T. pseudonana* and the coculture of the diatom with *R. pomeroyi* in the region containing DHPS carbons (Figure 2). Multiple peaks appeared to be drawn down by *R. pomeroyi*, but signal overlap and complicated multiplet structures made it difficult to identify the carbons of DHPS. Although a carbon detected 2D heteronuclear correlation (HETCOR) experiment would help with signal assignments, this was not attempted because of the low S/N and long acquisition time. Low-throughput, challenging peak identification, and inadequate S/N then led us to reconsider proton detected 2D ^{1}H-^{13}C-HSQC experiments to resolve both ^{1}H and ^{13}C nuclei with a 5-mm CN{H} TXO cryoprobe on a 900-MHz Bruker NEO spectrometer.

We analyzed samples of *T. pseudonana* cocultured with the *R. pomeroyi* transporter knockout mutant *ΔhpsKLM*. As a baseline, we first analyzed unmodified exudate to determine the feasibility of using ^{1}H-^{13}C-HSQC experiments in moderate salt concentrations. As expected, the

metabolites in this spectrum were too dilute to yield any usable peaks (Figure 3A). Next, we concentrated the exudate with rotary evaporation and reconstituted in D_2O, resulting in a spectrum in which all three peaks of DHPS were present (Figure 3B). However, the overall spectrum had few peaks (Figure 3D), and the starting exudate volume was 50 mL, which was a challenge—both upstream and downstream—in preparing large numbers of cultures. The salt content was now very high, reflected by the long ^{1}H and ^{13}C pulse widths (26.2 and 52.42 μs, respectively), while the S/N was relatively low (Figure 4). We elected to continue refining the method to further reduce starting sample volumes, experimental times, and salt.

3.5 | MeOH extraction

To reduce the salt concentration in the final NMR samples, we switched to extracting rotary evaporated samples with MeOH, a solvent that is suitable for both polar and nonpolar molecules.

3.5.1 | Rotary evaporation and MeOH extraction

The sample was dehydrated using rotary evaporation and subjected to MeOH extraction. This extract was rotary evaporated again and re-dissolved in D_2O. Rotary evaporation has several drawbacks. Heating samples impacts metabolite integrity[55] and is low throughput for multiple samples and replicates. Only one sample can be dried at a time, requiring continuous observation. There is also inevitable sample loss from solutes adhering to the walls of the relatively large volume flasks. Accordingly, variability with rotary evaporation is typically higher than other methods.

3.5.2 | MeOH extraction and ^{1}H-^{13}C-HSQC

The MeOH extract was rotary evaporated again and reconstituted in D_2O in a 3-mm NMR tube and analyzed on the CN{H} TXO cryoprobe (Figure 3C). In addition to the DHPS peaks, many other signals were faintly observed, indicating that the extraction was effective (Figure 3E).

The combination of lower salt and the smaller volume tube reduced the ^{1}H and ^{13}C pulse widths to 17 and 40.2 μs, respectively, and S/N was comparable, even although the starting culture volume was half as much (Figures 3B and 4). We aimed to further improve the method to increase S/N, decrease salt concentration, and decrease the volume of the coculture medium utilized.

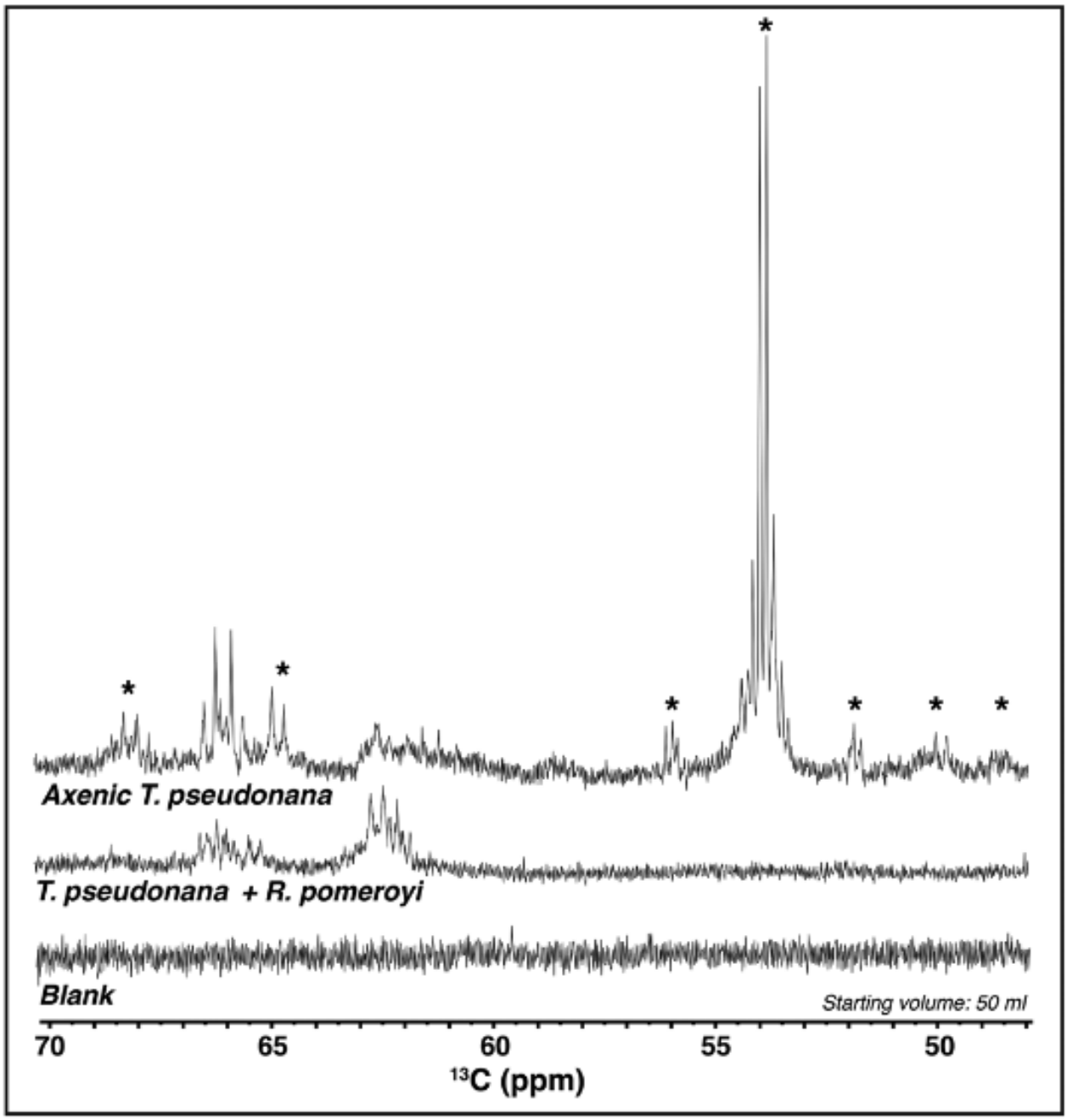

FIGURE 2 Direct ^{13}C NMR analysis of spent media. Spent media of axenic *T. pseudonana* and *T. pseudonana* cocultured with *R. pomeroyi* (*T. pseudonana* + *R. pomeroyi*) were concentrated to saturation by speed-vacuum and observed with a 5-mm DCH ^{13}C observe cryoprobe on a Bruker

NEO 600 MHz spectrometer. Peaks that differ between samples are denoted with an asterisk. The blank sample consisted of speed-vacuum concentrated media only.

3.6 | Other method considerations

Two important aspects of optimizing the method were the refinement of our drying technique and homogenization practices.

3.6.1 | Lyophilization

To achieve our goal of high-throughput sample drying, lyophilization was used instead of rotary evaporation. Lyophilization is the high-throughput process of removing liquid and volatile components from samples through freeze-drying with a vacuum 6–30 times the pressure of the SpeedVac.[52] In this process, the solvent sublimates from the sample, going directly from the solid to the gas phase.[52] Lyophilization has been shown to provide consistent results with strong reproducibility and minimal degradation of metabolites.[56] We transitioned to lyophilization in the middle of the DMSO-d_6 stage (see section 3.7) of method development.

3.6.2 | Homogenization of solid residue

Homogenization is a short but crucial step in sample preparation, affecting the surface area of the dried sample available to the solvent for extraction. Initially, dry solids in the rotary evaporated and lyophilized samples were manually ground using a metal spatula. The three main drawbacks to this method were sample loss, particle size heterogeneity, and low throughput. A significant portion of solid sample was unable to be scraped from the sides of the sample vessel and the resulting scraped solids varied greatly in size. This later impacted the reproducibility and extraction efficiency once solvent was added.

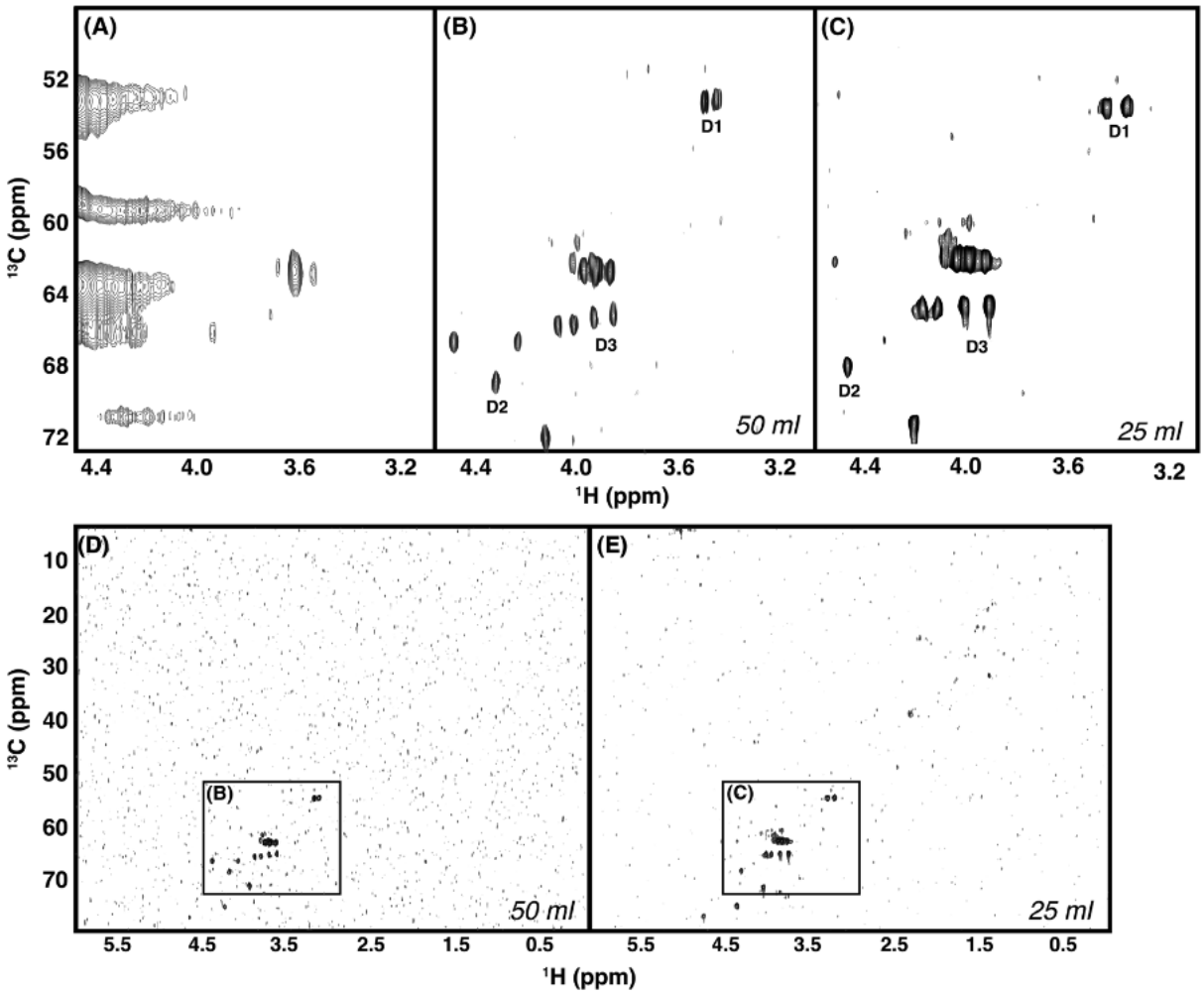

FIGURE 3 ^{1}H-^{13}C-HSQC spectra of D_2O reconstitution and MeOH extraction followed by reconstitution in D_2O allows visualization of all DHPS peaks in the knockout mutant *ΔhpsKLM*. (A) DHPS peaks were unidentifiable in the unconcentrated exudate. (B and C) All DHPS peaks (Figure1B) are present in 50 ml rotary evaporated exudate reconstituted in D_2O and 25 ml rotary evaporated exudate extracted with MeOH, rotary evaporated again, and reconstituted in D_2O in a 5- and 3-mm tube, respectively. (D) The full spectra of D_2O reconstituted exudate contained peaks in the region shown in (B) only. (E) MeOH extraction followed by D_2O reconstitution contained additional peaks of interest beyond what is shown in (C) in the full spectra. The starting exudate volume is listed in the bottom-right corner of each panel. DHPS, 2,3-dihydroxypropane 1-sulfonate; MeOH, methanol

To quantitatively and reproducibly extract the DOM, dried material must be ground to a fine powder. Our optimized method employed the use of a mechanical homogenizer to bead-beat the samples in two rounds: first dry, then again after the addition of deuterated solvent. Bead-beating is high throughput and produces a finely powdered sample compared with manual

homogenization. As such, the reconstitution solvent has greater access to the entirety of the sample, thus extracting more efficiently. The primary disadvantage of bead-beating is that the bead friction can introduce heat, potentially affecting temperature-sensitive metabolites.[57]

3.7 | DMSO-d_6 extraction

Based on the increased number of extracted components seen in the MeOH extract, we tried using DMSO-d_6 as a possibly more effective solvent. DMSO is often considered a universal solvent and is ideal for small polar and ionic organic compounds. The drawbacks are that the high viscosity of DMSO-d_6 can cause line broadening, and it can also be an oxidant to some molecules.[58] If later recovery is desired, DMSO-d_6 can be challenging to remove completely from the sample, even with the dehydration methods discussed above. Finally, DMSO-d_6 has a strong affinity for water, which can cause broad water peaks in the spectra if the solvent is left exposed to air or in an unsealed vial, even for short periods of time.[58] This can also make standardizing chemical shifts difficult as water/DMSO-d_6 ratios change over time or between samples.

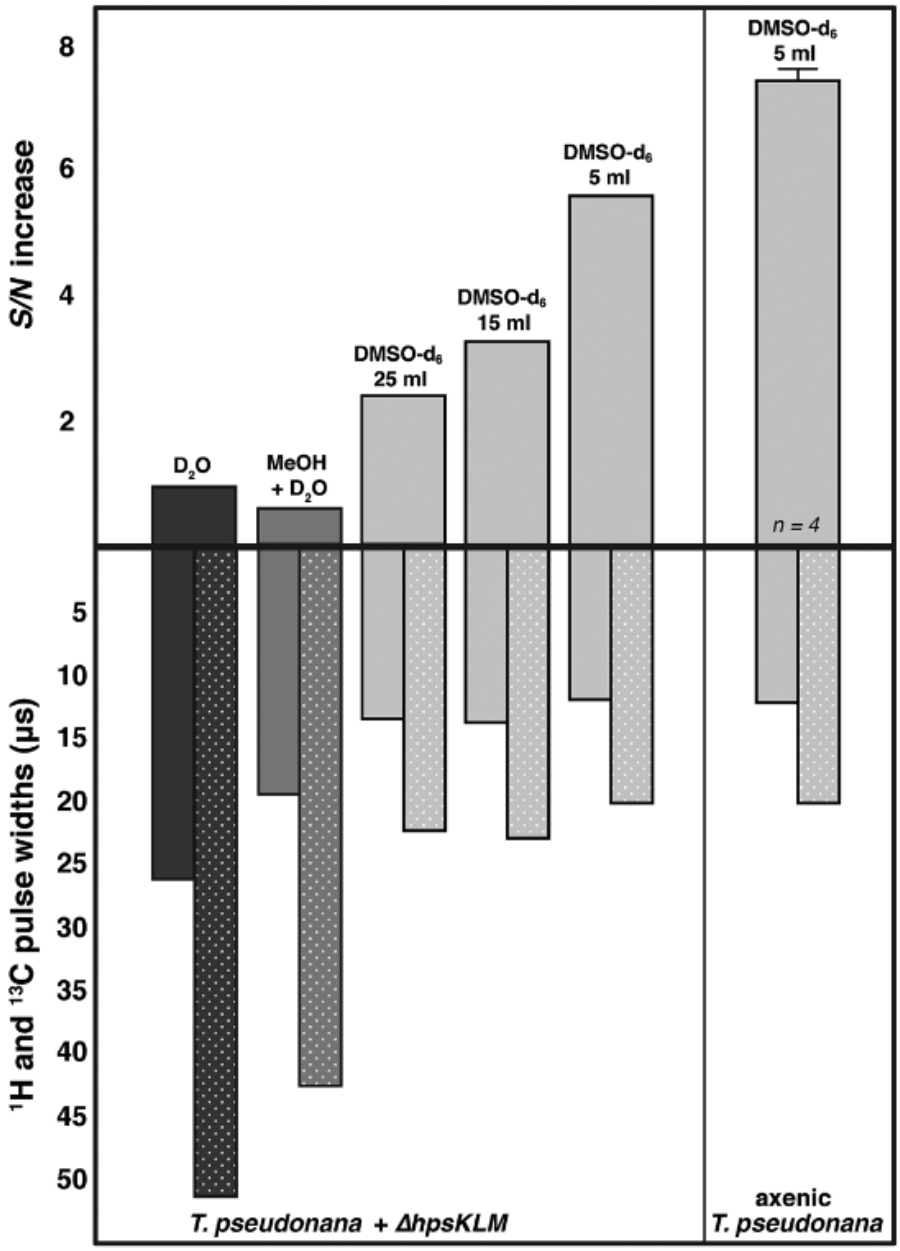

FIGURE 4 Signal-to-noise (S/N) and pulse widths are optimal when lyophilization, mechanical homogenization, DMSO-d_6 extraction, and analysis in a small-volume cryoprobe are performed. Top panel: The signal to noise (S/N) of all spectra with a clearly discernable peak D1 was determined using MNOVA NMR tool scripts, adjusted for spent media starting volume and number of scans, and normalized to reflect a factor increase over the initial D_2O extraction. D_2O, MeOH + D_2O, and DMSO-d_6 (25 and 15 ml) spectra were collected on a 900-MHz spectrometer with a CN{H} TXO cryoprobe. DMSO-d_6 (5 ml, both *T. pseudonana* + *ΔhpsKLM* and axenic) were collected on an 800-MHz spectrometer with a 1.7-mm TCI H cryoprobe. Bottom panel: The pulse widths are shown for ^{1}H (solid bars) and ^{13}C (patterned bars) nuclei in each extraction method. DMSO-d_6 extraction results in the shortest pulse widths of any tested method. DMSO-d_6, deuterated dimethyl sulfoxide; MeOH, methanol.

3.7.1 | DMSO-d_6 and ^{1}H-^{13}C-HSQC

Initially, rotary evaporated *T. pseudonana* + *ΔhpsKLM* coculture residue was extracted with a large volume of unlabeled DMSO, rotary evaporated again, then reconstituted in D_2O. This yielded a salty sample with residual DMSO that was difficult to remove further and obscured the region of the spectra containing DHPS and other organic acids (data not shown).

Using a smaller amount of deuterated DMSO for extraction and as the NMR solvent provided a promising spectrum. The ^{1}H-^{13}C-HSQC spectra of various starting volumes of exudate, lyophilized and extracted with DMSO-d_6, are shown in Figure 5. This method addressed all three main problems of analyzing spent media from marine microorganisms: high-salt concentrations, low concentrations of DOM, and difficulty in isolating small, polar metabolites. All three peaks of DHPS were visible with starting volumes of 25 (Figure 5A) and 15 ml (Figure 5B) exudate. DMSO-d_6 further reduced the ^{1}H and ^{13}C pulse widths (to ranges of 11–13 and 20–24 μs, respectively) and increased S/N by a factor of 2.5–3.5 (Figure 4).

To develop a higher throughput method for our future experimental needs of chemically differentiating between multiple cocultures with many replicates and monitoring cocultures grown under varied experimental conditions, we continued to reduce the starting volume. We utilized a 1.7-mm cryoprobe at 800 MHz that allowed starting culture volumes of 5 mL and final NMR sample volumes of 35–40 μL. Small-volume probes are advantageous for increasing S/N in mass-limited exudate samples.[51] The smaller diameter of both the probe and the sample decreases the effects of salt and increases the amount of the sample volume observed by the RF coil due to an improved filling factor.[59] When combined with high-temperature super conducting material, small-volume probes can improve mass sensitivity by up to 14 times compared with typical 5-mm probes.[59]

Our 800-MHz 1.7-mm cryoprobe provided high-quality, high-throughput spectra with just a small fraction of the starting volume of exudate and deuterated solvents required by the 5-mm tubes in the CN{H} TXO cryoprobe on the 900-MHz spectrometer. A 5 mL sample of exudate lyophilized, mechanically homogenized, and reconstituted in DMSO-d_6 contained all three DHPS peaks (Figure 5C), had the shortest pulse widths of all tested methods, and the highest S/N factor, an increase of approximately six times that of the D_2O reconstituted sample (Figure 4). The full spectrum of the lyophilized, bead-beaten, 5 mL axenic *T. pseudonana* exudate sample reconstituted in DMSO-d_6 demonstrates the breadth of visible peaks in the finalized method (Figure 6).

A summary of the S/N and pulse widths for each condition is shown in Figure 4. Ultimately, 5 mL of lyophilized, bead-beaten exudate reconstituted in DMSO-d_6 (Figure 4, top panel) had a 5.5–7.5-fold increase in S/N versus the 50 mL of sample exudate dried in a SpeedVac and reconstituted in D_2O (Figure 4, bottom panel). Initial ^{1}H and ^{13}C pulse widths in rotary evaporated exudate reconstituted in D_2O were greater than 25 and 52 μs, respectively while the lyophilized, bead-beaten, DMSO-d_6 reconstituted exudate in 1.7-mm tubes decreased the pulse widths by more than half.

To calculate extraction efficiency, three 1 mL replicates with 70 mM laboratory-synthesized DHPS dissolved in saltwater media were lyophilized and extracted using DMSO-d_6 with DSS. Measurements were collected using the 1.7-mm probe on the Bruker NEO 800 MHz spectrometer, and the percentage recovery was calculated. We quantified the extraction efficiency of the method by comparing the integral values for peak D1in the three replicates with the integral of a 70 mM stock solution of DHPS. The extraction efficiency was determined to be 40.3% ± 4.8%.

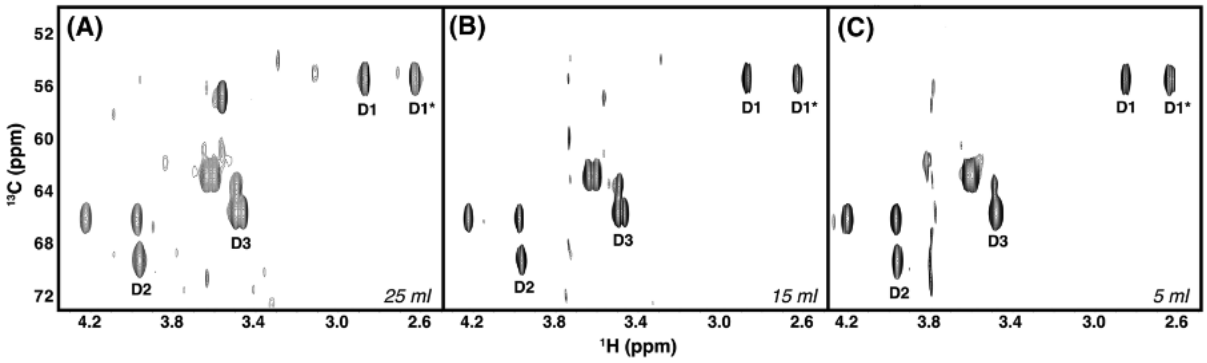

FIGURE 5 Lyophilization, mechanical homogenization, and reconstitution in DMSO-d6 successfully extracts the low concentrations of DHPS from a small volume of starting material. ^{1}H-^{13}C-HSQC spectra of *T. pseudonana* + *ΔhpsKLM* coculture spent media reveals superior peak resolution and separation in DMSO-d_6 versus former methods. (A and B) DHPS peaks (Figure 1B) were all identifiable and resolved in 25 and 15 ml of lyophilized exudate reconstituted in DMSO-d_6 in 5-mm tubes on a Bruker NEO 900 MHz NMR spectrometer with a CN{H} TXO cryoprobe. (C) All DHPS peaks are present in a lyophilized sample of 5 ml of spent media extracted with DMSO-d_6 on a Bruker NEO 800 MHz spectrometer with a small-volume 1.7-mm TCI cryoprobe. The starting exudate volumes are shown in the bottom right corner of each spectrum. DHPS, 2,3-dihydroxypropane 1-sulfonate; DMSO-d_6, deuterated dimethyl sulfoxide.

Spent media from a 5 mL culture of axenic *T. pseudonana* were extracted with DMSO-d_6 as described. Three aliquots with sequential 1% addition of 70 mM DHPS were measured using the 1.7-mm probe on the Bruker NEO 800-MHz spectrometer. The integral values of peak D1 were recorded from each spectrum, and values from the titrated samples were incorporated into a titration curve with accompanying trendline (Figure S1). This allowed us to calculate the concentration of endogenous DHPS present in the axenic sample as 28.4 μM.

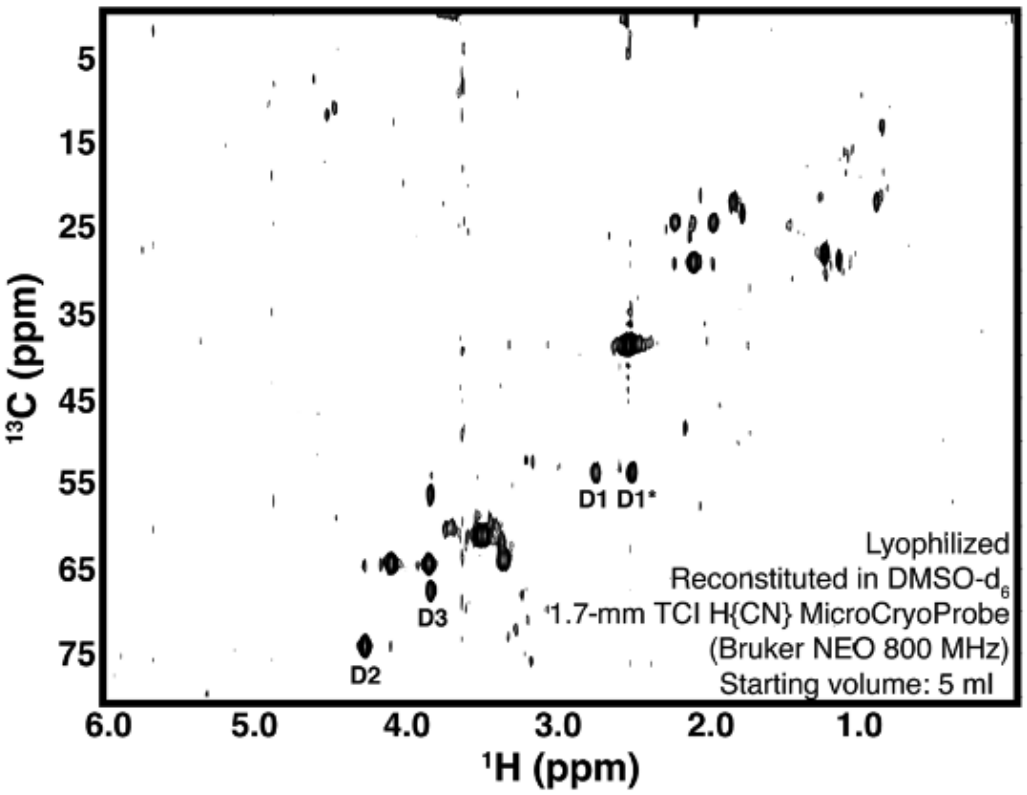

FIGURE 6 Full ^{1}H-^{13}C-HSQC spectra of lyophilized, mechanically homogenized, DMSO-d$_6$ extracted axenic *T. pseudonana* media contains a range of peaks. Five ml of axenic *T. pseudonana* lyophilized exudate was reconstituted in DMSO-d$_6$ and analyzed in a 1.7-mm tube on an 800 MHz spectrometer with a 1.7-mm TCI H cryoprobe. The spectrum contains all DHPS peaks, indicating extraction efficacy in addition to other peaks of further interest. DHPS, 2,3-dihydroxypropane 1-sulfonate; DMSO-d6, deuterated dimethyl sulfoxide

We used our optimized extraction method (Figure 6) to compare three different culture conditions with suitable numbers of replicates: axenic *T. pseudonana*, *T. pseudonana* + wild-type *R. pomeroyi*, and *T. pseudonana* + *ΔhpsKLM R. pomeroyi*. These cocultures were a proof-of-principle as we expected ^{13}C-DHPS to be present in the axenic culture and the *T. pseudonana* coculture with *ΔhpsKLM R. pomeroyi*, which lacked the DHPS transporter. It was expected that DHPS would be absent in the *T. pseudonana* + wild-type *R. pomeroyi* coculture because of the bacteria possessing a functional DHPS transporter. Our extraction method detected the disruption

of DHPS uptake in the mutant coculture and supported previous experimental annotation of the *hpsKLM* genes as DHPS transporter genes[45] (Figure 7).

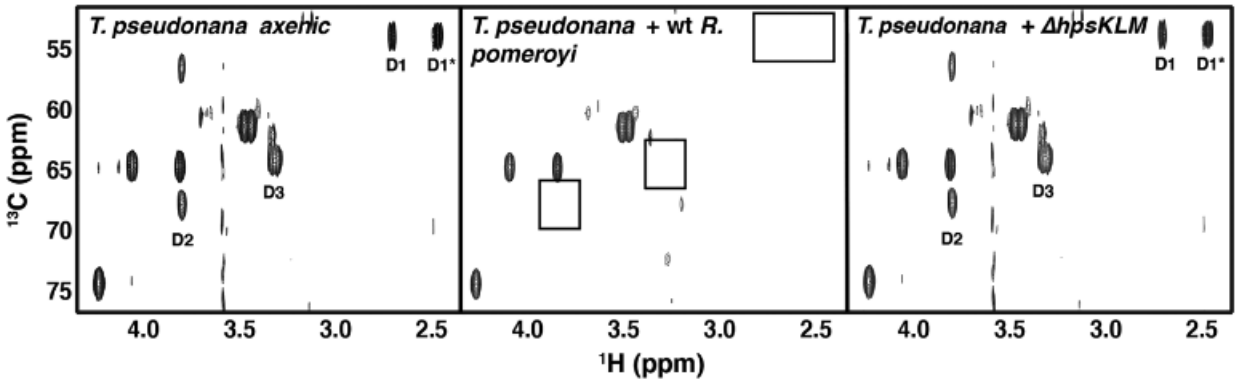

FIGURE 7 ^{1}H-^{13}C HSQC spectra of extracted spent media reveal disruption of ^{13}C-DHPS uptake in transporter knockout mutant (*ΔhpsKLM*) versus wild-type *R. pomeroyi* in coculture with *T. pseudonana*. Axenic *T. pseudonana* cultures (*T. pseudonana* axenic, left spectrum) have ^{13}C-DHPS characteristic peaks. D1* is the signal for one of the ^{13}C–^{1}H bonds at the D1 carbon. It lies within t1 noise and therefore cannot be integrated. Wild-type *R. pomeroyi* cocultures with *T. pseudonana* (*T. pseudonana* + wt *R. pomeroyi*, middle spectra) lack ^{13}C-DHPS peaks (the black boxes indicate absent peaks). Mutant *ΔhpsKLM* cocultures with *T. pseudonana* (*T. pseudonana* + *ΔhpsKLM*, far right spectra) have characteristic ^{13}C-DHPS peaks, indicating inhibited import of ^{13}C-DHPS. DHPS, 2,3-dihydroxypropane 1-sulfonate

4 | DISCUSSION

Through the development of this method, we addressed and resolved several key analytical challenges of high-salt exudates from cocultures of marine microorganisms. Our best result used DMSO-d_6 as an extraction solvent. Samples in DMSO-d_6 all had relatively short ^{1}H and ^{13}C 90-degree pulse lengths, indicating that salt was not a major factor. Surprisingly, we found that those samples still had high-salt concentrations, because when we removed much of the DMSO-d_6 and re-dissolved the sample in D_2O, the ^{1}H pulse width increased from 12 to more than 18 μs, consistent with a high-salt sample. Computational studies have found unusual electrostatic properties of DMSO that might account for its universal solvent properties.[60] This could perhaps be the reason why high salt does not behave the same in DMSO-d_6 NMR samples compared with

D_2O samples. We do not fully understand how DMSO-d_6 affects the sample and consider this an interesting phenomenon to investigate further.

Dispensing the sample into 1.7-mm tubes for analysis in a small-volume cryoprobe allows characterization of LMW DOM peaks of low con-centration via NMR spectroscopy. Ultimately, this method is a step forward in elucidating the metabolites present in DOM. It also provides additional benefits by requiring only small coculture volumes. Low culture sample volumes enhance the ability for high-throughput sample analysis in future experiments and conserve both ^{13}C label and deuterated solvents.

In the future, we hope to further concentrate the extracts to achieve de novo metabolite identification and chemical analysis, but this method also has potential as a genetic screening tool for microorganisms cultured in high-salt media. Extracted exudate from mutant microorganisms can be compared with axenic and wild-type cocultures to support gene assignment, as was demonstrated with the *R. pomeroyi ΔhpsKLM* mutant (Figure 7). Additionally, this method enables the discovery of metabolic interaction between ocean microbes across a range of bacterial taxa commonly found in ecological association with phytoplankton. This extraction method has already been utilized to support the hypothesis that metabolic interactions between phytoplankton and marine bacteria generate niche-specific footprints that differentiate cocultures.[27]

Extraction methods of greater complexity may be developed and optimized to extract metabolites in higher concentrations. One such method we explored is a two-step process employing lyophilization, MeOH extraction, a second round of lyophilization, and DMSO-d_6 extraction. This method resulted in good spectra, but DHPS peaks of interest were in lower concentrations than our optimized direct DMSO extraction (Figure S2). A drawback to multiday extraction methods is that they could add variation and greater potential for error.

The ocean absorbs approximately 26 million tons of CO_2 from anthropogenic sources each day.[61,62] As a result, oceans are acidifying and deoxygenating, causing a decrease in phytoplankton populations due to their sensitivity to environmental changes.[35,62] This has implications for species diversity, distribution, phytoplankton productivity, and marine food web structure, of which phytoplankton form the basis.[29,62] It is predicted that carbon fixation will decrease and selection will favor smaller over larger phytoplankton due to lower nutrient obtainability.[40] Our understanding of the chemical ecology of phytoplankton and marine bacteria is limited, with the bulk of seawater metabolites yet to be chemically characterized.[14] Doing so is essential for understanding metabolic turnover, reactivity, and chemical transformation to establish a baseline of carbon flux through the ocean and to monitor any changes caused by anthropogenic influences.

ACKNOWLEDGEMENTS

This is the NSF Center for Chemical Currencies of a Microbial Planet (C-CoMP) publication #008. The 600 MHz console used in this study was from an National Institutes of Health (NIH) grant to Jim Prestegard (1S10OD021623-01). The authors acknowledge Haris Panagos for beginning the exploration into high-salt spent media analyses, as well as Ricardo Borges and Mario Uchimiya for helpful discussions. The DHPS was obtained from Shawn Campagna and Stephen Dearth at the University of Tennessee. Support was provided by the National Science Foundation (1656311, 1948104, and OCE-2019589), the Georgia Research Alliance, and the Gordon and Betty Moore Foundation (5503).

Supplementary figures:

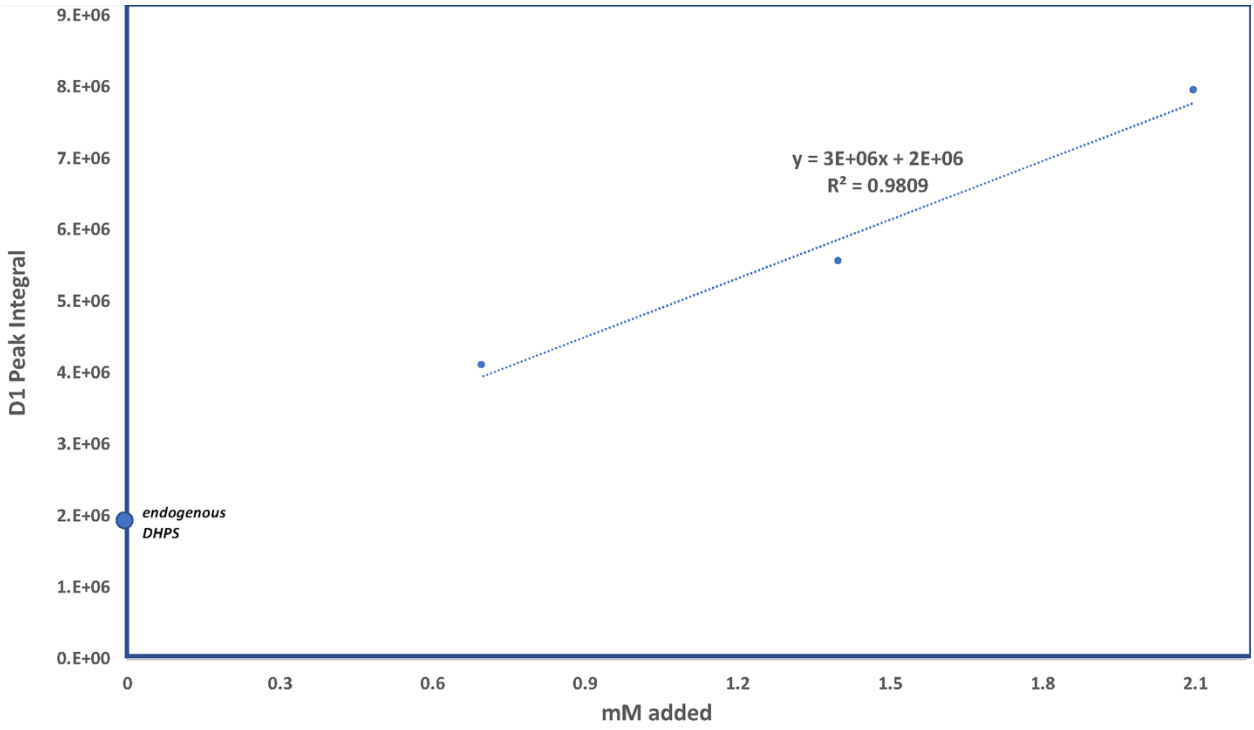

Figure S1. Titration curve of DHPS using DMSO-d_6 extraction method. A 5 ml axenic sample of spent media from *Thalassiosira pseudonana* was extracted according to method described herein. DHPS was added in three sequential 1mM final increments, and peak integrals were recorded. Each point corresponds to the addition of 1mM DHPS to the endogenous sample. The equation for the linear portion of the calibration curve is included.

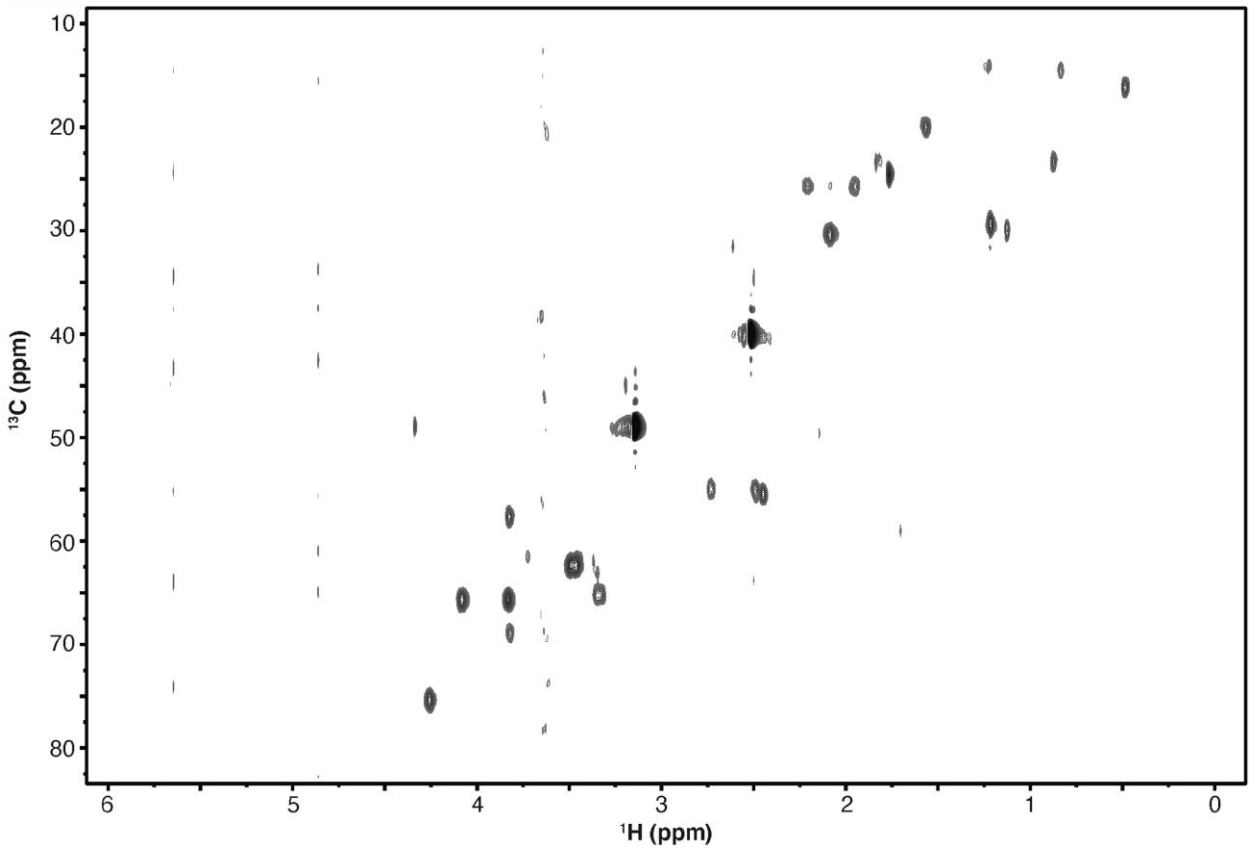

Figure S2. ^{1}H-^{13}C HSQC spectra of media subjected to MeOH extraction followed by DMSO-d_6 extraction. Axenic *Thalassiosira pseudonana* cultures were extracted by lyophilizing 5 mL of spent media, extracting with 3 ml of MeOH, lyophilizing the supernatant, and extracting with 200 µL DMSO-d_6. Peak integral of D1 is diminished to just 0.13% of the value of D1 in the DMSO-d_6 extraction.

CHAPTER 3

RESOURCE PARTITIONING OF PHYTOPLANKTON METABOLITES THAT SUPPORT BACTERIAL HETEROTROPHY[1]

Frank Xavier Ferrer-Gonzalez*, Brittany Widner*, Nicole R. Holderman*, John Glushka, Arthur S. Edison, Elizabeth B. Kujawinski, Mary Ann Moran

Chapter 3 was originally published in the ISME Journal and has been reproduced with permission. It is reproduced as written with supplementary figures incorporated following the main text. Mary Ann Moran, Elizabeth B. Kujawinski, and Arthur S. Edison conceptualized the study. Frank X. Ferrer-Gonzalez* assisted them in study design, performed the bacterial genetic transformations, and grew all samples under the advisement of Mary Ann Moran. Brittany Widner developed the derivatization method and performed LC-MS analysis on the samples under the advisement of Elizabeth B. Kujawinski. Nicole R. Holderman* performed the NMR method development on the samples with help from John Glushka and under the advisement of Arthur S. Edison. The paper was written by Frank, Brittany, Nicole, and Mary Ann with input from all authors.

*Co-first author

---

[1]Ferrer-González FX, Widner B, Holderman NR, Glushka J, Edison AS, Kujawinski EB, Moran MA (2021) Resource partitioning of phytoplankton metabolites that support bacterial heterotrophy. *ISME J.* **15:** 762-773. [Published] Reprinted here with permission of publisher.

ABSTRACT

The communities of bacteria that assemble around marine microphytoplankton are predictably dominated by Rhodobacterales, Flavobacteriales, and families within the Gammaproteobacteria. Yet whether this consistent ecological pattern reflects the result of resource-based niche partitioning or resource competition requires better knowledge of the metabolites linking microbial autotrophs and heterotrophs in the surface ocean. We characterized molecules targeted for uptake by three heterotrophic bacteria individually co-cultured with a marine diatom using two strategies that vetted the exometabolite pool for biological relevance by means of bacterial activity assays: expression of diagnostic genes and net drawdown of exometabolites, the latter detected with mass spectrometry and nuclear magnetic resonance using novel sample preparation approaches. Of the more than 36 organic molecules with evidence of bacterial uptake, 53% contained nitrogen (including nucleosides and amino acids), 11% were organic sulfur compounds (including dihydroxypropanesulfonate and dimethysulfoniopropionate), and 28% were components of polysaccharides (including chrysolaminarin, chitin, and alginate). Overlap in phytoplankton-derived metabolite use by bacteria in the absence of competition was low, and only guanosine, proline, and N-acetyl-D-glucosamine were predicted to be used by all three. Exometabolite uptake pattern points to a key role for ecological resource partitioning in the assembly marine bacterial communities transforming recent photosynthate.

1 | INTRODUCTION

The marine dissolved organic carbon (DOC) reservoir plays two critical roles in the global carbon cycle. The first is as a long-term repository of carbon nearly equal in magnitude to the inorganic carbon stored in the atmosphere. This role is fulfilled by ~660 Pg C of refractory organic compounds that accumulate in seawater, some with lifetimes of many thousands of years[63]. The second is as the primary source of substrates for heterotrophic marine microbes. This role is fulfilled by ~0.2 Pg of highly bioreactive organic compounds that are rapidly cycled by bacterioplankton[64], some with turnover times on the order of hours[65-67]. Recent chemical analysis of bulk marine DOC concentrated from seawater has shown it to be conservatively composed of tens of thousands of distinct organic compounds[68,69]. Yet chemical analysis of the bioreactive subset of marine DOC has thus far been dominated by targeted analysis of a limited number of core metabolites, such as amino acids, sugars, and select biopolymers[10,70-72]. Untargeted chemical approaches have lagged behind, plagued by low concentrations, similar physical properties of salt and polar metabolites, and short lifetimes of component metabolites. Thus, many critical but largely invisible chemical connections between marine microbes remain unstudied.

The primary source of labile metabolites for surface ocean bacteria is phytoplankton. It is estimated that these microbial autotrophs release 10–20% of net primary production (NPP) into

the marine DOC pool in coastal systems[39] and up to 40% in oligotrophic systems[73], although this percentage varies across species and growth conditions[74,75]. Mechanisms by which metabolites are released from phytoplankton cells range from passive leakage of small and uncharged molecules[76], to active exudation related to redox balance, defense, and signaling[77-79], to photosynthetic overflow due to stoichiometric imbalance[75]. Labile organic compounds also become available by phytoplankton cell death from processes such as viral lysis, protist grazing, and senescence[80-82]. Once metabolites are released or excreted from phytoplankton cells, heterotrophic bacteria play the dominant role in their transformation.

Three marine bacterial taxa have consistently been found associated with microphytoplankton in natural marine environments and phytoplankton cultures, and are thought to dominate processing of recently-fixed carbon using genes that allow them to quickly respond to transient nutrient pulses[1]. Members of these three groups, the Rhodobacterales, Gammaproteobacteria, and Flavobacteriales, appear to specialize on different components of bioreactive DOC[1,8,10,11]. Rhodobacterales typically play a prominent role in processing low molecular weight (LMW) phytoplankton-derived metabolites[83,84], Flavobacteriales largely transform high molecular weight carbohydrate polymers[85,86], and several copiotrophic Gammaproteobacteria families utilize compounds from both classes[87,88]. Here, we address the ecological basis of this widespread taxonomic pattern by generating metabolite uptake profiles for three model bacterial species, one from each of the major phytoplankton-associated groups, when growing on a microphytoplankton exometabolite pool in the absence of competition from other bacteria.

Pairwise co-culture systems were established with the diatom *Thalassiosira pseudonana* as the sole source of substrates for *Ruegeria pomeroyi* DSS-3

(Rhodobacterales), *Stenotrophomonas* sp. SKA14 (Xanthomonadales), or *Polaribacter dokdonensis* MED152 (Flavobacteriales). *T. pseudonana* was selected as the autotrophic member of the model systems because as a group, marine diatoms contribute ~20% of global NPP[21]. The heterotrophic bacterial strains were selected because they have high identity to 16S rRNA genes from phytoplankton cultures or flow-sorted phytoplankton cells, with percent similarities as high as 99.6% for *R. pomeroyi* [15,89-91], 98.8% for *Stenotrophomonas* sp. SKA14[89], and 97.2% for *P. dokdonensis*[90,92]. To overcome some challenges of direct chemical analysis of low-concentration compounds in seawater, we used two biological vetting approaches that highlighted metabolites most likely to be important in phytoplankton-bacteria carbon exchange. In the first, expression patterns of bacterial transporters and catabolic genes were used to identify the cellular machinery for carbon acquisition activated by each strain when growing in co-culture. In the second, drawdown of diatom-derived exometabolites from the co-culture media was used to distinguish compounds decreasing in the presence of bacteria. Metabolite concentrations were measured using liquid chromatography-mass spectrometry (LC-MS) and heteronuclear single quantum coherence (HSQC) nuclear magnetic resonance (NMR) spectroscopy. Both biological vetting strategies relied on bacterial activity to spotlight compounds within a complex pool of dilute metabolites that were likely supporting bacterial heterotrophy.

2 | METHODS

2.1 | Cocultures

Three bacterial strains were introduced individually into 7-day diatom co-cultures. Samples were collected after 8, 24, and/or 48 h and analyzed for bacterial response via transcriptomics (to measure regulation changes) or via mass spectrometry (MS) or NMR (to measure metabolite drawdown). To initiate co-cultures, *T. pseudonana* 1335 (National Center for

Marine Algae) was grown axenically in organic carbon-free medium L1 +Si[93] in 1900-ml vented polystyrene tissue culture flasks at 18 °C under 16 h light at 160 µmol photons m^{-2} s^{-1} and 8 h dark. For samples used in NMR analysis, ^{13}C bicarbonate was used to make the L1 medium. After the diatom cultures had been growing for 7 days, bacteria pre-grown in YTSS medium were washed five times in sterile L1 medium and inoculated into three replicate diatom cultures at ~10^6 cells ml^{-1}; three flasks remained uninoculated. Following incubation in the light for 8 h, *T. pseudonana* cells were removed by pre-filtration through 2.0-µm-pore-size filters, and bacteria were collected on 0.2-µm-pore-size filters. Filters were immediately flash frozen in liquid nitrogen and stored at −80 °C until processing and the filtrate was stored frozen for subsequent chemical analysis. Filtrate was also obtained 24 and 48 h after bacterial inoculation for chemical analysis. The control for transcriptome analysis was established by growing bacteria in a defined glucose medium (L1 medium +Si with 2.5 mM glucose); this masked signals of glucose utilization in the co-cultures but provided baseline transcriptomes of actively growing bacteria. Bacterial strains were similarly inoculated into the control medium, collected on 0.2 pore-size filters after 8 h, and flash frozen. Detailed methods are given in Supplementary File 1

2.2 | Cell counts

Culture samples were fixed to a final concentration of 1% glutaraldehyde, incubated at 4°C for 20 min, and stored at −80 °C. Just prior to analysis, an internal standard of 5-µm fluorescent beads was added (Spherotech, Lake Forest, IL, USA), followed by staining for 15 min with SYBR Green I (final concentration 0.75X; Life Technologies, Waltham, MA, USA). Samples were analyzed on an Agilent Quanteon flow cytometer (Acea, Biosciences Inc., San Diego CA). Fluorescence was detected with a 405 nm laser using a 530/30 bandpass filter for SYBR Green (bacteria) and a 695/40 bandpass filter for chlorophyll a. There was no bacterial contamination of

axenic cultures based on scattergrams from flow cytometry and aliquots from axenic cultures spread onto YTSS plates.

2.3 | RNA-seq analysis

Filters were incubated in SDS (0.6% final concentration) and proteinase K (120 ng μl^{-1} final concentration). RNA was extracted from duplicates of each treatment by adding an equal volume of acid phenol:chloroform:isoamyl-alcohol, followed by shaking, centrifugation, collection of the supernatant, and addition of an equal volume of chloroform:isoamyl-alcohol. RNA was recovered from the supernatant, treated to remove rRNA, and sequenced on an HiSeq Illumina 2500. Quality control of the 207 million 50-bp reads was performed using the FASTX toolkit. Reads aligning to rRNA were removed and remaining reads were mapped to the bacterial genomes. Genes with differential expression were determined with DESeq2[94], and are available in Supplementary Tables S1, S2, and S3. The dbCAN web resource was used for identification of carbohydrate-active enzyme annotations[95]. Raw RNA-seq data are available in the NCBI SRA BioProject database under accession PRJNA448168. Detailed methods are given in Supplementary File 1. Microbial genome sequences are available at NCBI RefSeq under accession numbers ASM14940v2 (*T. pseudonana* CCMP1335), ASM1196v2 (*R. pomeroyi* DSS-3), ASM15857v1 (*Stenotrophomonas* sp. SKA14), and ASM15294v2 (*P. dokdonensis* MED152).

2.4 | Mass spectrometry analysis

Chemical analysis was conducted on filtered spent media from the co-cultures and axenic *T. pseudonana* culture using an uninoculated L1 as the medium blank. For MS analysis, 8, 24, and 48 h co-culture spent media were analyzed. Metabolites were derivatized with benzoyl chloride[96] by modification of methods from Oehlke et al.[97] and Wong et al.[98], extracted using a solid phase resin (Agilent, Bond Elut PPL), and analyzed using ultra high performance liquid

chromatography coupled with electrospray ionization and tandem MS with modifications to Kido Soule et al.[99]. Metabolite peak areas were selected and integrated using Skyline[100,101] (Fig. S1). MS metabolites were evaluated statistically in MATLAB by comparing adjusted sample concentrations grouped across time points using a one-way ANOVA ($\alpha = 0.05$). Post hoc Dunnett's test was used to compare each co-culture to the axenic *T. pseudonana* treatment, and *p* values were adjusted for multiple comparisons. Outliers were defined as values that exceeded three scaled median absolute deviations and were excluded from statistical analysis. All MS data are available at MetaboLights under accession number MTBLS1751. Detailed methods are given in Supplementary File 1.

2.5 | NMR analysis

For NMR analysis, 5 ml of 48 h co-culture spent medium was lyophilized, homogenized dry using 5 × 3.5 mm glass beads, reconstituted in dimethyl-sulfoxide-d6, and re-homogenized. The supernatant was analyzed using two-dimensional HSQC NMR (Bruker 800 MHz NEO with 1.7 mm cryoprobe) using acquisition parameters modified from a hsqcetgpsisp2.2 pulse program (TopSpin V4.0.6). The indirect ^{13}C (f1) dimension had a spectral width of 90.0027 ppm, 128 data points, and a carrier frequency of 45 ppm. The direct ^{1}H dimension (f2) had a spectral width of 13.0255 ppm, 4166 data points, and a carrier frequency of 3.691 ppm. Spectra were processed in MNOVA and transformed spectra were auto-phased, baseline-corrected, and referenced along f1 and f2 to DSS-d6 (0.0, 0.0 ppm). All peaks above noise were manually integrated (Fig. S2). A MATLAB workflow was used to normalize, scale, and analyze spectral features. *p* values were calculated for all peak integrals using the [ttest] function in MATLAB for sample pairs. False discovery rates and *q* values were calculated using MATLAB built-in function [mafdr]. Raw data,

peak lists, and analysis scripts are available at MetaboLights under accession MTBLS1544. Detailed methods are given in Supplementary File 1.

3 | RESULTS

Identification of ecologically relevant exometabolites was carried out in co-culture systems in which marine phytoplankter *T. pseudonana* CCMP1335 served as the sole carbon source for three bacterial strains. *R. pomeroyi* DSS-3, *Stenotrophomonas* sp. SKA14, and *P. dokdonensis* MED152 were individually inoculated into a *T. pseudonana* culture that had accumulated exometabolites over 7 days. Bacterial gene expression in response to compounds in the exometabolite pool was identified after 8 h by comparison to gene expression in a single-substrate (glucose) control. Drawdown of *T. pseudonana* exometabolites in the co-culture spent medium was analyzed after 8, 24, and 48 h by LC-MS (Table S4)[96] and after 48 h incubations by 2D HSQC NMR (Holderman et al. in prep.). The control for the chemical analyses was spent medium from axenic *T. pseudonana* cultures. Microscopic observations did not reveal close physical attachment of the bacteria to diatom cells, although *P. dokdonensis* appeared associated with diatom extracellular polysaccharides after 48 h in co-culture. There was no evidence of altered growth rates by the diatom in the presence of the bacteria (Kruskal Wallis, $p = 0.30$, $n = 3$, $T = 253$ h; Fig. 1).

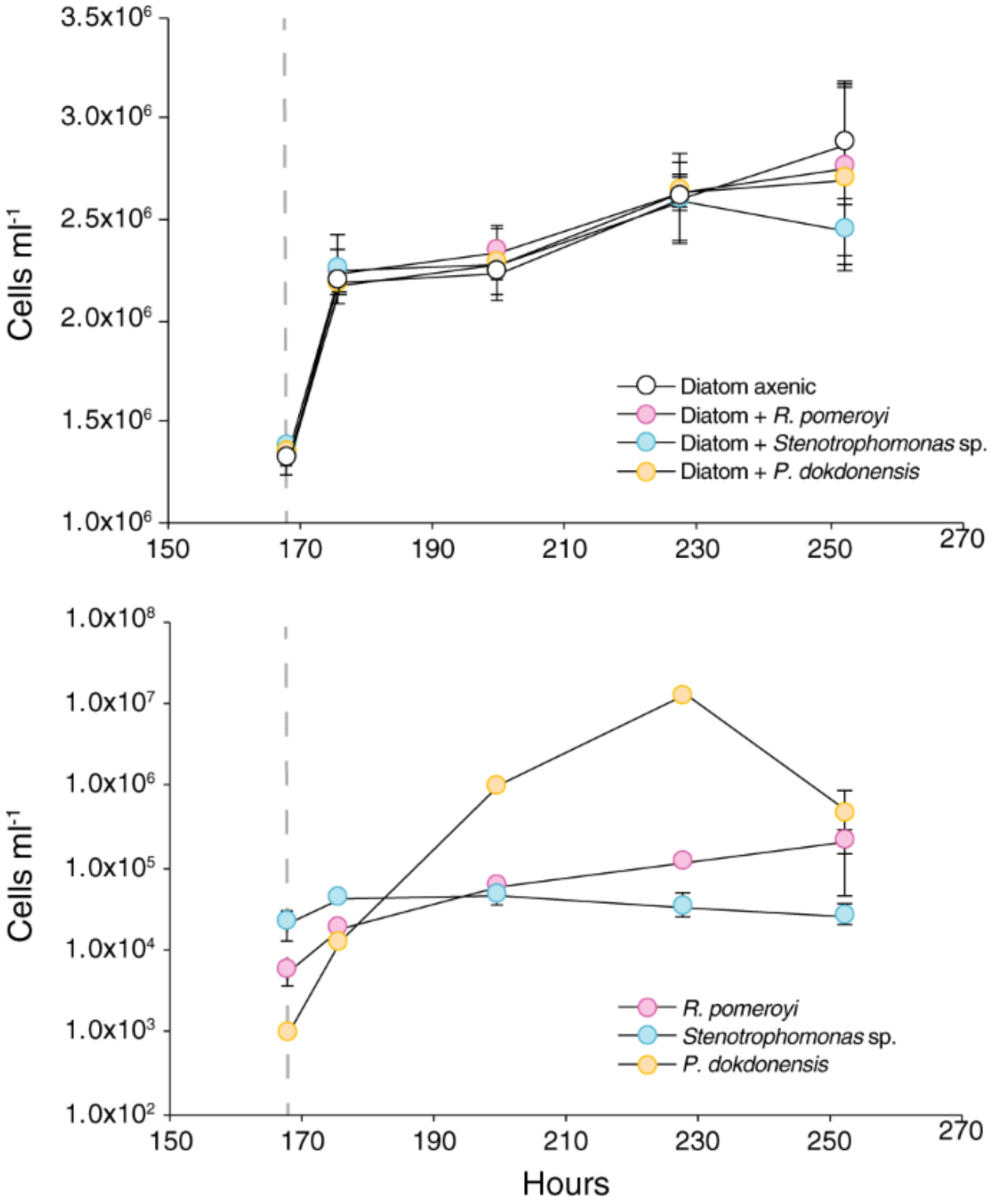

Fig. 1: Cell numbers in co-culture experiments after inoculation of bacterial strains into *T. pseudonana* cultures at 168 h (day 7; gray dashed line). Top: growth of *T. pseudonana* under axenic conditions and in cultures with each bacterial strain. Bottom: growth of bacterial strains in co-culture with *T. pseudonana*. $n = 3$; error bars represent ±1 standard deviation.

3.1 | *Ruegeria pomeryi* DSS-3 metabolite utilization

R. pomeroyi transporters that were enriched in the co-cultures compared to the glucose control included ABC and TRAP transporters, both employing dedicated solute binding proteins that recognize substrates with high affinity, as well as permeases that depend largely on diffusion. Five enriched transporters had hypothesized annotations for amino acid uptake (Fig. 2 and Table S5). Spent medium drawdown patterns were consistent with this, and specifically indicated that concentrations of arginine and the branched chain amino acids valine, leucine, and isoleucine were lower in co-cultures with *R. pomeroyi* compared to axenic *T. pseudonana* cultures (Fig. 3). Nucleoside uptake was also indicated by spent medium drawdown, with significantly lower concentrations of guanosine and thymidine (Figs. 3 and S1).

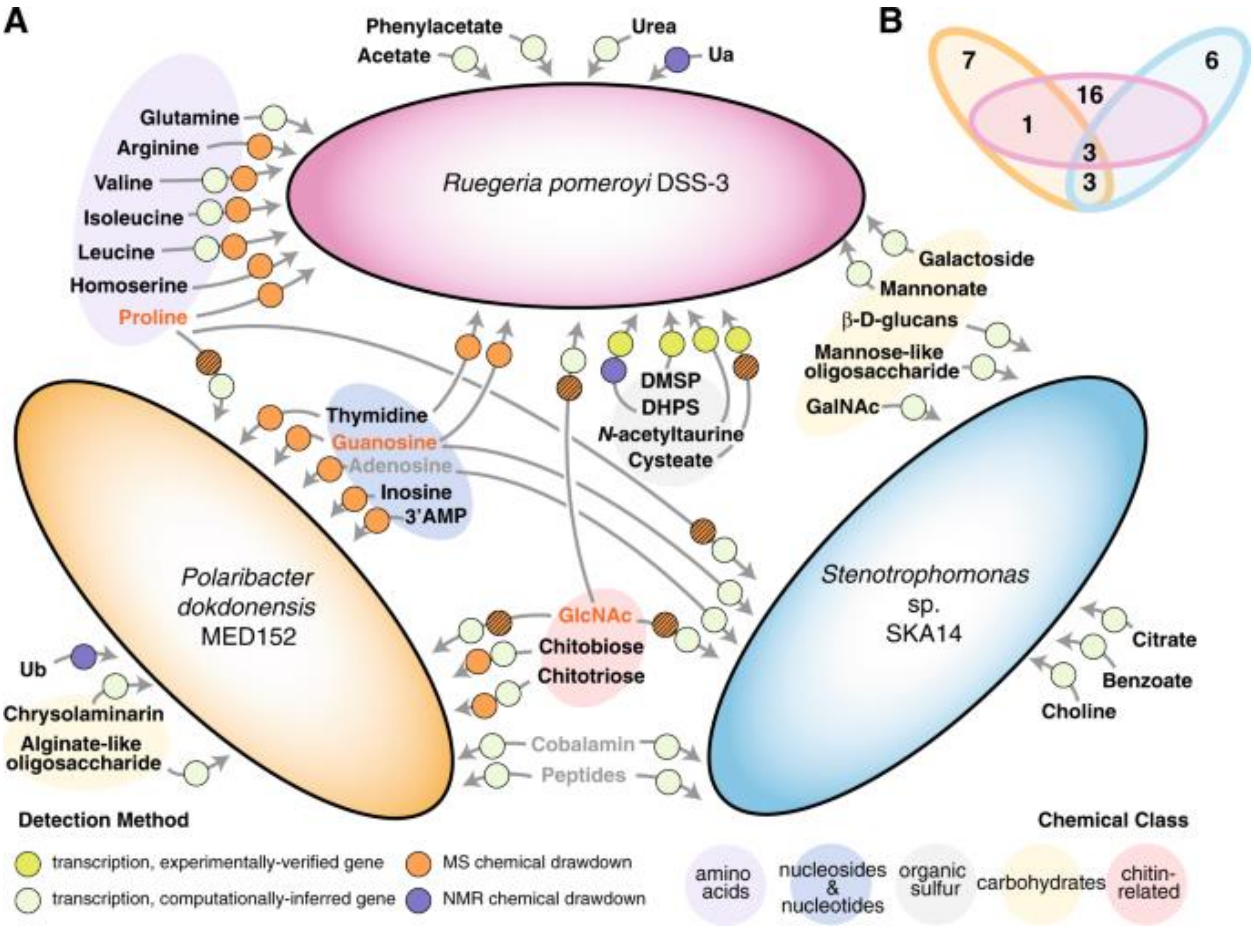

Fig. 2: Metabolites involved in autotroph-heterotroph carbon transfer for three model marine bacteria when co-cultured with *T. pseudonana*. A. Summary of results from exometabolite chemical analysis and bacterial gene expression. Black font indicates metabolites unique to a single strain; gray font indicates metabolites shared by two strains; and orange font indicates metabolites shared by three strains. Circles specify the detection method(s), with hatched symbols indicating a mismatch between expression and drawdown methods. Metabolites Ua and Ub are unidentified compounds detected by ^{13}C-HSQC NMR. **B** Venn diagram summary of unique and shared metabolites.

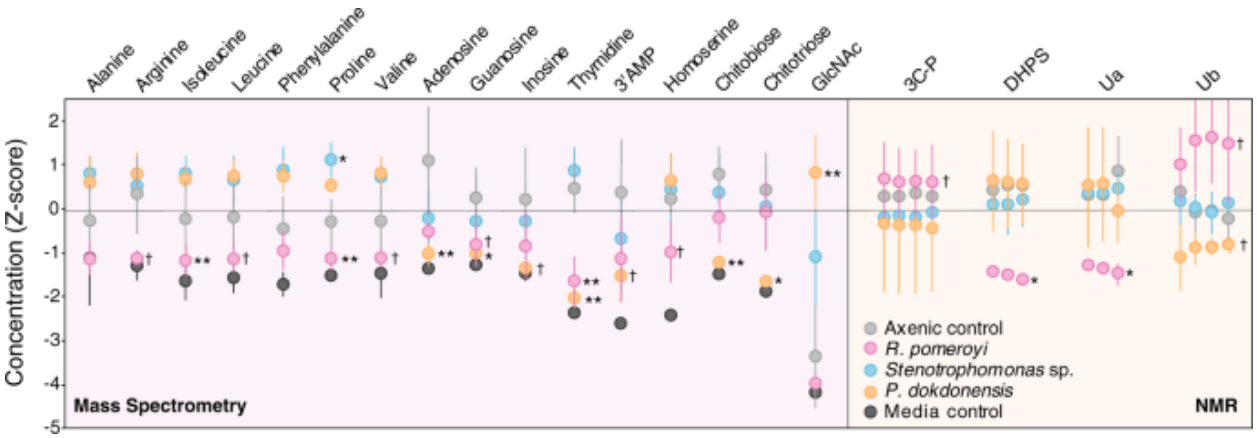

Fig. 3: Bacterial drawdown of diatom exometabolites compared to axenic diatom cultures based on analysis of spent media by targeted LC-ESI-MS (left) and ^{13}C-HSQC NMR (right). Data are *Z* scores of adjusted concentration (MS analysis) and scaled area (NMR analysis). Grouped data points indicate linked carbon atoms in NMR analysis. See Fig. S1 for time course of MS data and Fig. S2 for contour plots of NMR features. $n = 3–7$. ** = treatments significantly different from the axenic diatom cultures at adjusted $p \leq 0.01$; * = treatments different from the axenic diatom cultures at $p \leq 0.05$; † = treatments different from the axenic diatom cultures at $p < 0.10$.

Organic sulfur substrates indicated by transcript enrichment included 2,3,-dihydroxypropane-1-sulfonate (DHPS) and cysteate and *N*-acetyltaurine each containing a nitrogen atom as well (Tables 1 and S5). For all of these, the transporter genes have been verified experimentally in *R. pomeroyi* (Table 1). In the case of DHPS, spent medium drawdown analysis further indicated bacterial consumption based on significantly lower concentrations in the co-cultures. Drawdown analysis also indicated homoserine consumption (Fig. 3). Although the transporter for dimethylsulfoniopropionate (DMSP) has not yet been identified in the *R. pomeroyi* genome, enrichment of transcripts for functionally verified genes *dmdA* (DMSP demethylase)[102] and *acuI* (acrylyl-CoA reductase)[103] (Tables 1 and S5) suggested uptake of this organic sulfur metabolite.

Substrate	*R. pomeroyi*	*Stenotrophomonas*	*P. dokdonensis*	References
Organic nitrogen				
3′ AMP			M	
Adenosine		G	M	
Arginine	M			
Chitobiose			M, G	
Chitotriose			M, G	
Choline		G		
N-acetyl-D-galactosamine		G[a]		[53]
N-acetyl-D-glucosamine	G	G	G	
Glutamine	G			
Guanosine	M	G	M	
Homoserine	M			
Inosine			M	
Isoleucine	M, G			
Leucine	M, G			
Peptides		G	G	
Proline	M	G	G	
Thymidine	M		M	
Urea	G			
Valine	M, G			
Organic nitrogen and sulfur				
Cysteate	G[a]			[98]
N-acetyltaurine	G[a]			[99]
Organic sulfur				
DHPS	M, G[a]			[100]
DMSP	G[a]			[47, 48]
Carbon only				
Acetate	G			
Alginate-like oligosaccharide			G	
β-D-Glucans		G		
Benzoate		G		
Chrysolaminarin			G	
Citrate		G		
Mannonate	G			
Mannose-like oligosaccharide		G		
Phenylacetate	G			
Galactoside	G			
Others				
Cobalamin		G	G	
Ua	M			
Ub			M	

Metabolites Ua and Ub are unidentified compounds detected by ^{13}C-HSQC NMR (Fig. S2).

M uptake suggested from metabolomics analysis, *G* uptake suggested from gene expression.

[a]Gene function is experimentally verified.

Table 1 Metabolites hypothesized to support bacterial heterotrophy in diatom co-cultures based on significant changes in bacterial gene expression (adjusted $p < 0.05$) or metabolite concentrations in spent media (adjusted $p < 0.10$) for three bacterial strains, and the methodological approach providing support.

For five enriched transporter systems, computationally inferred target substrates included urea, phenylacetate, mannonate, acetate, and a galactoside. Transcriptome analysis indicated uptake of six additional metabolites by transporters with general (e.g., sugar and dicarboxylate) or no substrate annotation (Fig. 2 and Table S5). Drawdown analysis revealed a lower concentration of one unidentified metabolite (designated Ua). In two cases there were higher concentrations of compounds in the co-culture spent media (phosphate-containing three carbon compound 3C-P and Ub; Fig. 3), suggesting either release of these unidentified metabolites by *R. pomeroyi* or enhanced export by *T. pseudonana* in the presence of the bacterium. Overall, the transcriptome and spent medium analyses of the *T. pseudonana–R. pomeroyi* co-culture indicated that at least 20 components of the diatom exometabolite pool were used by this bacterium, 13 of which were organic nitrogen molecules and 4 of which were organic sulfur molecules.

3.2 | *Stenotrophomonas sp.* SKA14 metabolite utilization

Of the 23 organic compound transporters significantly enriched in the *Stenotrophomonas* sp. SKA14 transcriptome, six are TonB-dependent transporters (TBDTs) functioning in the outer membrane to bring molecules into the periplasm using energy from TonB proteins located in the inner membrane (Table S6); subsequent passage of substrates into the cytoplasm is typically carried out by permeases or other types of inner membrane transporters. Among the enriched TBDTs, three are annotated as cobalamin/B_{12} receptors and likely involved in vitamin acquisition. Other types of enriched transporters indicate uptake of peptides (major facilitator superfamily (MFS) and oligopeptide family transporters), amino acids (two permeases, a serine/alanine/glycine transporter), and benzoate (Fig. 2 and Table S6). However, there were no decreases in amino acids in the spent medium compared to the *T. pseudonana* axenic control. An actual increase in proline and phenylalanine concentrations (Fig. 3) suggested either release of

these metabolites by *Stenotrophomonas* or their enhanced export by *T. pseudonana* when *Stenotrophomonas* was present. Transporters for purines (MFS transporter) and nucleosides (NupC) were upregulated in co-culture (Table 1).

Carbohydrate utilization was important in the *Stenotrophomonas* co-cultures and accomplished largely via polysaccharide utilization loci (PULs), genomic regions that provide Gammaproteobacteria[69] and Flavobacteriales[104] with the capacity to hydrolyze polysaccharide structures while retaining the resulting monomers in the periplasm until passage inside the cell. Both TBDTs and carbohydrate degrading enzymes (CAZymes) are common in these regions. Among the four PULs containing enriched genes in the *Stenotrophomonas* co-culture transcriptome is a likely *N*-acetyl-D-glucosamine (GlcNAc) PUL (Fig. 4) containing an enriched glycoside hydrolase (GH) that acts on *N*-acetylglucosides (GH-20), a glucokinase that phosphorylates glucose, a sugar membrane permease, and several GlcNAc catabolic enzymes (such as *nagA*)[105,106]. The two chitinases also present in this PUL were not enriched, a pattem suggesting that *Stenotrophomonas* sp. SKA14 was targeting GlcNAc or chitin oligosaccharides in the *T. pseudonana* exometabolite pool. The hypothesized mannose oligosaccharide PUL system includes two GHs annotated as a β-mannosidase (GH2) and α-1,2-mannosidase (GH92). The likely *N*-acetyl-D-galactose PUL (GalNAc PUL) has a gene content consistent with activity toward galactose-containing carbohydrates[107-109], and is homologous to an operon in *Stenotrophomonas maltophilia* K279a verified experimentally to catabolize *N*-acetyl-D-galactosamine[108]. Significantly enriched genes in the co-culture transcriptome (Fig. 4) included an MFS transporter that brings *N*-acetyl-D-galactosamine through the inner membrane (AgaP), a tagatose-biphosphate aldolase (AgaY) that carries out the final step in *N*-acetyl-D-galactosamine catabolism, and a GH containing a carbohydrate binding module with activity against substrates

such as galactose oligosaccharides, galactomannans, and galactolipids (Table S6). Finally, a likely 1,3/1,4-β-D-glucan PUL contains an upregulated exo 1,3/1,4-β-D-glucan glucohydrolase (GH3) predicted to hydrolyze residues of β-D-glucans[110].

Fig. 4: Polysaccharide utilization loci (PULs) containing genes enriched in diatom co-cultures relative to glucose controls.
A *Stenotrophomonas* sp. SKA14. **B** *Polaribacter dokdonensis* MED152. Gene annotations and fold-change data are given in Tables S6 and S7. There were also seven carbohydrate-active enzymes located outside PUL regions among the enriched *Stenotrophomonas* sp. genes (Table S6), two of which have computationally derived annotations for utilization of choline and chitin. Overall, transcriptomes and drawdown assays hypothesized at least 12 diatom metabolites serving as substrates for *Stenotrophomonas* in the co-cultures (Table 1), 7 of which contain nitrogen and 4 of which are carbohydrates.

3.3 | *Polaribacter sp.* MED152 metabolite utilization

In the co-culture transcriptomes of *P. dokdonensis*, components of 13 organic molecule transporters were significantly enriched compared to the glucose control (DeSeq2; $p < 0.01$) (Fig. 2 and Table S7). Six of these are TBDTs, most located in PULs with carbohydrate utilization functions but one annotated for cobalamin uptake. Of the seven other transporters, one is a general MFS transporter with no substrate information, and one is annotated as a putative amino acid transporter. Exometabolite analysis showed no evidence of amino acid drawdown in the *P.*

dokdonensis co-culture, but did indicate decreases in concentrations of inosine, adenosine, thymidine, and guanosine (Fig. 3). Peaks putatively assigned to unidentified metabolite Ub were also drawn down in the *P. dokdonensis* co-culture relative to axenic *T. pseudonana*.

Carbohydrate utilization via PULs was also important in the *P. dokdonensis* co-cultures. PUL2 (designations from the CAZy database)[110] (Fig. 4) is predicted to degrade chrysolaminarin, a glucose storage glucan synthesized by diatoms[111,112] that is ubiquitous in ocean organic matter pools[113]. The enriched substrate binding proteins (*susD*) is an ortholog of a Flavobacterales gene demonstrated to bind laminarin[114], a storage glucan similar to chrysolaminarin found in brown macroalgae. For PUL3 of *P. dokdonensis* (Fig. 4), we hypothesize a function in transport and catabolism of fucose-like or maltooligosaccharide-containing compounds based on inner membrane transporters (Table S7). PUL5 was the most enriched PUL in the *P. dokdonensis* transcriptome, and we predict it transports and catabolizes GlcNAc in the form of chitin monomers or oligomers. This PUL aligns modularly with a Bacteroidaceae PUL in a bacterium confirmed to grow on GlcNAc[115], and the enriched MFS transporter (Table S7) is an ortholog of a gene in the GlcNAc PUL of a *Stenotrophomonas* species. Genes encoding chitin hydrolysis were not found in the *P. dokdonensis* genome, suggesting this bacterium is only able to use monomers and oligomers of chitin. Bacterial drawdown analysis agreed with this annotation by indicating significantly lower concentrations of chitobiose and chitotriose in the co-culture spent medium (Fig. 3), but concentrations of GlcNAc were higher. PUL6 and PUL7 are co-located (Fig. 4) and we predict they target glycans containing guluronic acid and mannuronic acid, the two primary monomers of alginate. While alginate has not been reported as a component of *T. pseudonana* polysaccharides, guluronic acid is present in diatom cell walls[116] and the *P. dokdonensis* PUL6 is highly syntenic with those of previously described alginate-catabolizing

Flavobacteriales[117-120]. The enriched components of PUL6 and PUL7 include a poly(β-D-mannuronate) lyase and two alginate lyases, also supporting a function for this genomic region in utilization of an alginate-like polysaccharide (Table S7). Nine enriched CAZymes that were not associated with PULs included a gene with catabolic activity against β-1,3 glucans, a gene with activity toward various β-1,3 and β-1,4 glucans, and an alginate lyase. A total of 14 possible substrates were identified for *P. dokdonensis*, 10 of which were organic nitrogen compounds and 5 of which were carbohydrates (Table 1).

4 | DISCUSSION

Metabolites passed between marine microbes play key roles in ocean ecosystems, influencing bacterial community assembly and diversity[120,121], mediating competition, antagonism, and mutualisms [11], and serving as currencies of carbon flux. The last of these roles is a central function in global carbon cycling by which ~50% of marine photosynthate is transferred from phytoplankton to heterotrophic bacteria via the labile DOC pool [63,122,123]. There are two primary reasons why little is known about the metabolites linking marine phytoplankton and bacteria[38]. One is that the most biologically reactive components of marine DOC do not accumulate and therefore account for an extremely small fraction of the total reservoir[63]; and the other is that direct chemical analysis, especially in a seawater matrix, is challenging unless the identity of a compound is already known[124].

Our approach delineated clear differences in resource use patterns by bacteria individually inoculated into identical exometabolite pools formed during exponential through stationary growth phases of a diatom. Of the 36 molecules (Fig. 2) covering chemical classes ranging from amino acids to organic sulfur compounds, monosaccharides, oligosaccharides, nucleosides, and organic acids, 29 (80%) were targeted for uptake up by only one of the three representative bacterial strains.

Rhodobacterales member *R. pomeroyi* was hypothesized to uniquely utilize four amino acids, the organic sulfur compounds DHPS, cysteate, DMSP, and *N*-acetyltaurine, the carboxylic acids acetate and phenylacetate, two carbohydrates, and urea, suggesting a substrate suite that is diverse, dominated by LMW compounds, and distinguished by a focus on organic sulfur metabolites. Gammaprotebacteria member *Stenotrophomonas* sp. SKA14 was hypothesized to uniquely utilize three carbohydrates plus benzoate, citrate, and choline. Flavobacteriales member *P. dokdonensis* uniquely utilized the chitin oligomers chitobiose and chitotriose, the carbohydrate storage compound chrysolaminarin, an alginate-like carbohydrate, 3′AMP, and the nucleoside inosine. The latter two bacteria had substrate use linked to polymeric and oligomeric carbohydrates that, particularly in the case of *P. dokdonensis*, is consistent with significant roles in aging blooms[1,10]. Low overlap in the utilization of labile organic matter has been proposed to explain the predictable co-occurrence of Rhodobacterales, Gammaproteobacteria, and Flavobacteriales with microphytoplankton in the surface ocean [1,10,84,125,126]. Our analyses concur that substrate overlap is low among these groups when processing a natural pool of phytoplankton-derived molecules. Furthermore, they point to resource-based niche partitioning of the available resources, rather than competition for them, as the underlying ecological explanation.

Seven of the 36 metabolites, however, were targeted for uptake by more than one bacterial strain: proline, GlcNAc, peptides, cobalamin, and the nucleosides adenosine, guanosine, and thymidine. All of these are organic nitrogen compounds and one is also a vitamin, suggesting these may be resources for which there is competition among the marine bacteria growing at the expense of diatom exometabolites. Proline, guanosine, and GlcNAc were targeted for uptake by all three strains, with the availability of GlcNAc possibly linked to the chitin present in diatom cell walls[42].

Organic nitrogen compounds were also common in the non-shared metabolites, making up ~45% of metabolites.

Previous studies of endometabolite composition of diatom cells reported some of the same compounds identified here in the *T. pseudonana* exometabolome (Table 1). These include the amino acids glutamine, arginine, valine, isoleucine, leucine, and proline[127,128], the organic sulfur compounds DMSP and DHPS[129,130], choline [127,131], galactose[132], and chrysolaminarin[130]. Previous studies have also shown chemotaxis by marine bacteria to several compounds identified in the *T. pseudonana* exometabolome. These include valine, proline, DMSP, and GlcNAc[7,133]. Evidence that these compounds are present in diatom cells, function as attractants in chemotaxis, and are taken up differentially by heterotrophic bacteria suggests they play roles in the chemical ecology of bacterial community assembly. Niche dimensions unrelated to carbon and nutrient acquisition were not examined here, but may also influence ecological differentiation among co-existing bacterial species in the surface ocean; such factors include physical conditions[134], growth kinetics[135], antimicrobial defenses[136], and death processes through viral and protist grazing[137].

Some metabolites had different patterns in gene expression compared to drawdown. Examples are the enrichment of transcripts from the experimentally verified cysteate transporter in *R. pomeroyi* (Tables 1 and S5) but no evidence of cysteate release by axenic diatoms; and enrichment of transcripts from possible proline transporters in both *Stenotrophomonas* sp. and *P. dokdonensis* (Tables 1, S6, and S7) but no evidence of proline drawdown for either (Fig. 3). Differential exometabolite release by the diatom in axenic versus co-culture (i.e., different composition or rate of exometabolite release in the presence versus absence of bacteria) could explain these methodological mismatches. There is growing evidence that marine phytoplankton can detect the presence of bacteria, including a potential recognition cascade invoked by *T.*

pseudonana when growing with *R. pomeroyi* [138]. Other scenarios that could lead to mismatches between these methodological approaches include lower bacterial drawdown rates than diatom release rates, and bacterial metabolite release. A potential example of the last scenario is the accumulation of GlcNAc in the *P. dokdonensis* co-culture but not the axenic diatom culture. In this case, *Polaribacter* hydrolysis of chitobiose and chitotriose (Fig. 3) may be outpacing its uptake of the hydrolysis product GlcNAc[139].

The interpretation of gene expression patterns used here assumed that upregulation of transport and catabolic genes was stimulated by the availability of a substrate. This is based on the unfavorable energetics of across-the-board synthesis of transporter systems that may not yield benefits[140], as well as previous observations of transporter expression changes when the substrates available to heterotrophic marine bacteria are manipulated[83,141,142]. Other regulatory strategies are possible, however, such as constitutive regulation, posttranscriptional regulation, or co-regulation, and these may not be detected in this study or could mislead interpretation. Finally, gene expression interpretations assume that computationally inferred annotations of transporter and catabolic genes in the bacterial genomes are generally correct, which is not always the case [143]. Across the three bacterial genomes, half the upregulated transporters have either general annotations or no annotations regarding their target substrates (Tables S5, S6, and S7), emphasizing the limitation of comparative genome analysis alone to address bacterial resource dimensions.

The role of resource competition in determining bacterial community assembly has been explored recently both in experimental systems and metabolic models[121,144-146]. Yet current knowledge of microbial metabolites is hindered by barriers to capturing and identifying microbial products, and further exacerbated by the difficulty of microbial gene annotation. Thus, it is

challenging to go beyond generic products of central metabolism in addressing resource-based bacterial niche dimensions. Indeed, metabolites of noncore processes that are by and large missing from experiments and models may be the compounds most likely to support resource-based niche differentiation. For example, DHPS release by marine diatoms (Fig. 2) was mentioned only two times in the oceanographic literature[147,148] before it emerged as a major resource for certain taxa of heterotrophic bacteria[83]. Two types of information are critical for improving understanding of bacterial resource partitioning. The first is a chemical database that captures the diversity of microbial metabolites. The second is experimental annotation of bacterial transporter genes that hold important clues about resource-based niche dimensions in the surface ocean[38].

High turnover rates and low concentrations make identification of the labile organic matter released by phytoplankton problematic. Here we used biological vetting based on bacterial activity to identify the molecules most likely to shape heterotrophic bacterial communities reliant on recent photosynthate. Progress in closing the knowledge gap of marine metabolites will enable new insights into the transfer of carbon between major ocean reservoirs.

Acknowledgements

The authors thank S. Roth, J. Nelson, J. Schreier, B. Nowinski, C. Smith, S. Sharma, M. Uchimiya, M. Olofsson, H. Panagos, H. Fu, and M. Kido Soule for advice and assistance, and J. Pinhassi for bacterial strains. This work was supported by grants from the Gordon and Betty Moore Foundation (5503) and the National Science Foundation (IOS-1656311) to MAM, ASE, and EBK, and by the Simons Foundation grant 542391 to MAM within the Principles of Microbial Ecosystems (PriME) Collaborative.

Author notes

1. These authors contributed equally: Frank Xavier Ferrer-González, Brittany Widner, Nicole R. Holderman

Authors and Affiliations

1. **Department of Marine Sciences, University of Georgia, Athens, GA, 30602, USA**
   Frank Xavier Ferrer-González & Mary Ann Moran

2. **Department of Marine Chemistry and Geochemistry, Woods Hole Oceanographic Institution, Woods Hole, MA, 02543, USA**
   Brittany Widner & Elizabeth B. Kujawinski

3. **Department of Biochemistry and Complex Carbohydrate Research Center, University of Georgia, Athens, GA, 30602, USA**
   Nicole R. Holderman, John Glushka & Arthur S. Edison

Contributions

MAM, EBK, and ASE conceptualized the study. FXF-G, ASE, EBK, and MAM designed the study. BW, NRH, ASE, and EBK designed and developed chemical methodologies. FXF-G, BW, and NRH generated and analyzed data. FXF-G, BW, NRH, and MAM wrote the paper with input from all authors.

5 | SUPPLEMENTARY MATERIAL

Three bacterial strains were introduced individually into 7 d diatom co-cultures. Samples were collected after 8 h, 24 h, and/or 48 h and analyzed for bacterial response via transcriptomics (to measure regulation changes) or via MS or NMR (to measure metabolite drawdown) (Fig. 1).

Co-cultures and axenic cultures of *Thalassiosira pseudonana* 1335 culture (National Center for Marine Algae) were grown in organic-carbon free medium L1 +Si (1) in 1900 ml vented polystyrene tissue culture flasks at 18° C under 16 h light at 160 µmol photons m^{-2} s^{-1} and 8 h dark. For samples used in NMR analysis, ^{13}C bicarbonate was used to make the L1 medium. After the diatom cultures had been growing for 7 d, bacteria pre-grown in YTSS medium were washed 5 times in sterile L1 medium and inoculated into the diatom cultures at ~10^6 (*Stenotrophomonas sp.* and *P. dokdonensis*) or ~10^7 (*R. pomeroyi*) cells ml^{-1} . Three replicate co-cultures were established for each bacterial strain. After incubation in the light for 8 h, *T. pseudonana* cells were removed by pre-filtration through polycarbonate 2.0 µm pore-size filters, and bacteria were collected on 0.2 µm pore-size Supor filters. Filters were immediately flash frozen in liquid nitrogen and stored at -80° C until processing, and the filtrate was stored frozen for subsequent chemical analysis. Filtrate was also obtained 24 h and 48 h after bacterial inoculation for chemical analysis. An additional treatment was established in which strains were introduced individually into a defined medium with glucose as the carbon source (L1 medium +Si with 2.5 mM glucose), and this served as the control treatment for co-culture transcriptome analysis (Fig. 1). Bacterial strains were similarly inoculated into the medium, collected on 0.2 pore-size filters after 8 h, and flash frozen.

Cell counts

Culture samples were fixed to a final concentration of 1% glutaraldehyde, incubated at 4°C for 20 min, and stored at −80°C. Just prior to analysis, an internal standard of 5 µm fluorescent beads was added (Spherotech, Lake Forest, IL, USA), followed by stained for 15 min with SYBR Green I (final 2 concentration 0.75X; Life Technologies, Waltham., MA, USA). Samples were analyzed on an Agilent Quanteon flow cytometer (Acea, Biosciences Inc, San Diego CA). Flouorescence was detected with a 405 nm laser using a 530/30 bandpass filter for SYBR Green

(bacteria) a 695/40 bandpass filter for chlorophyll a. There was no bacterial contamination of axenic cultures based on scattergrams from flow cytometry and aliquots from axenic cultures spread onto YTSS plates.

RNA-seq Analysis

Filters were cut into pieces using sterile technique and incubated at room temperature for 1 h in TE buffer, SDS (0.6% final concentration), and proteinase K (120 ng μl^{-1} final concentration). An equal volume of acid phenol:chloroform:isoamyl-alcohol was added and samples were shaken, incubated for 15 min, and centrifuged at 4°C for 15 min for collection of the supernatant. This process was repeated on the supernatant with addition of an equal volume of chloroform:isoamyl-alcohol. The resulting supernatant was mixed with 1 volume of isopropanol and sheared by passage through a 21 g syringe needle. Samples were incubated overnight at -20° C, centrifuged at 4°C for 30 min, washed twice with 75% ethanol, and dried and resuspended in RNAse-free water. Potential traces of DNA were removed using the Turbo DNA-free kit (Invitrogen, Waltham, MA, USA). Samples were tested for residual DNA by a 40-cycle PCR targeting the 16S rRNA gene of the bacterial strains. Duplicates of each treatment were randomly selected for carrying forward through rRNA depletion using the Ribo-Zero Bacteria kit (Illumina, San Diego, CA, USA), library preparation using the KAPA Stranded RNA-Seq Kit (Kapa Biosystems, Wilmington, MA, USA), and sequencing on a HiSeq Illumina 2500 at the Hudson Alpha Institute for Biotechnology (Huntsville, AL, USA). Raw data were deposited in the NCBI SRA BioProject database under accession PRJNA448168.

Quality control was performed on 207 million 50-bp reads using the FASTX toolkit, imposing a minimum quality score of 20 over 80% of read length. Reads aligning to an in-house rRNA database were removed (blastn, score cutoff > 50). Remaining reads were mapped to the *R.*

pomeroyi, Stenotrophomonas sp. SKA14, or *P. dokdonensis* MED152 genomes (Bowtie 2; (2) and counted (HTSeq; (3), conserving strand information and removing reads that mapped to more than one location. Genes with differential expression were determined with DESeq2 (4). Annotations of the bacterial genomes were updated by comparison to closely-related genomes in the IMG (5) and NCBI (6, 7) databases, and to a database of TnSeq derived annotations (8). The dbCAN web resource was used for identification of carbohydrate-active enzyme annotations, taking into account results of HMMs, peptide pattern 3 recognitions, and protein alignments (9). Reciprocal best hit analysis was carried out against genomes of well-annotated Gammaproteobacteria (*Stenotrophomonas maltophila* K279a), and Flavobacteriia (*Formosa sp.* Hel_1_33_133, *Bacteriodetes ovatus* ATCC8433, *Gramella forsetii* KT0803, and *Zobellia galactanivorans* DsijT).

Mass Spectrometry and NMR Analysis

Chemical analysis was conducted on filtered spent media from the co-cultures and axenic *T. pseudonana* culture and on uninoculated L1 as the medium blank. For mass spectrometry analysis, 8, 24, and 48 h co-culture spent media were analyzed. Metabolites were derivatized with benzoyl chloride (Widner et al. in prep) by modification of methods from Oehlke et al. (10) and Wong et al. (11), extracted using a solid phase resin (Agilent, Bond Elut PPL), and analyzed using ultra high performance liquid chromatography coupled with electrospray ionization and tandem mass spectrometry (UHPLC-ESIMSMS) with modifications to Kido Soule et al. (12). Unless otherwise noted, all samples and reagents for mass spectrometry analysis were stored and transferred with acid-washed (10% HCl), combusted (450° C for 5 hours) glassware, and all solvents were Thermo Fisher Optima Grade. Standards were obtained from Sigma-Aldrich at the highest purity available. Filtered (0.2 µm) samples were divided into two 1 mL aliquots and one

was spiked with a standard mix (100 ng/mL final concentration; Table S4) to correct for matrix effects. Each sample was combined with 300 µL sodium carbonate, 30 µL sodium hydroxide, and 200 µL working reagent (5% benzoyl chloride in acetone V:V). After vortexing for 5 min, samples were acidified with concentrated phosphoric acid to pH 2-3 (15 µL). The acetone was evaporated using a vacufuge (Eppendorf), and an equivalent volume of Milli-Q water was added to replace the acetone. One mL of the aqueous phase was loaded onto solid phase extraction cartridges (1g/6ml, Bond Elut PPL, Agilent, conditioned according to manufacturer's specifications). Samples were eluted from the cartridge with methanol (6 mL), dried down (vacufuge), reconstituted in 90:10 water:acetonitrile (100 µL), and stored at -20 °C until analysis.

Mass spectrometry samples were analyzed on a Vanquish UHPLC system [Waters Acquity HSS T3 column (2.1 x 100 mm, 1.8 µm) with a Vanguard pre-column at 40 °C] coupled via heated electrospray ionization (H-ESI) to an ultrahigh resolution tribrid mass spectrometer, the Orbitrap Fusion Lumos (Thermo Fisher Scientific). The column was eluted with mobile phase (A) 0.1% formic acid in water and (B) 0.1% formic acid in acetonitrile at a flow rate of 0.5 mL min^{-1} . The gradient conditions were 0-0.5 min (1% B), 2 min (10% B), 2-5 min (10% B), 7 min (25% B), 7-9 min (25% B), 12.5 min (50% B), 13 min (95% 4 B), 13-14.5 min (95% B). The system was then returned to 1% B for re-equilibration prior to the next injection (total gradient time 16 min). Separate injections of 5 µL each were made for positive and negative ion modes. The electrospray voltages were 3600 V (positive) and 2600 V (negative), and the source gases were 55 (sheath) and 20 (auxiliary), and 1 (sweep). The capillary temperature was 350 °C and the vaporizer temperature was 400 °C. The Lumos was operated in full-scan MS mode with data dependent tandem mass spectrometry, guided by a list of user-defined parent ions with a retention time window for each (full MS/ddMS2 with inclusion list). In this targeted quantitation approach, data are collected in

full-scan mode in the Orbitrap analyzer (resolution 60,000 fwhm, at m/z 200). When any of the parent ions on the inclusion list are detected within the retention time window, MS/MS scans are automatically acquired (resolution 7,500 fwhm, at m/z) and then the instrument resumes full-scan operation. Data obtained in full-scan mode were used for detection and quantification, while MS/MS data were used for identification and confirmation. Full-scan MS data were collected between 170-1000 m/z, and the automatic gain control (AGC) setting was 4e5 with a max injection time of 50 msec. MS/MS data were collected using higher energy collisional dissociation (HCD) with collision energy at 35% and intensity threshold at 2e4. The MS/MS AGC target setting was 5e4 with a max injection time of 22 msec. Parent ions were isolated within the quadrupole at an isolation width of 1 m/z. All data were collected in profile mode. See Table S4 for retention times and parent and product ion values. Standards were prepared in duplicate in L1 medium from 0.5 to 500 ng/mL. Sample and standard peaks were integrated using Skyline (13, 14), and standard curves were calculated using at least 5 standards. Standard curve R squared values were required to be greater than 0.92 for metabolite quantification (Table S4). In preliminary experiments (Widner et al. in prep), we determined that the instrument response could be enhanced or suppressed in some spent culture media relative to the standards in L1 medium. The analytical recoveries were calculated as the difference between the calculated concentrations of the spiked sample (sample concentration + 100 ng/mL spike) and the unspiked sample divided by the spike concentration (100 ng/mL). The concentration of each sample was corrected for matrix effects by multiplying the raw concentration by the average analytical recovery for that culture media type. Because of these corrections, we are reporting 'adjusted concentration' for metabolites. Mass spectrometry metabolites were evaluated statistically in Matlab by comparing adjusted sample concentrations (from all time points) by treatment using a one-way ANOVA ($\alpha = 0.05$) and post-

5 hoc Dunnett's test to compare each co-culture to the axenic *T. pseudonana*. Outliers were defined as values that exceeded 3 scaled median absolute deviations and were excluded from statistical analysis. For NMR analysis, 5 ml of 48 h co-culture spent medium were lyophilized, homogenized dry (MP Biomedicals FastPrep-96) through 3 x 30 s cycles at 1800 rpm using 5 x 3.5 mm glass beads, reconstituted in 200 µL dimethyl-sulfoxide-d6 (DMSO-d6) with 50 µM sodium trimethylsilylpropanesulfonate-d_6 (DSS-d_6, Cambridge Isotope Laboratories, Inc.) and re-homogenized through 3 x 30 s cycles at 1800 rpm. Following centrifugation for 10 min at 22 °C and 5000 x g, the supernatant was centrifuged for 15 min at 5000 x g and added in 40 µL aliquots to 1.7 mm NMR tubes in a 96 tube rack. Two-dimensional HSQC-NMR spectra were collected (Bruker 800 MHz NEO with 1.7 mm cryoprobe) with an automatic and refrigerated (279 K) sample changer (SampleJet) using IconNMR (V5.1). Before NMR data acquisition, samples were preincubated for 5 min in the probe for temperature equilibration at 300 K. 2D data were collected using acquisition parameters modified from a hsqcetgpsisp2.2 pulse program (TopSpin V4.0.6). Spectra were acquired in Echo-Antiecho acquisition mode in 3 h 58 min with presaturation of residual water using 64 scans and 32 dummy scans. The indirect 13C (f1) dimension had a spectral width of 90.0027 ppm, 128 data points, and an offset of 45 ppm. In the direct 1 H dimension (f2) had a spectral width of 13.0255 ppm, 4166 data points, and an offset of 3.691 ppm. Spectra were processed in MNOVA by applying a 90° sine square apodization, 4K zero-filling, and Fourier-transformation. Transformed spectra were auto-phased, baseline-corrected and referenced along f1 and f2 to DSS-d6 (0.0, 0.0 ppm). All peaks above the noise were manually integrated. These peaks were divided into four sub-regions for visualization (Figure S2) and analysis using MATLAB. Raw data, peak lists, and analysis scripts are available on MetaboLights under accession MTBLS1544. The peak integral values were imported into a MATLAB workflow to

normalize, scale, and analyze spectral features. The peak integral table was normalized using built-in probabilistic quotient normalization (PQN), mean-centering, and univariate scaling functions. The built-in MATLAB principal components analysis (PCA) function was applied to feature integrals across co-culture conditions, and a loadings plot along principal component 1 was generated to determine which peaks accounted for the largest proportion of variance among samples. The loadings plot informed our decision for which peaks to analyze further, and all peaks between the covariance threshold of -0.5 and 0.5 were omitted from 6 further analysis as they accounted for the least between-sample variation. From these data, P-values, false discovery rates (FDR), and q-values were calculated using MATLAB built-in functions.

Supplementary references

1. Guillard R, Hargraves P. Stichochrysis immobilis is a diatom, not a chrysophyte. Phycologia. 1993;32(3):234-6.

2. Langmead B, Salzberg SL. Fast gapped-read alignment with Bowtie 2. Nat Meth. 2012;9(4):357.

3. Anders S, Pyl PT, Huber W. HTSeq—a Python framework to work with high-throughput sequencing data. Bioinformatics. 2015;31(2):166-9.

4. Love MI, Huber W, Anders S. Moderated estimation of fold change and dispersion for RNA-seq data with DESeq2. Genome Biol. 2014;15(12):550.

5. Chen I-MA, Chu K, Palaniappan K, Pillay M, Ratner A, Huang J, et al. IMG/M v. 5.0: an integrated data management and comparative analysis system for microbial genomes and microbiomes. Nucleic Acids Res. 2018;47(D1):D666-D77.

6. O'Leary NA, Wright MW, Brister JR, Ciufo S, Haddad D, McVeigh R, et al. Reference sequence (RefSeq) database at NCBI: current status, taxonomic expansion, and functional annotation. Nucleic Acids Res. 2015;44(D1):D733-D45.

7. Tatusova T, DiCuccio M, Badretdin A, Chetvernin V, Ciufo S, Li W. Prokaryotic genome annotation pipeline. The NCBI Handbook [Internet] 2nd edition: National Center for Biotechnology Information (US); 2013.

8. Price MN, Wetmore KM, Waters RJ, Callaghan M, Ray J, Liu H, et al. Mutant phenotypes for thousands of bacterial genes of unknown function. Nature. 2018;557(7706):503.

9. Zhang H, Yohe T, Huang L, Entwistle S, Wu P, Yang Z, et al. dbCAN2: a meta server for automated carbohydrate-active enzyme annotation. Nucleic Acids Res. 2018;46(W1):W95-W101.

10. Oehlke J, Brudel M, Blasig IE. Benzoylation of sugars, polyols and amino acids in biological fluids for high-performance liquid chromatographic analysis. J Chromatogr B: Biomedical Sci Appl. 1994;655(1):105-11.

11. Wong J-MT, Malec PA, Mabrouk OS, Ro J, Dus M, Kennedy RT. Benzoyl chloride derivatization with liquid chromatography–mass spectrometry for targeted metabolomics of neurochemicals in biological samples. J Chromatogr A. 2016;1446:78-90.

12. Soule MCK, Longnecker K, Johnson WM, Kujawinski EB. Environmental metabolomics: Analytical strategies. Mar Chem. 2015;177:374-87.

13. Henderson CM, Shulman NJ, MacLean B, MacCoss MJ, Hoofnagle AN. Skyline performs as well as vendor software in the quantitative analysis of serum 25-hydroxy vitamin D and vitamin D binding globulin. Clinical Chem. 2018;64(2):408-10.

14. Pino LK, Searle BC, Bollinger JG, Nunn B, MacLean B, MacCoss MJ. The Skyline ecosystem: Informatics for quantitative mass spectrometry proteomics. Mass Spectrom Rev. 2017.

Supplementary Figures:

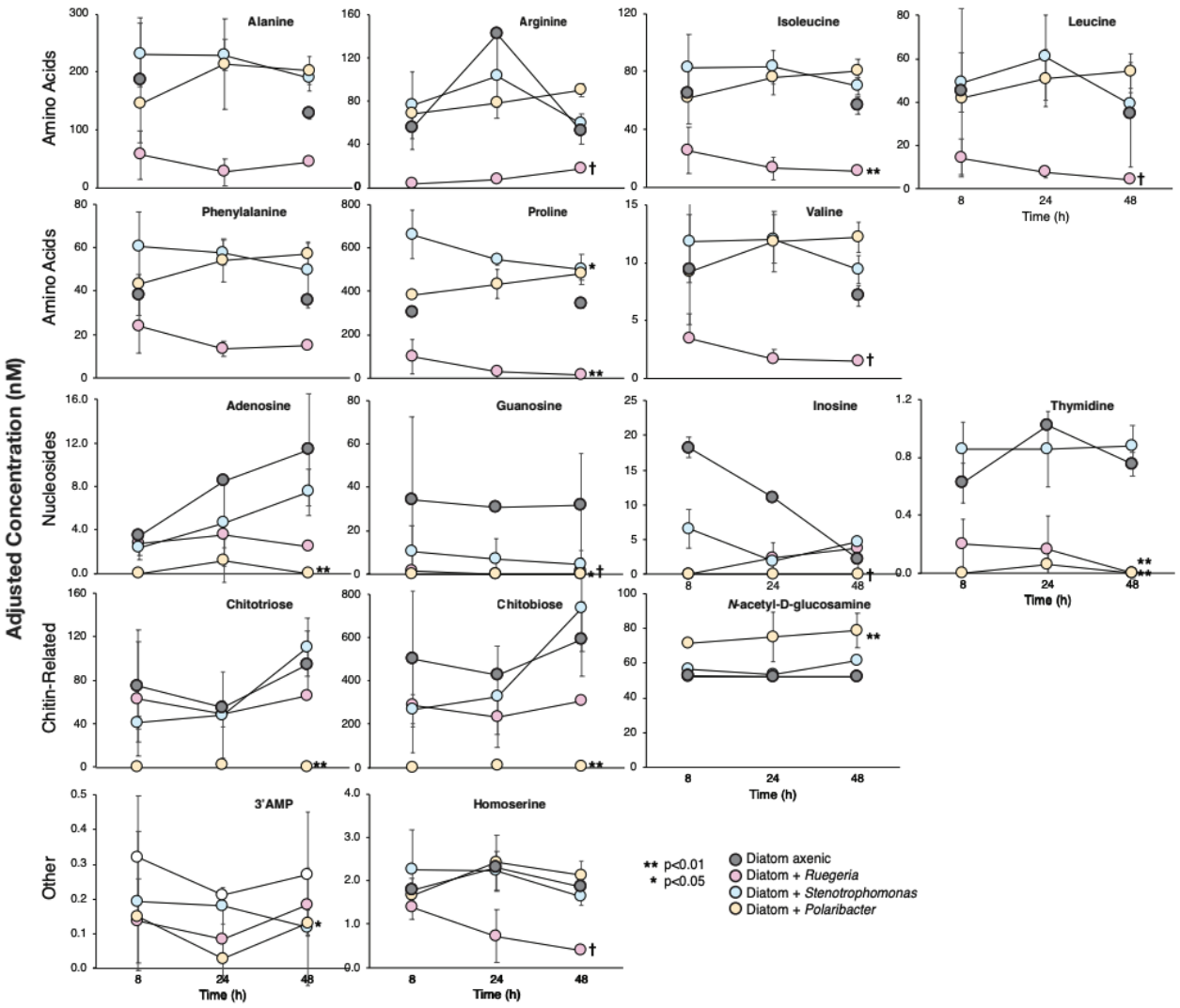

Figure S1. Time course of exometabolite concentrations based on targeted LC-ESI-MS analysis of axenic and co-culture spent media. ** = treatments significantly different from the axenic diatom cultures in the grouped analysis presented in Fig. 3 at $p < 0.01$; * = treatments significantly different from the axenic diatom cultures in the grouped analysis presented in Fig. 3 at $p < 0.05$ in Fig. 4. Error bars indicate standard deviations.

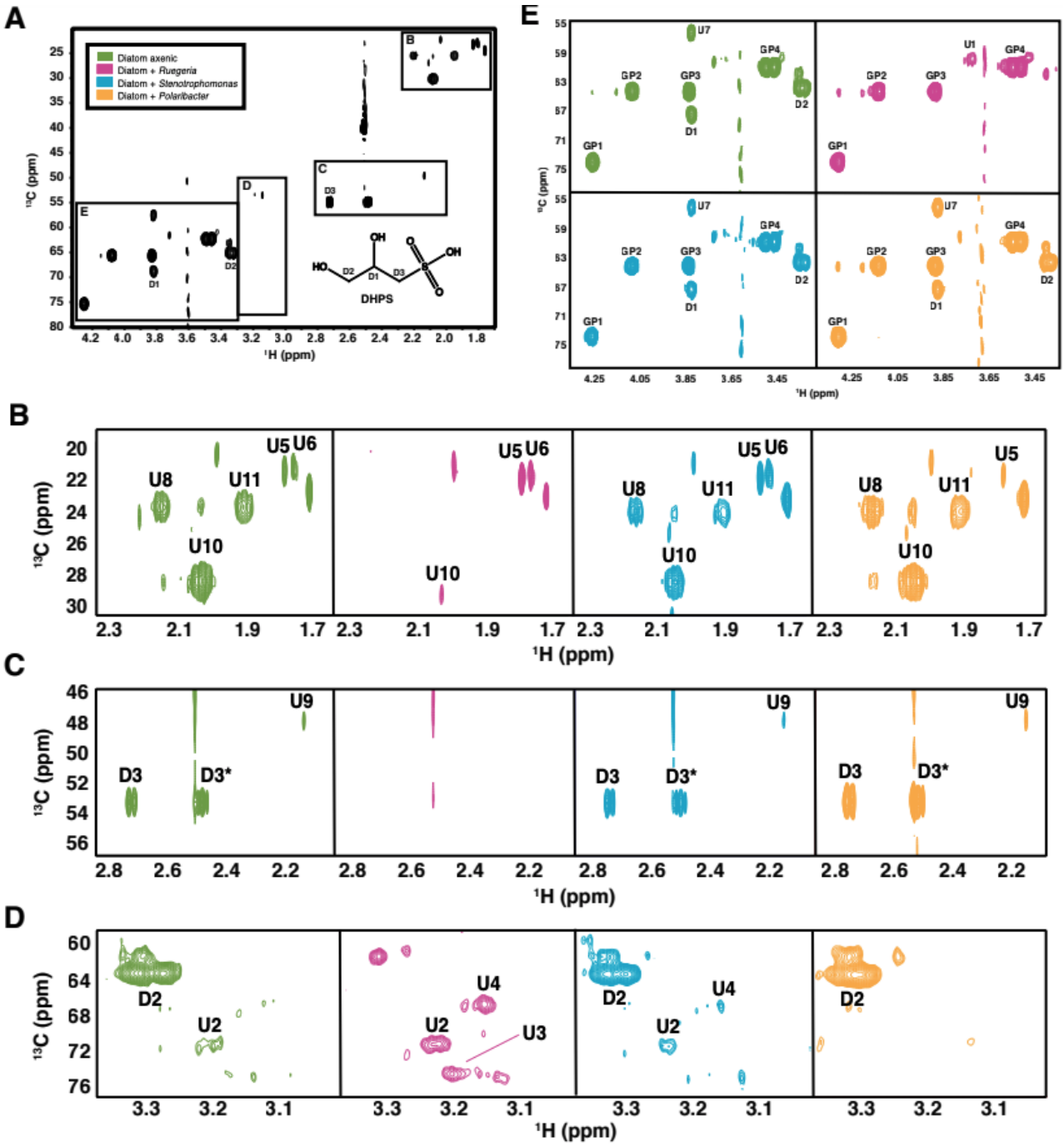

Figure S2. 13C-HSQC NMR spectra of metabolite uptake in co-cultures. (A) Full representative spectra from *T. pseudonana* with insets B, C, D, and E. The structure of DHPS is shown with numbered peaks (D1, D2, and D3) corresponding to each C-H bond in the compound. (B-E) Detailed NMR signals of 18 features in axenic and co-culture spent media. Spectra from one of 3 replicate samples is shown. The peak labeled with an asterisk in panel C indicates a C – H bond in DHPS that lies within T1 noise.

Supplementary Tables:

Table S1*. RNA-seq data for *R. pomeroyi* DSS-3. Log2 fold-differences that are negative are enriched in the co-culture, differences that are positive are enriched in the glucose control.

Table S2*. RNA-seq data for *Stenotrophomonas sp.* SKA14. Log2 fold-differences that are negative are enriched in the co-culture, differences that are positive are enriched in the glucose control.

Table S3*. RNA-seq data for *P. dokdonensis* MED152. Log2 fold-differences that are negative are enriched in the co-culture, differences that are positive are enriched in the glucose control.

*Due to file size, these tables are available at: https://www.nature.com/articles/s41396-020-00811-y#Sec13

Compound	Retention Time (min)	Parent (m/z)	Product 1 (m/z)	Product 2 (m/z)	Adduct	# bz	Correlation Coefficient (R2)	# Standards
2,3 -Dihydroxybenzoic acid	12.6	257.0455	121.0282	N/A	-H	1	0.950	8
2'deoxycitidine	7.8	332.1241	105.0330	216.0776	+H	1	0.986	9
2'deoxyguanosine	8.5	370.1157	121.0281	150.0406	-H	1	0.983	7
3'AMP	5	450.0820	134.0456	78.9579	-H	1	0.987	7
4-aminobenzoic acid	10.9	240.0666	196.0762	N/A	-H	1	0.997	7
5'AMP	6.7	450.0820	134.0456	78.9579	-H	1	0.984	7
5'deoxyadenosine	7.7	354.1208	238.0727	N/A	-H	1	0.986	10
adenine	7.4	240.0880	105.0328	137.0449	+H	1	0.978	7
adenosine	8.5	372.1302	105.0328	136.0612	+H	1	0.938	7
alanine	6.6	192.0666	148.0762	120.0443	-H	1	0.996	8
AmMP	3.7	243.1240	122.0714	81.0445	+H	1	0.988	5
arginine	3.3	279.1452	105.0330	220.0962	+H	1	0.993	5
asparagine	3.4	237.0870	105.0328	122.0595	+H	1	0.989	5
aspartate	4.5	236.0564	115.0023	120.0443	-H	1	0.996	8
chitobiose	7	529.2028	126.0543	204.0860	+H	1	0.981	7
chitotriose	7	732.2822	126.0543	138.0550	+H	1	0.986	7
ciliatine	3	230.0577	105.0328	95.0484	+H	1	0.989	9
citrulline	4.6	278.1146	191.1194	235.1069	-H	1	0.992	8
cysteate	2.8	274.0380	166.9789	184.9895	+H	1	0.964	6
cysteine	11.2	449.0846	105.0330	224.0368	+H (dimer)	1	0.938	7
cytidine	7.4	346.1044	213.0661	135.0191	-H	1	0.996	5
desthiobiotin	7.3	215.1390	179.1161	197.1281	+H	0	0.976	9
DHPS	5.4	259.0282	121.0285	N/A	-H	1	0.988	8
ectoine	5.4	265.1187	105.0330	98.0596	+H	1	0.993	9
GABA	6.8	208.0968	105.0328	95.0484	+H	1	0.993	5
glucosamine 6-phosphate	2.4	362.0646	78.9579	96.9681	-H	1	0.964	8
glutamic acid	5.5	250.0721	121.0290	162.0925	-H	1	0.997	6
glutamine	3.8	249.0881	120.0443	187.0880	-H	1	0.990	6
glycine	4.3	178.0510	132.0438	134.0607	-H	1	0.992	8
guanosine	8.2	388.1251	105.0328	152.0556	+H	1	0.931	7
histidine	2.7	258.0884	120.0443	81.0452	-H	1	0.996	8
HMP	6.3	244.1080	105.0330	123.0456	+H	1	0.940	7
homoserine	4.2	222.0772	120.0449	178.0872	-H	1	0.991	7
homoserine betaine	5	266.1387	105.0330	207.0643	+H	1	0.995	5
inosine	1.9	269.0881	137.0449	N/A	+H	0	0.939	7
isethionate	6.4	229.0176	121.0289	N/A	-H	1	0.977	6
isoleucine	11.4	234.1136	190.1247	82.0660	-H	1	0.988	8
kynurenine	11.2	313.1183	105.0330	146.0598	+H	1	0.990	5
leucine	11.2	236.1281	105.0333	86.0960	+H	1	0.999	8
lysine	11	355.1652	105.0328	188.1072	+H	2	0.979	9
methionie	9.4	252.0700	160.0753	146.0599	-H	1	0.978	7
MTA	1.7	314.0918	136.0616	97.0282	+H (oxidizec	0	0.998	5
n-acetyl muramic acid	8.1	380.1338	105.0330	126.0543	+H (water lc	1	0.982	7
n-acetyl-D-glycosamine	7.1	326.1234	105.0330	126.0539	+H	1	0.956	9
ornithine	10.4	339.1350	120.0442	174.0911	-H	2	0.976	8
pantothenic acid	10.9	324.1442	184.0966	202.1063	+H	1	0.992	9
phenylalanine	11.7	268.0979	120.0442	91.0507	-H	1	0.977	8
proline	7.9	220.0968	105.0330	70.0648	+H	1	0.990	5
putrescine	11.2	297.1597	105.0330	176.1076	+H	2	0.944	9
pyridoxine	7.3	274.1074	105.0330	256.0957	+H	1	0.951	9
S-(1,2-dicarboxyethyl)glutathione	6.5	526.1142	143.0448	115.0023	-H	1	0.985	8
S-(5'-adenosyl)-L-homocysteine	3.4	505.1511	136.0611	97.0279	+H (oxidizec	0	0.942	7
sarcosine	6.1	194.0812	105.0330	95.0487	+H	1	0.990	5
serine	3.6	208.0615	134.0606	146.0595	-H	1	0.994	8
spermidine	8	354.2176	162.0911	105.0328	+H	2	0.959	7
syringic acid	5.4	197.0456	123.0071	166.9982	-H	0	0.938	8
taurine	3.3	228.0336	106.9800	79.9564	-H	1	0.996	6
taurocholic acid	12	514.2844	N/A	N/A	-H	0	0.973	7
threonine	5.5	224.0917	105.0329	56.0491	+H	1	0.998	5
thymidine	2.5	241.0830	125.0342	N/A	-H	0	0.980	6
tryptophan	11.4	307.1088	120.0442	134.0606	-H	1	0.999	5
tyrosine	8.4	284.0928	119.0492	120.0442	-H	1	0.999	5
valine	9.4	220.0979	176.1062	68.0495	-H	1	0.995	8
xanthine	6.9	255.0523	N/A	N/A	-H	1	0.975	8
xanthosine	8.5	387.0946	151.0247	193.0350	-H	1	0.978	6

Table S4. Targeted metabolites that could be quantified by mass spectrometry in culture media with a calibration curve R2 > 0.92. Each parent ion was fragmented into one or more product ions (Product 1, Product 2). N/A = absence of a product ion; # bz = number of benzoyl groups added to the target compound in the derivatization process; # Standards = number of standards in the calibration curve.

SPO	Protein Tag	Fold Change	Adjusted p	Description
Transporter Systems				
SPO0591	WP_011046347.1	58.3	**	Dihydroxypropanesulfonate (DHPS) TRAP transporter, DctP
SPO0592	WP_011046348.1	43.5	**	Dihydroxypropanesulfonate (DHPS) TRAP transporter, DctQ
SPO0593	WP_011046349.1	37.9	**	Dihydroxypropanesulfonate (DHPS) TRAP transporter, DctM
SPO0608	WP_044027876.1	96.7	**	sugar ABC transporter, substrate binding protein
SPO0609	WP_011046365.1	60.7	**	sugar ABC transporter, ATP binding protein
SPO0610	WP_011046366.1	52.5	**	sugar ABC transporter, ATP binding protein
SPO0611	WP_011046367.1	50.3	**	sugar ABC transporter, permease
SPO0612	WP_011046368.1	46.4	**	sugar ABC transporter, permease
SPO0660	WP_011046411.1	3.6	**	*N* -acetyltaurine ABC transporter, substrate binding protein
SPO0661	WP_084791036.1	4.3	**	*N* -acetyltaurine ABC transporter, permease
SPO0662	WP_011046413.1	3.7	**	*N* -acetyltaurine ABC transporter, permease
SPO0663	WP_011046414.1	5.0	**	*N* -acetyltaurine ABC transporter, ATP-binding protein
SPO0664	WP_011046415.1	4.1	**	*N* -acetyltaurine ABC transporter, ATP-binding protein
SPO1017	WP_011046765.1	3.9	**	branched-chain amino acid ABC transporter, ATP binding protein
SPO1018	WP_011046766.1	4.3	**	branched-chain amino acid ABC transporter, ATP binding protein
SPO1019	WP_011046767.1	6.2	**	branched-chain amino acid ABC transporter, permease
SPO1020	WP_044027955.1	6.5	**	branched-chain amino acid ABC transporter, permease
SPO1021	WP_011046769.1	7.0	**	branched-chain amino acid ABC transporter, substrate binding protein
SPO1112	WP_011046859.1			TRAP transporter, DctP
SPO1113	WP_011046860.1	2.5	**	TRAP transporter, DctQ
SPO1114	WP_011046861.1	2.9	**	TRAP dicarboxylate transporter, DctM
SPO1485	WP_044028096.1	7.9	**	sodium:galactoside symporter family protein
SPO1490	WP_011047227.1	3.1	**	branched-chain amino acid ABC transporter, substrate binding protein
SPO1491	WP_011047228.1	3.1	*	branched-chain amino acid ABC transporter, permease
SPO1492	WP_011047229.1			branched-chain amino acid ABC transporter, permease
SPO1493	WP_011047230.1			branched-chain amino acid ABC transporter, ATP binding protein
SPO1707	WP_011047441.1	3.4	*	urea ABC transporter, ATP binding protein
SPO1707a	WP_011047442.1	3.5	**	urea ABC transporter, ATP binding protein
SPO1708	WP_011047443.1	4.2	**	urea ABC transporter, permease
SPO1709	WP_011047444.1	3.2	*	urea ATP transporter, permease
SPO1710	WP_044029188.1	4.3	**	urea ABC transporter, substrate binding protein
SPO1719	WP_011047455.1	3.7	**	TRAP dicarboxylate transporter, DctM (mannonate, putative)
SPO1720	WP_011047456.1	4.0	**	TRAP dicarboxylate transporter, DctQ
SPO1721	WP_044028157.1	3.1	**	TRAP dicarboxylate transporter, DctP
SPO1810	WP_011047543.1	4.8	**	sodium/solute symporter family protein (acetate, putative)
SPO1820	WP_011047553.1			sugar ABC transporter, substrate binding protein (glycerol-3-phosphate, putative)
SPO1821	WP_044028198.1	3.8	*	sugar ABC transporter, permease
SPO1822	WP_011047555.1	4.1	*	sugar ABC transporter, permease
SPO1823	WP_011047556.1			sugar ABC transporter, ATP binding protein
SPO1846	WP_011047579.1			branched-chain amino acid ABC transporter, substrate binding protein
SPO1848	WP_011047581.1	2.2	*	branched-chain amino acid ABC transporter, ATP binding protein
SPO1849	WP_011047582.1	2.3	**	branched-chain amino acid ABC transporter, ATP binding protein
SPO1850	WP_011047583.1	2.2	**	branched-chain amino acid ABC transporter, permease
SPO1851	WP_011047584.1	2.9	**	branched-chain amino acid ABC transporter, permease
SPO2530	WP_011048237.1			branched-chain amino acid ABC transporter, permease
SPO2531	WP_011048238.1			branched-chain amino acid ABC transporter, permease
SPO2532	WP_011048239.1			branched-chain amino acid ABC transporter, ATP binding protein
SPO2533	WP_011048240.1	4.6	**	branched-chain amino acid ABC transporter, ATP binding protein
SPO2534	WP_011048241.1			branched-chain amino acid ABC transporter, substrate binding protein
SPO2571	WP_011048276.1	3.2	**	TRAP transporter, DctM
SPO2572	WP_044028481.1	3.5	**	TRAP transporter, DctQ
SPO2573	WP_011048278.1	3.6	**	TRAP transporter, DctP
SPO2626	WP_011048328.1	2.9	**	TRAP transporter, DctM
SPO2627	WP_011048329.1	2.6	*	TRAP transporter, DctQ
SPO2628	WP_011048330.1	2.3	*	TRAP transporter, DctP
SPO2658	WP_011048360.1	47.8	**	cysteate ABC transporter, substrate binding protein
SPO2659	WP_011048361.1	51.4	**	cysteate ABC transporter, permease
SPO2660	WP_011048362.1	23.8	**	cysteate ABC transporter, permease

SPO2661	WP_011048363.1	22.2	**	cysteate ABC transporter, ATP binding protein
SPO2802	WP_011048502.1	2.9	**	sugar ABC transporter, substrate binding protein
SPO2803	WP_011048503.1	3.3	**	sugar ABC transporter, ATP binding protein
SPO2804	WP_011048504.1	5.2	**	sugar ABC transporter, permease
SPO2805	WP_044028562.1	6.3	**	sugar ABC transporter, permease
SPO3040	WP_011048734.1	157.6	**	polar amino acid ABC transporter, substrate binding protein (glutamine, putative
SPO3041	WP_044028642.1	116.0	**	polar amino acid ABC transporter, permease
SPO3042	WP_011048736.1	52.4	**	polar amino acid ABC transporter, permease
SPO3043	WP_011048737.1	23.2	**	polar amino acid ABC transporter, ATP binding protein
SPO3290	WP_011048973.1	9.4	**	branched chain ABC transporter, ATP binding protein (phenylacetate, putative)
SPO3291	WP_011048974.1	4.7	**	branched chain ABC transporter, substrate binding protein
SPO3292	WP_011048975.1	6.8	**	branched chain ABC transporter, permease
SPO3294	WP_011048977.1	12.7	**	branched chain ABC transporter, permease
SPO3295	WP_044028707.1	16.5	**	branched chain ABC transporter, ATP binding protein
CAZymes				
SPO1844	WP_011047577.1	3.1	**	*N*-acetylglucosamine-6-phosphate deacetylase (CE9)
SPO3258	WP_011048948.1	2.8	**	glycosyl hydrolase 25 (GH25)
SPO0190	WP_011045959.1	2.7	**	oxidoreductase (AA3_2)
DMSP Demethylation				
SPO1913	WP_011047644.1	3.6	**	dimethylsulfoniopropionate demethylase
SPO1914	WP_011047645.1	3.6	**	acrylyl-CoA reductase

Table S5. Significantly enriched transporter systems and carbohydrate active enzymes in the transcriptome of *R. pomeroyi* DSS-3 in co-culture with *T. pseudonana*. ** $p < 0.01$, * = $p < 0.05$, NS = not 8 significant. GH = glycoside hydrolase, AA = auxiliary activity, CE = carbohydrate esterase. Alternating shading highlights multi-protein transporters.

Locus Tag	Protein Tag	Fold Change	Adjusted p	Description
Transporter Systems				
SSKA14_4109	WP_008268431.1	11.2	**	TonB Dependent Receptor (GluNac PUL)
SSKA14_4041	WP_008268362.1	8.7	**	NCS2 family permease: Xanthine/Uracil Family Permease
SSKA14_445	WP_008264850.1	8.3	**	TonB Dependent Receptor (Man PU)
SSKA14_174	WP_008264603.1	7.4	**	MFS transporter
SSKA14_3190	WP_040007328.1	6.7	**	TonB-dependent receptor, cobalamin
SSKA14_1710	WP_008266061.1	5.3	**	MFS transporter
SSKA14_2888	WP_008267272.1	5.0	**	sugar MFS transporter (GlcNac PUL)
SSKA14_2052	WP_008266402.1	4.3	**	MFS transporter of the (GalNac PUL)
SSKA14_3787	WP_008268127.1	4.0	**	amino acid permease
SSKA14_2708	WP_008267086.1	3.8	**	sugar MFS transporter (β-D-glucan PUL)
SSKA14_3866	WP_040009399.1	3.7	**	CitMHS family transporter, citrate transporter
SSKA14_993	WP_040009025.1	3.7	**	TonB-dependent vitamin B12 receptor
SSKA14_2346	WP_040009051.1	3.7	**	D-serine/D-alanine/glycine transporter
SSKA14_1433	WP_008265791.1	3.6	**	TonB-dependent receptor, cobalamin
SSKA14_1406	WP_006461445.1	3.5	**	arginine/agmatine antiporter
SSKA14_1199	WP_040008529.1	3.2	**	oligopeptide transporter, OPT family
SSKA14_103	WP_008264537.1	3.1	**	peptide MFS transporter
SSKA14_4238	WP_040007848.1	3.0	**	amino acid permease
SSKA14_3225	WP_008267572.1	2.7	**	hypothetical protein, possible xanthine/uracil family permease (IMG)
SSKA14_2695	WP_008267073.1	2.4	**	dicarboxylate/amino acid:cation symporter
SSKA14_2274	WP_004154263.1	2.3	**	nucleoside transporter NupC
SSKA14_2109	WP_008266462.1	2.2	**	proline/glycine betaine transporter ProP
SSKA14_582	WP_040006829.1	2.0	**	benzoate/H(+) symporter BenE family transporter
CAZymes				
SSKA14_1062	WP_008265435.1	9.8	**	DUF5110 domain-containing protein (GH31,CBM32,CBM51, GalNac PUL)
SSKA14_4140	WP_008268466.1	7.9	**	hypothetical protein (CBM32)
SSKA14_2691	WP_008267069.1	6.2	**	glycoside hydrolase family 92 protein (GH92)
SSKA14_1430	WP_040007852.1	5.3	**	glycoside hydrolase family 92 protein (GH92, Man PUL)
SSKA14_4417	WP_008268752.1	5.1	**	choline dehydrogenase (AA3)
SSKA14_2242	WP_040007085.1	4.8	**	family 20 glycosylhydrolase (GH20, GlcNac PUL)
SSKA14_158	WP_008264589.1	4.0	**	glycoside hydrolase family 2 protein (GH2, Man PUL)
SSKA14_1256	WP_008265632.1	3.1	**	glycoside hydrolase family 92 protein (GH92)
SSKA14_2811	WP_008267196.1	3.0	**	cellulose-binding protein (AA10,CBM73)
SSKA14_1958	WP_008266306.1	2.5	**	tetratricopeptide repeat protein (GT41)
SSKA14_133	WP_008264568.1	2.4	**	*N* -acetylglucosamine-6-phosphate deacetylase (CE9, GlcNac PUL)
SSKA14_150	WP_008264581.1	2.0	**	glycosyltransferase (GT2,GT4)
SSKA14_2339	WP_008266696.1	1.1		exo 1,3/1,4-beta-D-glucan glucohydrolase (EC 3.2.1.21)
GlcNac PUL				
SSKA14_2242	WP_040007085.1	4.8	**	beta-hexosaminidase (GH20)
SSKA14_4109	WP_008268431.1	11.2	**	TonB-dependent receptor
SSKA14_173	WP_008264602.1	12.4	**	glucokinase (EC 2.7.1.2)
SSKA14_2888	WP_008267272.1	5.0	**	sugar MFS transporter
SSKA14_413	WP_006391719.1			LacI family DNA-binding transcriptional regulator
SSKA14_1007	WP_008265386.1	2.0	*	glutamine-fructose-6-phosphate transaminase
SSKA14_133	WP_008264568.1	2.4	**	*N* -acetylglucosamine-6-phosphate deacetylase (CE9)
SSKA14_3769	WP_008268111.1			putative heparan-alpha-glucosaminide N-acetyltransferase
Man PUL				
SSKA14_158	WP_008264589.1	4.0	**	beta-mannosidase (EC 3.2.1.25) (GH2)
SSKA14_826	WP_008265210.1	2.0	*	N-acylglucosamine 2-epimerase
SSKA14_3154	WP_008267508.1			fructokinase
SSKA14_738	WP_008265126.1			L-fucose:H+ symporter permease
SSKA14_980	WP_008265359.1			transcriptional regulator, LacI family
SSKA14_1430	WP_040007852.1	5.3	**	alpha-1,2-mannosidase, putative subfamily (GH92)
SSKA14_445	WP_008264850.1	8.3	**	TonB-dependent receptor
SSKA14_2050	WP_008266400.1	4.8	**	TonB-dependent receptor
GalNac PUL				
SSKA14_2052	WP_008266402.1	4.3	**	MFS transporter (AgaP)
SSKA14_3302	WP_008267642.1	1.9	*	N-acetylglucosamine-6-phosphate deacetylase (CE9, AgaA)

SSKA14_1063	WP_008265436.1			transcriptional regulator, DeoR family (AgaR)
SSKA14_4056	WP_008268376.1	12.8	**	tagatose-bisphosphate aldolase noncatalytic subunit (AgaZ)
SSKA14_1072	WP_008265444.1			*N*-acetyl-D-glucosamine kinase (AgaK)
SSKA14_2667	WP_008267043.1			galactosamine 6-phosphate isomerase (AgaS)
SSKA14_1062	WP_008265435.1	9.8	**	(GH31,CBM32,CBM51)
SSKA14_802	WP_008265187.1	4.2	*	TonB-dependent receptor (Omp_Aga)
SSKA14_240	WP_040009289.1			Gfo/Idh/MocA family oxidoreductase (GH109)
β-D-glucan PUL				
SSKA14_1589	WP_008265935.1	2.4	*	sensor domain-containing diguanylate cyclase
SSKA14_1295	WP_008265669.1	1.4		cupin-like domain-containing protein
SSKA14_1667	WP_040006978.1	1.5		TonB-dependent receptor
SSKA14_2708	WP_008267086.1	3.8	**	sugar MFS transporter
SSKA14_1577	WP_040006979.1	1.4		LacI family DNA-binding transcriptional regulator
SSKA14_2339	WP_008266696.1	1.1		exo 1,3/1,4-beta-D-glucan glucohydrolase (EC 3.2.1.21)
SSKA14_1033	WP_008265408.1	1.3		hypothetical protein

Table S6. Significantly enriched transporter systems and carbohydrate active enzymes in the transcriptome of *Stenotrophomonas sp.* SKA14 in co-culture with *T. pseudonana* and their location in PULs. ** $p < 0.01$, * = $p < 0.05$. GH = glycoside hydrolase, CBM = carbohydrate binding module, AA = auxiliary activity, CE = carbohydrate esterase, GT = glycosyl transferase.

Locus Tag	Protein Tag	Fold Change	Adjusted p	Description
Transporter Systems				
MED152_00420	WP_015479862.1	10.1	**	TonB-dependent receptor, PUL2
MED152_05095	WP_015480785.1	6.0	**	MFS transporter, PUL3 (fucose)
MED152_05115	WP_015480789.1	3.3	**	MFS transporter, PUL3
MED152_05120	WP_015480790.1	6.7	**	MFS transporter, PUL3
MED152_05155	WP_015480797.1	4.9	**	TonB-dependent receptor, PUL3
MED152_06260	WP_015481012.1	2.3	**	peptide MFS transporter
MED152_06860	WP_015481128.1	2.8	**	Na+/proline symporter, PUL4
MED152_08060	WP_015481364.1	2.0	**	branched-chain amino acid transport system II carrier protein
MED152_08460	WP_015481441.1	4.0	**	sugar MFS transporter, PUL5
MED152_08475	WP_015481444.1	126.0	**	TonB-dependent receptor, PUL5
MED152_09830	WP_015481710.1	3.9	**	TonB-dependent receptor, PUL6
MED152_09865	WP_015481717.1	17.9	**	TonB-dependent receptor, PUL7
MED152_12804	WP_015482283.1	9.8	**	TonB-dependent receptor (cobalamin)
CAZymes				
MED152_11564	WP_015482037.1	9.2	**	family 16 glycosylhydrolase (GH16)
MED152_09780	WP_015481700.1	5.4	**	alginate lyase (PL6, PUL6)
MED152_00755	WP_015479928.1	4.5	**	T9SS C-terminal target domain-containing protein (GH81, CBM6)
MED152_07070	WP_051058582.1	4.3	**	glycoside hydrolase (GH113)
MED152_09875	WP_015481719.1	3.8	**	hypothetical protein (PL6)
MED152_09820	WP_015481708.1	3.3	**	heparinase (PL17, PUL6)
MED152_03735	WP_015480517.1	3.2	**	T9SS C-terminal target domain-containing protein (PL6)
MED152_09785	WP_015481701.1	3.0	**	polysaccharide lyase family 7 protein (PL7, PUL6)
MED152_08695	WP_015481488.1	2.5	**	glycosyl transferase family 2 (GT2)
MED152_03105	WP_041383822.1	2.2	**	response regulator (GT2)
MED152_05855	WP_015480934.1	2.2	**	glycogen synthase (GT4)
MED152_04045	WP_015480579.1	2.2	**	glycosyltransferase (GT2)
MED152_08490	WP_015481447.1	2.2	**	beta-N-acetylhexosaminidase (GH20, PUL5)
not assigned	WP_015480999.1	2.1	**	polysaccharide lyase family 7 protein (PL7)
PUL2				
MED152_00360	WP_015479851.1			LacI family transcriptional regulator
MED152_00365	WP_015479852.1			MFS transporter (maltose/moltooligosaccharide transporter)
MED152_00370	WP_015479853.1			beta-phosphoglucomutase
MED152_00375	WP_015479854.1			maltose phosphorylase (GH65)
MED152_00380	WP_015479855.1			sulfatase
MED152_00385	WP_015479856.1			alpha-amylase (GH13)
MED152_00390	WP_015479857.1			esterase
MED152_00395	WP_015479858.1			alpha-glucosidase/oligosaccharide 4-alpha-D-glucosyltransferase (GH31)
MED152_00400	WP_015479859.1			alpha-amylase (GH13)
MED152_00405	WP_015479860.1			alpha-amylase (GH13)
MED152_00410	WP_041383244.1			hypothetical protein
MED152_00415	WP_015479861.1			hypothetical protein (regulatory protein, LuxR family)
MED152_00420	WP_015479862.1	10.1	**	TonB-dependent receptor
MED152_00425	WP_041383746.1	7.3	**	RagB/SusD family nutrient uptake outer membrane protein
MED152_00430	WP_015479864.1	4.2	**	hypothetical protein
MED152_00435	WP_015479865.1	3.2	**	hypothetical protein
MED152_00440	WP_015479866.1			hypothetical protein (glycosyl hydrolase)
MED152_00445	WP_015479867.1			hypothetical protein (GH149)
MED152_00450	WP_015479868.1			glycosyl hydrolase family 17 (GH17)
MED152_00455	WP_015479869.1			glycosyl hydrolase family 30 (GH30)
MED152_00460	WP_015479870.1			MFS transporter (glycoside/pentoside/hexuronide:cation symporter, GPH family)
PUL3				
MED152_05050	WP_015480776.1			beta-glucosidase (GH3)
MED152_05055	WP_015480777.1			hypothetical protein
MED152_05060	WP_015480778.1			DNA polymerase III subunit epsilon
MED152_05065	WP_015480779.1			polyphosphate kinase
MED152_05070	WP_015480780.1			hypothetical protein
MED152_05075	WP_015480781.1	1.9	*	maltooligosyl trehalose synthase (GH13)
MED152_05080	WP_041383396.1	3.6	**	sugar kinase
MED152_05085	WP_015480783.1	2.0	*	solute:sodium symporter family transporter (putative myo-inositol cotransporter)
MED152_05090	WP_015480784.1			alpha-glucosidase (GH13)
MED152_05095	WP_015480785.1	6.0	**	MFS transporter (fucose permease)

MED152_05100	WP_015480786.1			glycoside hydrolase family 65 protein (GH65), trehalose and maltose hydrolase
MED152_05105	WP_015480787.1			mannan endo-1,4-beta-mannosidase (GH5)
MED152_05110	WP_015480788.1			trehalase (GH37)
MED152_05115	WP_015480789.1	3.3	**	MFS transporter (fucose permease)
MED152_05120	WP_015480790.1	6.7	**	MFS transporter (maltose/moltooligosaccharide transporter)
MED152_05125	WP_015480791.1			hypothetical protein
MED152_05130	WP_015480792.1			ASPIC-like protein
MED152_05135	WP_015480793.1			ASPIC-like protein
MED152_05140	WP_015480794.1			hypothetical protein
MED152_05145	WP_015480795.1			ASPIC-like protein
MED152_05150	WP_015480796.1			RagB/SusD family nutrient uptake outer membrane protein
MED152_05155	WP_015480797.1	4.9	**	SusC/RagA family TonB-linked outer membrane protein
MED152_05160	WP_015480798.1			DUF1080 domain-containing protein
MED152_05165	WP_015480799.1			sugar phosphate isomerase/epimerase
MED152_05170	WP_015480800.1			gfo/Idh/MocA family oxidoreductase
MED152_05175	WP_015480801.1			nucleoside symporter
MED152_05180	WP_015480802.1	2.2	**	sugar phosphate isomerase/epimerase
MED152_05185	WP_015480803.1	2.2	**	AraC family transcriptional regulator
MED152_05190	WP_015480804.1	2.4	**	oxidoreductase (AA3)
MED152_05195	WP_015480805.1			gluconate 2-dehydrogenase subunit 3 family protein
PUL4				
MED152_06840	WP_015481124.1			hypothetical protein
MED152_06845	WP_015481125.1			hypothetical protein
MED152_06850	WP_015481126.1			SusC/RagA family TonB-linked outer membrane protein
MED152_06855	WP_015481127.1			SusD/RagB family nutrient-binding outer membrane lipoprotein
MED152_06860	WP_015481128.1	2.8	**	sodium:solute symporter "proline symporter"
MED152_06865	WP_015481129.1			diadenosine tetraphosphatase
MED152_06870	WP_015481130.1			rhodanese-like domain-containing protein
MED152_06875	WP_015481131.1			hypothetical protein
MED152_06880	WP_015481132.1			purine-nucleoside phosphorylase
MED152_06885	WP_015481133.1			DUF1679 domain-containing protein
PUL5				
MED152_08455	WP_015481440.1			aldose 1-epimerase
MED152_08460	WP_015481441.1	4.0	**	sugar MFS transporter
MED152_08465	WP_015481442.1	3.7	**	DNA-binding response regulator
MED152_08470	WP_015481443.1	9.1	**	histidine kinase
MED152_08475	WP_015481444.1	14.0	**	SusC/RagA family TonB-linked outer membrane protein
MED152_08480	WP_015481445.1	9.4	**	SusD/RagB family nutrient-binding outer membrane lipoprotein
MED152_08485	WP_015481446.1	6.7	**	glucosamine-6-phosphate deaminase
MED152_08490	WP_015481447.1	2.3	**	beta-N-acetylhexosaminidase (GH20)
MED152_08495	WP_015481448.1			N-acetylglucosamine kinase
MED152_08500	WP_015481449.1			hypothetical protein
PUL6 and 7				
MED152_09760	WP_015481697.1			adenosylhomocysteinase
MED152_09765	WP_015481698.1	9.2	**	PepSY domain-containing protein, Uncharacterized iron-regulated membrane protein
MED152_09770	WP_015481699.1			sodium:sulfate symporter
MED152_09780	WP_015481700.1	5.4	**	poly(beta-D-mannuronate) lyase (PL6)
MED152_09785	WP_015481701.1	3.0	**	polysaccharide lyase family 7 protein (PL7)
MED152_09790	WP_015481702.1			gluconokinase
MED152_09795	WP_015481703.1			6-phosphogluconate dehydrogenase
MED152_09800	WP_015481704.1	2.9	**	putative Mn2+ Fe2+ transporter
MED152_09805	WP_015481705.1			polysaccharide lyase family 7 protein (PL7)
MED152_09810	WP_015481706.1			3-oxoacyl-ACP reductase FabG
MED152_09815	WP_015481707.1	14.5	**	Por secretion system C-terminal sorting domain-containing protein
MED152_09820	WP_015481708.1	3.3	**	heparinase (PL17)
MED152_09825	WP_015481709.1			cupin domain-containing protein
MED152_09830	WP_015481710.1	3.9	**	TonB-dependent receptor
MED152_09835	WP_015481711.1	2.0	*	RagB/SusD family nutrient uptake outer membrane protein
MED152_09840	WP_015481712.1			hypothetical protein
MED152_09845	WP_015481713.1			PKD domain-containing protein
MED152_09850	WP_015481714.1			FadR family transcriptional regulator
MED152_09855	WP_015481715.1			MFS transporter
MED152_09860	WP_015481716.1			Short-chain dehydrogenase/reductase
MED152_09865	WP_015481717.1	17.9	**	TonB-dependent receptor
MED152_09870	WP_015481718.1	7.8	**	RagB/SusD family nutrient uptake outer membrane protein
MED152_09875	WP_015481719.1	3.8	**	poly(beta-D-mannuronate) lyase (PL6)
MED152_09880	WP_083903258.1			ATP-binding protein
MED152_09885	WP_041383578.1	2.1	**	hypothetical protein

Table S7. Significantly enriched transporter systems and carbohydrate active enzymes in the transcriptome of *Polaribacter dokdonensis* MED152 in co-culture with *T. pseudonana* and their location in PULs. ** $p < 0.01$, * = $p < 0.05$. GH = glycoside hydrolase, CBM = carbohydrate binding module, AA = auxiliary activity, CE = carbohydrate esterase, GT = glycosyl transferase.

CHAPTER 4

NMR METHODS TO OBSERVE *IN VIVO* METABOLISM IN *RUEGERIA POMEROYI*[1]

Nicole R. Holderman, Christa Smith, Mary Ann Moran, and Arthur S. Edison[1]

Chapter 4 is recent, unpublished pilot research conducted by Nicole Holderman. The CIVM-NMR method was originally conceptualized and published by Arthur S. Edison and Michael Judge for use in the filamentous fungus *Neurospora crassa*. Holderman optimized the method for use in *R. pomeroyi* and here reports the use of CIVM-NMR to observe substrate utilization by the bacteria. Mary Ann Moran, Arthur Edison, and Nicole Holderman designed the experiments. Christa Smith grew the *R. pomeroyi* cell cultures.

[1] Holderman, N., Smith, C., Moran, M. A., Edison, A. To be submitted to NMR in Biomedicine.

1 | INTRODUCTION

NMR spectroscopy has played a powerful role in deciphering metabolic processes for more than half a century.[149] The non-destructive nature of NMR makes it ideal for recording *in vivo* metabolism. One of the first studies to leverage NMR for developing our understanding of metabolism was conducted by Wilson, Burlingame and colleagues in 1974.[149,150] This study used ^{2}H- and ^{1}H-decoupled ^{13}C-NMR to detect the *in vivo* effects of deuterated ethanol by analyzing ^{2}H-incorporation into rat bile acids. While this was not authentic *in vivo* NMR, it set the stage for future studies that would continue to push the frontiers of this analytical platform.

Magic angle spinning (MAS) originated from a novel technique developed for solid-state NMR in 1958 when a sodium chloride crystal spun at 50 kHz exhibited narrowed spectral peaks versus a static crystal in ^{23}Na NMR.[151] The effects of molecular interactions between nuclei depend on the angle between the internuclear vector and the direction of the applied magnetic field. Time-averaged molecular interactions (sources of inhomogeneity that cause broad peaks and poor spectral resolution) disappear when the vector is a "magic angle" (54.74°) away from the direction of the magnetic field.[152]

One of the first applications of what would later be termed "high-resolution magic angle spinning (HR-MAS)" NMR was described in 1996 from an analysis of intact tissues *ex vivo*. Prior

to the advent of HR-MAS, NMR spectra collected from tissue analysis would suffer from sample heterogeneity and line broadening as described above. By quickly spinning (~2 kHz) a rotor at the magic angle, researchers could enhance spectral resolution and decrease line width to delineate differences in malignant versus healthy rat lymph nodes.[153] This technique was then applied to an analysis of human brain samples from healthy donors versus those with the neurodegenerative Pick disease and is the first reference to HR-MAS in the literature.[154] HR-MAS has since expanded into a robust tool for NMR metabolomics.

While a majority of HR-MAS studies have centered on the versatility and success of the technique in biomedicine and diagnostics, recent advances have been made in recording true *in vivo* metabolism in live organisms or cells over the course of hours or days. The Edison lab first published on the utility of a technique termed "continuous metabolism" by NMR (CIVM-NMR) in 2019.[28] CIVM-NMR measurements are instrumental for observing metabolic dynamics across a time series. Other methods of time series sampling to ascertain changing metabolic state(s) of an organism can be expensive in terms of time, resources, and material. Thus, researchers often make compromises on numbers of replicates, experimental duration, and/or temporal resolution.[28] Preparing these samples for analysis can then introduce extraction biases[155] or variability,[156] further complicating interpretation of metabolic data.

Judge and colleagues reported on the use of CIVM-NMR to elucidate branched chain amino acid (BCAA) flux in myeloid leukemia cells and to study the metabolism of *Neurospora crassa* under aerobic and anerobic conditions. CIVM-NMR revealed unidirectional metabolite flux of the BCAA ^{13}C-valine from isotopically labeled ^{13}C-keto-isovalerate media, an unexpected but profound discovery.[28,157] In *N. crassa*, glucose utilization in aerobic cultures caused concomitant acidification of the culture until substrate depletion after which point pH increased

slightly. The pH in anaerobic samples decreased with glucose consumption but persisted at the more acidic pH following glucose depletion.[28]

Here, we use CIVM-NMR to demonstrate *R. pomeroyi* substrate utilization of acetate, glucose, acetate + glucose, and 2[^{13}C-Me]-DMSP. The general procedure for this process is to culture *R. pomeroyi*, count the cells, load cells into a specialized rotor for the HR-MAS probe, spin at 3.5-4 kHz, collect 1D NMR data, and use a MATLAB workflow[28] to create a stacked plot of the spectra to represent the evolution of peaks over time (Figure 1).

DMSP catabolism is crucial to the global sulfur cycle as a precursor of dimethylsulfide (DMS), the primary contributor of naturally occurring sulfur to the atmosphere. The oxidation products of DMS (sulfate, sulfur dioxide, and methanesulfonic acid) are released into the atmosphere, functioning as a crucial regulator of climate.[24,25] The oxidation products significantly impact the amount of solar radiation reaching earth by directly scattering solar energy and operating as cloud condensation nuclei upon which water droplets condense in the initial stages of cloud formation.[25,26] For its ecological importance, DMSP was selected as an exemplar substrate to observe via CIVM-NMR. We were able to follow the utilization of 2[^{13}C-Me]-DMSP and observe its conversion through putative assignment of chemical shifts (Figure 3).

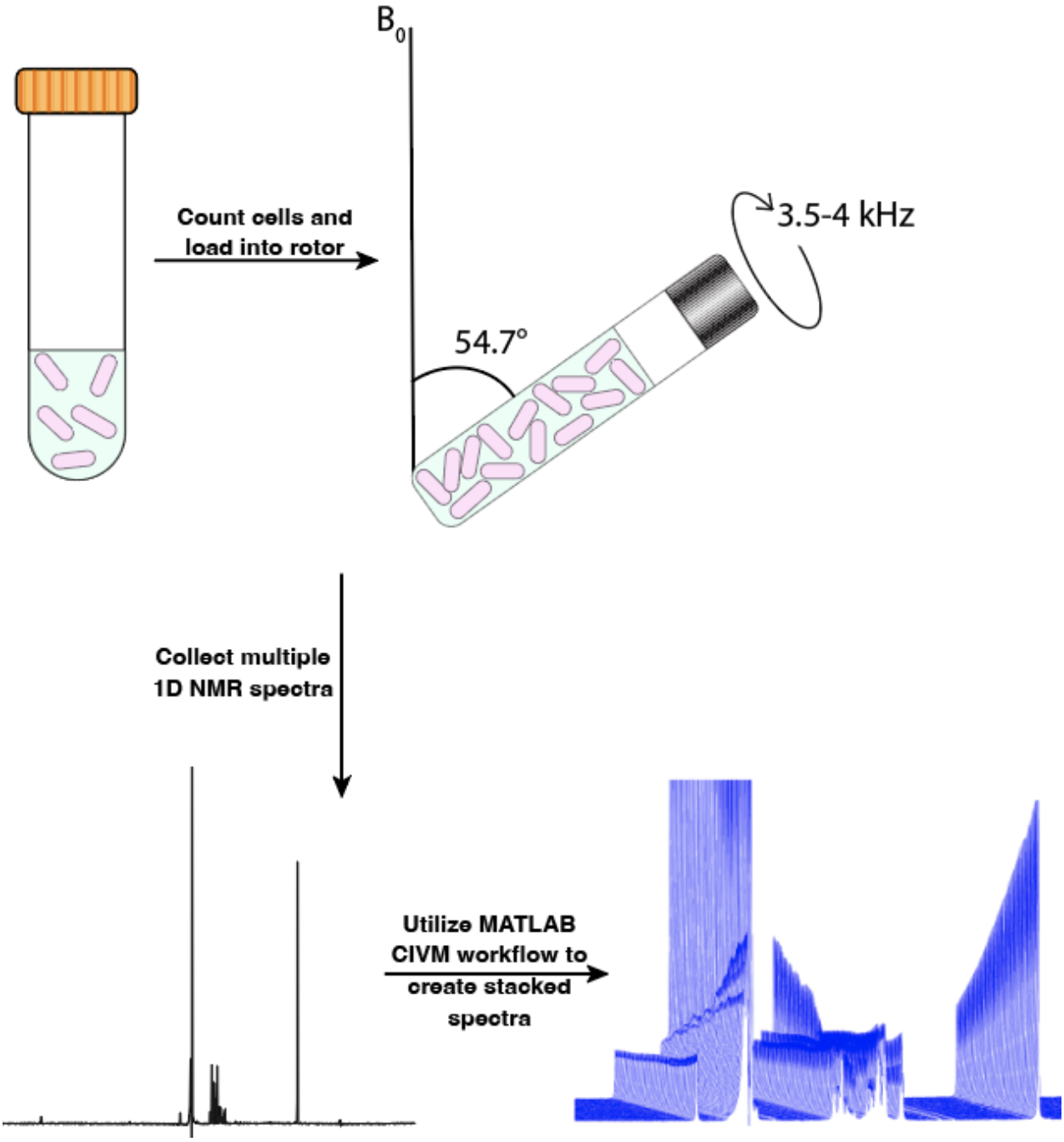

Figure 1: CIVM Workflow. *Ruegeria pomeroyi* cells were grown for 18 h after which cells were counted, washed, and loaded into a zirconia rotor for analysis in the HR-MAS probe. The sample was spun at 3.5 kHz for the 2[^{13}C-Me] DMSP substrate, and 4 kHz for acetate and glucose substrates. Multiple 1D NMR spectra were collected, and a MATLAB workflow was utilized to create a stacked spectra showing peak changes over time.

Acetate and glucose were of interest to us due to evidence in the literature regarding the differential use of both substrates for central metabolism, energy biosynthesis, and the electron transport chain (ETC). In a study utilizing core metabolic modeling (CMM), modeled pathways were mapped against pathway co-occurrence in central metabolism for a phylogenetically diverse collection of model microorganisms.[158] Alphaproteobacteria, of which *R. pomeroyi* is a member, demonstrated full correlation between CMM predictions and acetate metabolism pathways but comparatively lighter correlation between CMM predictions and its ability to perform glycolysis.[158] This indicates that acetate degradation pathways are present in all Alphaproteobacteria genomes but glucose degradation is not. *R. pomeroyi* is able to perform glucose and acetate degradation, but the incomplete coverage of glycolysis across all Alphaproteobacteria led to the hypothesis that *R. pomeroyi* may prefer acetate to glucose.

2 | EXPERIMENTAL

2.1 | Cell culture

Ingredients for MBM (20 ppt sea salt solution, 100 μM FeEDTA, 250 mL basal medium, 1 mL vitamin supplement, and ddH_2O to 1 L) were filter-sterilized through a 0.2-micron filter and aliquoted into sterile 50 mL Falcon tubes. Sea salt solution (5.79 g NaCl, 0.97 g Na2SO4, 0.164 g KCl, 23.6 mg KBr, 6.26 mg H_3BO_3, 0.752 mg NaF, 47.4 mg $NaHCO_3$, 2.62 g $MgCl_2$•$6H_2O$, 0.367 g $CaCl_2$•$2H_2O$, 6 mg $SrCl_2$•$6H_2O$), basal medium (1M Tris HCl pH 7.5, 0.34 g NH_4Cl, 182.98 mg K_2HPO_4, 375 mL ddH_2O), and vitamin supplement (100 mL ddH_2O, 2 mg biotin, 2 mg folic acid, 10 mg pyridoxine HCl, 5 mg riboflavin, 5 mg thiamine, 5 mg nicotinic acid, 5 mg pantothenic acid, 0.1 mg cyanocobalamin, 5 mg p-aminobenzoic acid) ingredients were dissolved and mixed in glass bottles. *R. pomeroyi* bacteria were incubated overnight (~18 h) at 30º C with a shaking

speed of 180 rpm in minimal basal medium (MBM) preconditioned with 10 mM glucose as the sole carbon source.

2.2 | Cell counts

Cells were counted prior to inoculating into the HR-MAS rotor using a Thermo Scientific (Waltham, MA, USA) NanoDrop 2000 UV Visible spectrophotometer.

2.3 | Preparation for HR-MAS

10 mM 2[^{13}C-Me]-DMSP pilot experiment

R. pomeroyi cells were washed twice in sterile carbon-free MBM and a cell suspension (36 µL) was loaded into a clean 4 mm diameter zirconia HR-MAS rotor (Bruker BioSpin) at 5e9 total cells. Substrate dissolved in 100% D_2O was loaded into the rotor immediately prior to analysis for a final D_2O concentration of 10%. A spacer (Bruker BioSpin) modified with a 0.016-inch diameter hole drilled using a lathe[159] was inserted to the top of the sample and a Kel-F rotor cap (Bruker BioSpin), with an o-ring for sealing and a hole to allow gas exchange, was placed on top of the spacer (Figure 1). The sample was inspected for any gaps between the cap and rotor, and the bottom edge of the rotor was marked with permanent marker before placing into the magnet bore with the cap pointing upwards.

5 mM acetate, 5 mM glucose, and 5 mM acetate + 5 mM glucose

R. pomeroyi cells were washed twice in sterile carbon-free MBM and a cell suspension (36 µL) was loaded into a clean 4 mm diameter zirconia HR-MAS rotor (Bruker BioSpin) at a density of 2.5e8 cells ml^{-1}. Substrate with 1 mM DSS-d_6 as an internal standard dissolved in 100% D_2O was loaded into the rotor immediately prior to analysis for a final D_2O concentration of 10%. A spacer (Bruker BioSpin) modified with a 0.016-inch diameter hole drilled using a lathe[159] was inserted to the top of the sample and a Kel-F rotor cap (Bruker BioSpin), with an o-ring for sealing

and a hole to allow gas exchange, was placed on top of the spacer (Figure 1). The sample was inspected for any gaps between the cap and rotor, and the bottom edge of the rotor was marked with permanent marker before placing into the magnet bore with the cap pointing upwards.

2.4 | NMR analysis

10 mM 2[^{13}C-Me]-DMSP pilot experiment

For measurement of ^{13}C, an hsqcetgpsisp (TopSpin) gradient heteronuclear single quantum coherence spectroscopy (HSQC) experiment run as a 1D experiment to visualize protons connected to ^{13}C was used with the parameters shown in Table 1.

5 mM acetate, 5 mM glucose, and 5 mM acetate + 5 mM glucose

An lc1pnf2 experiment was run to visualize ^{1}H and to set a secondary presaturation of the Tris buffer peak present in MBM. Parameters are shown in Table 1.

Substrate	Number of points	Ns/time point	Sweep Width (ppm)	Acquisition Time (ms)	Temp. (K)	Pulse width (µs)	Spin Speed (kHz)
2[^{13}C-Me] DMSP	4096	128	13.02	0.52	283.0	14.72	3.5
Acetate, Glucose, Acetate + Glucose	16384	64	19	1.376	303.15	13.4	4

Table 1: NMR experiment parameters. RG was set to 101 in both conditions. Data were collected on a Comprehensive Multi-Phase (CMP) HR-MAS probe installed on a 600 MHz Bruker NEO system

2.5 | Data processing

Batch processing for *in vivo* NMR was performed in NMRPipe using parameters optimized based on consistency between spectra from several time points for each sample. A custom bash script (modified from Judge et al., 2019)[28] ran NMRPipe[160] using the optimized parameters on all spectra for each sample. This script included all NMRPipe commands necessary for file conversions and NMR data processing including: apodization using an exponential decaying

window function with a line broadening of 3 Hz, Fourier transformation, 0- and 1st-order phasing, end removal, and baseline correction using automatic polynomial fitting.

For each sample, scripts written in MATLAB R2017b (The MathWorks, Inc., Natick, Massachusetts, USA) were adapted from Judge et al., 2019[28] in NMRbox.[160] These scripts loaded the processed spectra, ppm vectors, and measurement start times from ft and Bruker acqus files. Spectra were referenced to DSS automatically, stored as a matrix, and saved as a MATLAB workspace in .mat format. The matrix was normalized via a min/max normalization process to allow relative quantification of differences, and every eight spectra starting with the first timepoint were averaged as a moving average to improve signal-to-noise. All scripts are available at: https://github.com/artedison/Edison_Lab_Shared_ Metabolomics_UGA.

3| RESULTS

For the 10 mM 2[^{13}C-Me]-DMSP pilot experiment, only one replicate was observed due to interest in other substrates at the time. The extracted traces for this replicate are displayed. For statistical significance, additional replicates must be studied. The 5 mM acetate, 5 mM glucose, and 5 mM acetate + 5 mM glucose experiment contained three biological replicates of each substrate condition with traces displayed below.

3.1 | CIVM-NMR measurement detects metabolism of 2[^{13}C-Me]-DMSP by cleavage pathway(s)

R. pomeroyi catabolizes DMSP in three possible ways, two are via cleavage (Figure 2) and the third is through demethylation.[25] Due to the position of the ^{13}C labels in this study, we can most readily observe the two cleavage pathways. In one such pathway, 2[^{13}C-Me]-DMSP undergoes cleavage to form 2[^{13}C-Me]-dimethyl sulfide (DMS) and acrylate, and, in the other, 2[^{13}C-Me]-DMS and 3-hydroxypropanoyl-CoA. A fourth possible fate of DMSP in this

experiment is the oxidation of the 2[^{13}C-Me]-DMS product to 2[^{13}C-Me]-dimethyl sulfoxide (DMSO).

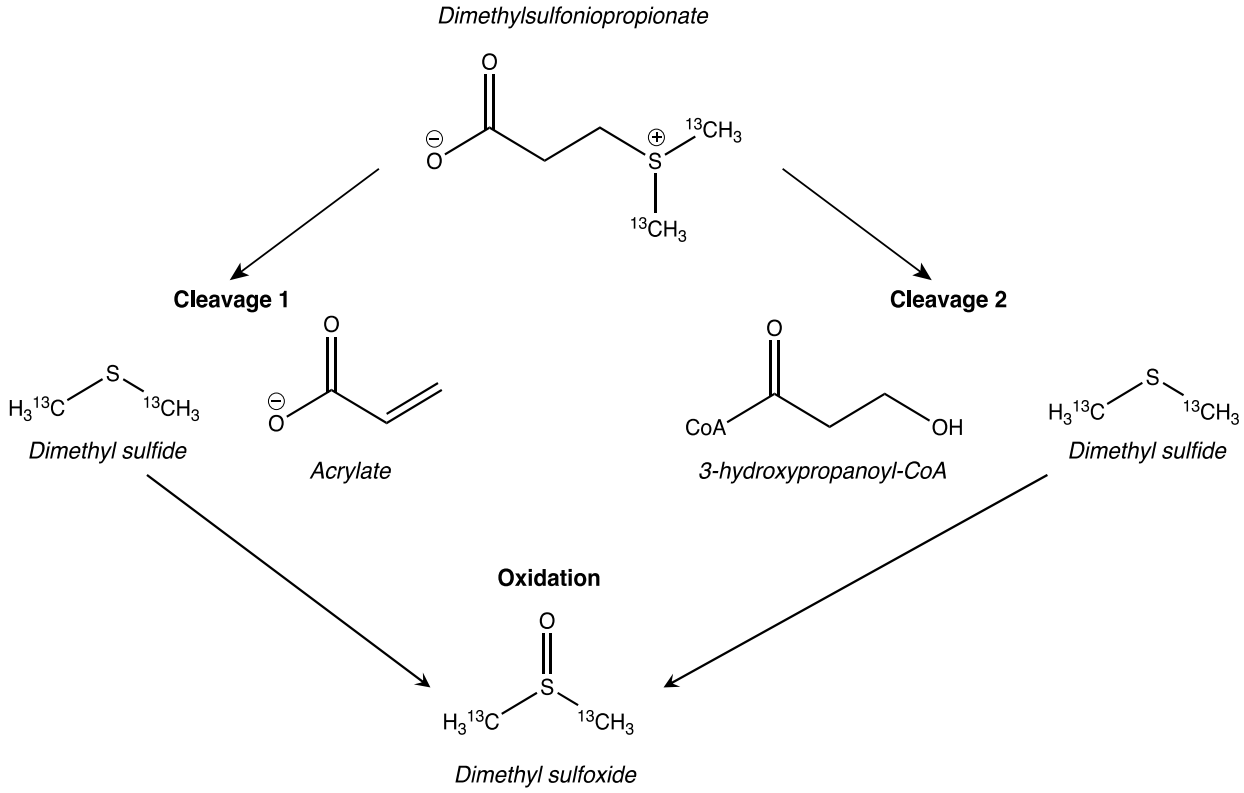

Figure 2: Possible fates of 2[^{13}C-Me]-DMSP. 2[^{13}C-Me]-DMSP can undergo one of two cleavage pathways to form either 2[^{13}C-Me]-DMS and acrylate or 2[^{13}C-Me]-DMS and 3-hydroxypropanoyl-CoA. 2[^{13}C-Me]-DMSO may also form as an oxidation product of 2[^{13}C-Me]-DMS. There also exists a demethylation pathway (not shown), for which products were unable to be putatively assigned. (DMSP, dimethylsulfoniopropionate; DMS, dimethyl sulfide; DMSO, dimethyl sulfoxide)

R. pomeroyi cells were cultured as described (see Experimental section), counted, pelleted and washed twice in MBM. A total of 5e9 cells were resuspended in sterile carbon-free MBM, and a cell suspension (36 µL) was loaded into a clean 4 mm diameter zirconia HR-MAS rotor (Bruker BioSpin). 2[^{13}C-Me]-DMSP dissolved in 100% D_2O was loaded into the rotor (4 µL, 10 mM final 2[^{13}C-Me]-DMSP) immediately prior to analysis, giving a final D_2O concentration of 10% for the NMR lock signal. A spacer (Bruker BioSpin) was inserted to the top of the sample and a Kel-F

rotor cap (Bruker BioSpin), with an o-ring for sealing and a hole to allow gas exchange, was placed on top of the spacer (Figure 1). The sample was inspected for any gaps between the cap and rotor and placed into the magnet. We recorded 1D HSQC spectra every 11 min while spinning at the magic angle (54.7°) at 3.5 kHz. A hole in the rotor cap and spacer allowed for gas exchange.

The intensity of the 2[^{13}C-Me]-DMSP peak at 2.729 ppm was monitored over 12 h (Figure 3). A peak at 2.54 and 1.915 ppm were monitored as well and are putatively assigned as the oxidation product 2[^{13}C-Me]-DMSO and 2[^{13}C-Me]-DMS, respectively. Putative assignments were made using chemical shift distances from 2[^{13}C-Me]-DMSP compared to literature values. More replicates and further peak validation need to be performed for positive peak assignment.

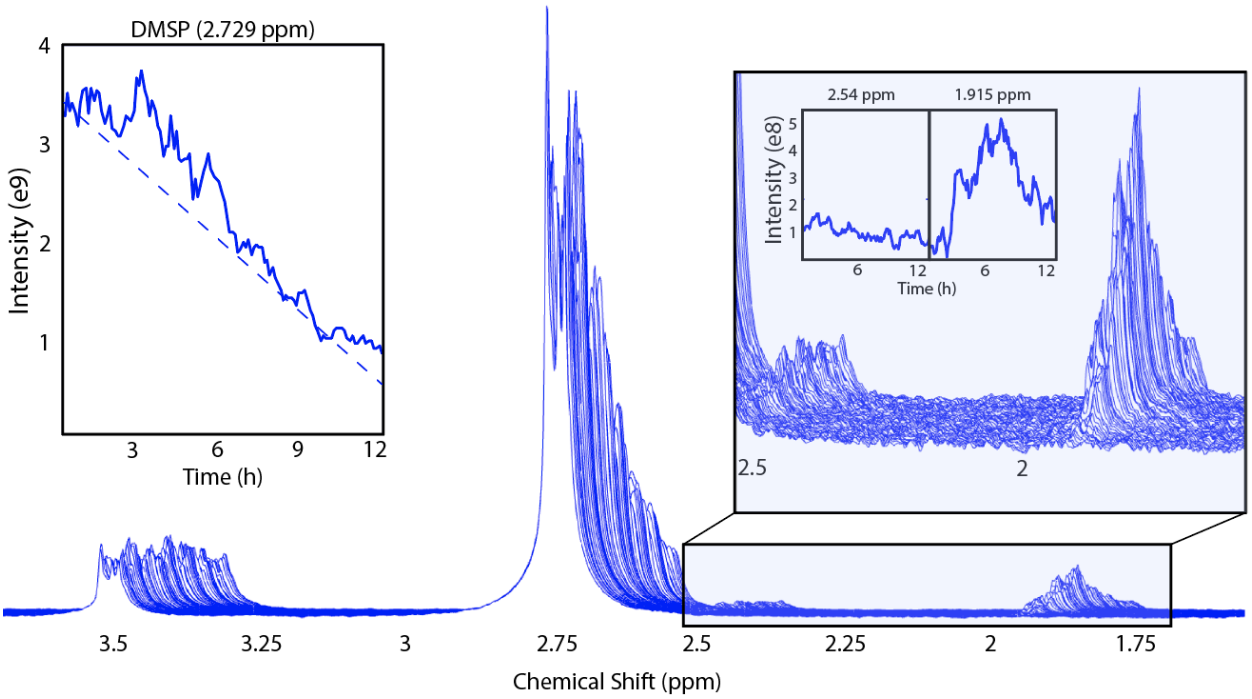

Figure 3: 2[^{13}C-Me]-DMSP utilization by *R. pomeroyi* in CIVM-NMR and putative cleavage and oxidation product formation
Putative assignment was determined by known chemical shift differences between (DMSP and DMS) and (DMSP and DMSO) to those visualized on the spectra (2.729 ppm for DMSP, 2.54 ppm for DMSO, and 1.915 ppm for DMS). The intensity of 2[^{13}C-Me]-DMSP decreases over time, 2[^{13}C-Me]-DMSO remains relatively steady, and 2[^{13}C-Me]-DMS increases then decreases sharply over the 12 h. Further validation is needed for spectral assignment. Additional replicates are needed as well to extend this research beyond a pilot study.

3.2 | CIVM-NMR measurement detects differential rates of substrate utilization between acetate and glucose

R. pomeroyi cells were cultured as described (see Experimental section), counted, pelleted and washed twice in MBM. A 2.5e8 cells ml^{-1} were resuspended in sterile carbon-free MBM and a cell suspension (36 µL) was loaded into a clean 4 mm diameter zirconia HR-MAS rotor (Bruker BioSpin). Acetate, glucose, or acetate + glucose dissolved in 100% D_2O for 5 mM final of each substrate was loaded into the rotor (4 µL) immediately prior to analysis, giving a final D_2O concentration of 10% for the NMR lock signal. A spacer (Bruker BioSpin) was inserted to the top of the sample and a Kel-F rotor cap (Bruker BioSpin), with an o-ring for sealing, was placed on top of the spacer (Figure 1). A hole in the rotor cap and spacer allowed for gas exchange. The sample was inspected for any gaps between the cap and rotor and placed into the magnet. We recorded 1D ^1H spectra (lc1pnf2) every 6 min while spinning at the magic angle (54.7°) at 4 kHz for 18 h.

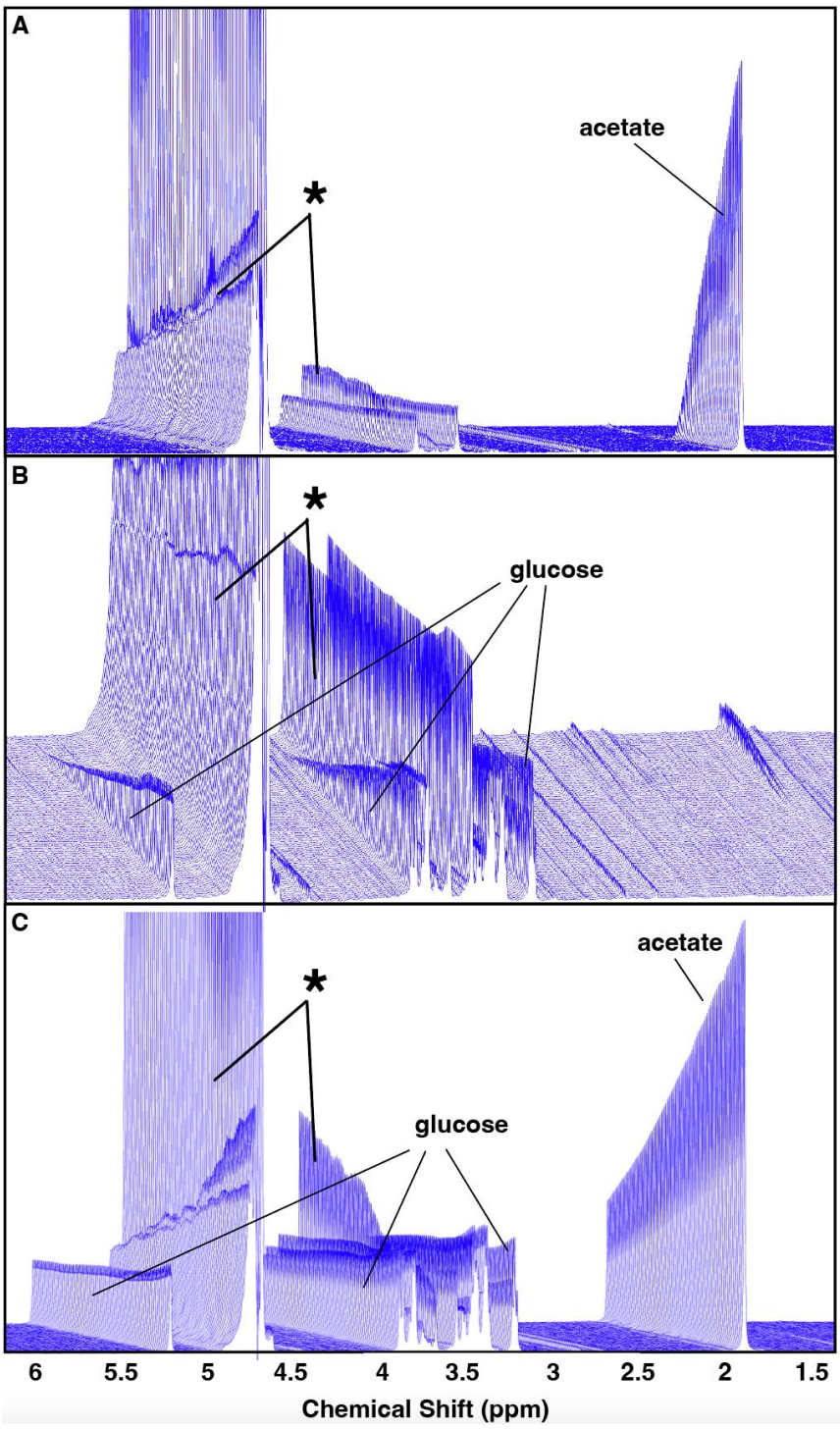

Figure 4: Acetate and glucose utilization in *R. pomeroyi* by CIVM-NMR over 18 h
T0 is the front-most trace, and time progresses as the traces advance into the page. The regions with asterisks are the two areas of presaturation for water and Tris buffer. Shown are stacked plots of (A) 5 mM acetate (B) 5 mM glucose and (C) 5 mM acetate an 5 mM glucose metabolism by *R. pomeroyi.*

Using MATLAB CIVM-NMR scripts, we extracted acetate and glucose peaks as regions of interest (ROIs) within a matrix and performed min/max normalization to obtain relative intensity of the substrate peaks. This was plotted as a function of time for all replicates (Figure 5). As anticipated, the rates of acetate utilization in both the acetate-only and acetate + glucose conditions were faster than rates of glucose utilization across all conditions. Acetate utilization was fastest when it was the sole carbon source. Likewise, when glucose was the sole carbon source, utilization was faster than glucose utilization in the acetate + glucose condition.

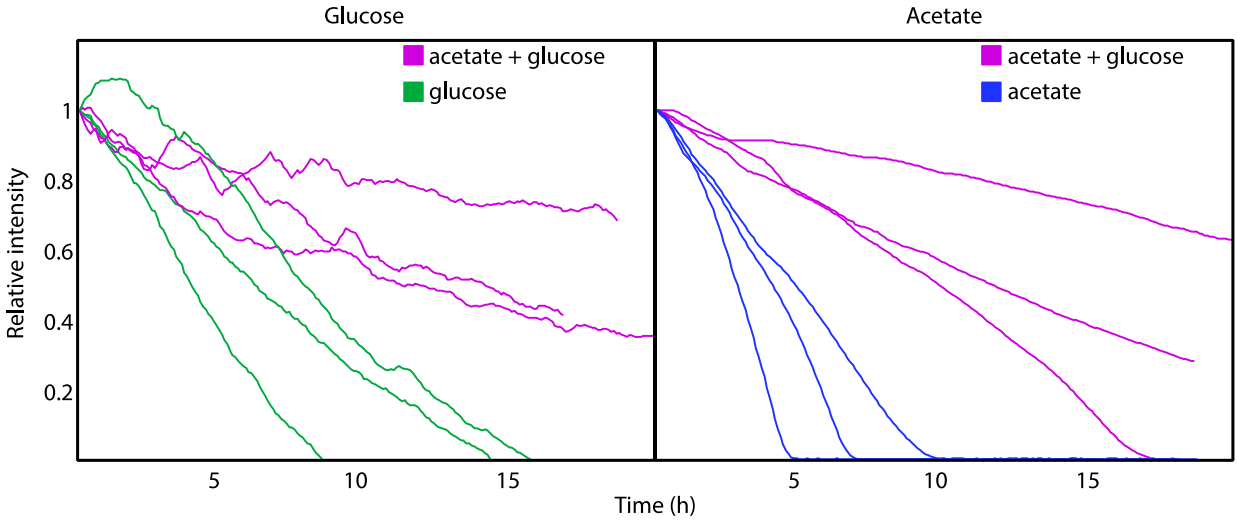

Figure 5: Relative rates of acetate and glucose utilization by CIVM-NMR
Normalized spectral intensity data for glucose, acetate, and acetate + glucose conditions were plotted, displaying all three replicates for each condition. In the left plot, the normalized relative intensities for the glucose peak in the 5 mM glucose condition (green) and 5 mM acetate + glucose condition (purple) are plotted for each replicate over 20 h. In the right plot, the normalized relative intensity for acetate is plotted in the 5 mM acetate condition (blue) and the 5 mM acetate + glucose condition (purple).

4 | DISCUSSION

The approach presented here allows us to monitor multiple substrates—2[^{13}C-Me]-DMSP, acetate, and glucose—and their metabolism in *R. pomeroyi in vivo* and in real-time. This process circumvents other methods of metabolic monitoring that involve variability-introducing extraction

methods, allowing for the continuous observation of unmodified samples in as close to ecological conditions as possible compared to other metabolic sampling methods.

We observed the cleavage of 2[^{13}C-Me]-DMSP to 2[^{13}C-Me]-DMS and oxidation to 2[^{13}C-Me]-DMSO, though the oxidation process cannot be positively attributed to metabolic activity by *R. pomeroyi* and could be a naturally occurring chemical process. We cannot say with certainty which cleavage pathways were utilized in the transformation from 2[^{13}C-Me]-DMSP to 2[^{13}C-Me]-DMS—it could be cleavage forming 2[^{13}C-Me]-dimethyl sulfide (DMS) and acrylate, 2[^{13}C-Me]-DMS and 3-hydroxypropanoyl-CoA, or a combination of both pathways.

We also observed differential utilization of acetate and glucose substrates—first, visually by CIVM-NMR and second by extracting acetate and glucose peaks as regions of interest (ROIs), normalizing, and comparing relative intensity for all replicates (Figure 5). Rates of acetate utilization in both the acetate-only and acetate + glucose conditions were faster than rates of glucose utilization across all conditions, as expected from predictions based on metabolic modeling.[158]

Future studies should explore additional replicates of 2[^{13}C-Me]-DMSP (1D-HSQC NMR experiment) or unlabeled DMSP (lc1pnf2 ^{1}H NMR experiment) if it is of interest to the community. The replicates of acetate and glucose substrate utilization may be of interest as complimentary research on substrate preference is currently being conducted in the Department of Marine Sciences at UGA.

ACKNOWLEDGEMENTS

The authors wish to thank Michael Judge for his helpful input throughout the process of data analysis and Chris Esselman for migrating the CIVM workflow onto NMRbox. Thank you to Christa Smith for growing the *R. pomeroyi* cell cultures. This study made use of NMRbox:

National Center for Biomolecular NMR Data Processing and Analysis, a Biomedical Technology Research Resource (BTRR), which is supported by NIH grant P41GM111135 (NIGMS).

CHAPTER 5

DISCUSSION AND FUTURE DIRECTIONS

This work has centered on the use of NMR spectroscopy to investigate metabolic flux in marine microorganisms. Through the development of the extraction method for high-salt samples (Chapter 2), we were able to elucidate differential flux of dihydroxypropanesulfonate (DHPS) between *T. pseudonana* and *R. pomeroyi* versus *T. pseudonana* and the Δ*hpsKLM* mutant lacking a functional DHPS transporter. Future work could utilize this method as a genetic screening tool to test DOM drawdown in other bacterial knockout mutants.

We extended our high-salt extraction method to investigate differential carbon flux between marine bacteria from varying clades and *T. pseudonana* (Chapter 3), demonstrating the robustness of the extraction protocol. Future investigators could repeat this process with additional species of phytoplankton and marine bacterial co-cultures. Currently, the method has been expanded for use of DMSO-d_6 in another area of research (biofluids) in the Edison lab. Our latest work on CIVM-NMR shows promise for future investigations into substrate utilization by *R. pomeroyi* and potentially additional marine bacteria.

We have sought to unravel data about how carbon fluxes in the ocean. We urgently need to expand our knowledge on ocean carbon flux due to widespread anthropogenic changes to the composition of seawater on chemical, phenotypic, and species levels. One such implication of these changes is the increased amount of atmospheric CO_2 absorbed by the ocean, decreasing ocean pH and increasing water temperature at an energetic cost to some phytoplankton. Deleterious anthropogenic changes causing an increased amount of atmospheric CO_2 absorbed by

the ocean are impacting the fitness of phytoplankton through a reduction in available nutrients and oxygenated water combined with an increase in ocean temperature, acidity, and evaporation[3]. Phytoplankton are decreasing in size and accelerating in growth rates, resulting in an overall reduction in net carbon flux.[4,5,6] In the past 50 years, water temperatures in the Antarctic Peninsula have increased at five times the rate of the global average, which has led to a 12% reduction in phytoplankton, carbon turnover, and photosynthetic output.[14]

Increased water temperatures and water acidity may inhibit enzymatic reactions or denature critical enzymes in some microorganisms allowing others to incur fitness advantages over the more vulnerable species.[10] Microorganisms endogenous to tropical oceans would be better suited for adapting to increasing ocean temperatures, dramatically altering species dynamics through the expansion of their geographic range. This phenomenon has already been observed in several species including tropical Radiolaria plankton which are now being found in Arctic waters.[15]

As phytoplankton are the lynchpin of the marine food web, these effects have potential to cascade through the entire ocean food chain.,[17] Phytoplankton provide nutrients in the form of DOM to symbiotic bacteria and are key food sources for herbivores such as birds, certain species of whales, shellfish, and small fish; the latter two which are important food sources for marine carnivores.[16] Warming waters are also shifting the temporal pattern of phytoplankton blooms.[18] Typically, phytoplankton populations surge during warm months, and many species migrate through waters to feed on these blooms. One such example is the Atlantic cod, which has now been found more than 300 kilometers north of their typical species distribution area where phytoplankton have been extending due to water warming.[19]

The implications for anthropogenic impacts are vast with effects so far reaching we likely do not yet appreciate. Thus, we face an urgent need to ascertain the current conditions of metabolic

exchange between phytoplankton and bacteria in order to closely monitor anthropogenic effects on these essential marine microorganisms. Through this work and similar, we can begin to accomplish this crucial research.

REFERENCES

1 Buchan, A., LeCleir, G. R., Gulvik, C. A., and González, J. M. Master recyclers: features and functions of bacteria associated with phytoplankton blooms. *Nat Rev Microbiol* **12**, 686-698, doi:10.1038/nrmicro3326 (2014).

2 Geng, H., and Belas, R. Molecular mechanisms underlying roseobacter-phytoplankton symbioses. *Curr Opin Biotechnol* **21**, 332-338, doi:10.1016/j.copbio.2010.03.013 (2010).

3 Zark, M., Christoffers, J., and Dittmar, T. Molecular properties of deep-sea dissolved organic matter are predictable by the central limit theorem: Evidence from tandem FT-ICR-MS. *Marine Chem* **191**, 9-15, doi:https://doi.org/10.1016/j.marchem.2017.02.005 (2017).

4 Hedges, J. I. *Why Dissolved Organics Matter*. 1-33 (Academic Press, 2002).

5 Riedel, T., and Dittmar, T. A method detection limit for the analysis of natural organic matter via fourier transform ion cyclotron resonance mass spectrometry. *Anal Chem* **86**, 8376-8382, doi:10.1021/ac501946m (2014).

6 Sogin, E. M., Puskás, E., Dubilier, N., and Liebeke, M. Marine metabolomics: a method for nontargeted measurement of metabolites in seawater by gas chromatography-mass spectrometry. *mSystems* **4,** e00638-19, doi:10.1128/mSystems.00638-19 (2019).

7 Bell, W. M., and Mitchell, R. Chemotactic and growth responses of marine bacteria to algal extracellular products. *Biol Bulletin* **143**, doi:https://doi.org/10.2307/1540052 (1972).

8 Sapp, M. *et al.* Species-specific bacterial communities in the phycosphere of microalgae? *Microb Ecol* **53**, 683-699, doi:10.1007/s00248-006-9162-5 (2007).

9 Sunagawa, S. *et al.* Ocean plankton. Structure and function of the global ocean microbiome. *Science* **348**, 1261359 (2015).

10 Teeling, H. *et al.* Substrate-controlled succession of marine bacterioplankton populations induced by a phytoplankton bloom. *Science* **336**, 608-611, doi:10.1126/science.1218344 (2012).

11 Amin, S. A., Parker, M. S., and Armbrust, E. V. Interactions between diatoms and bacteria. *Microbiol Mol Biol Rev* **76**, 667-684, doi:10.1128/mmbr.00007-12 (2012).

12 Noriega-Ortega, B. E. *et al.* Does the chemodiversity of bacterial exometabolomes sustain the chemodiversity of marine dissolved organic matter? *Front Microbiol* **10**, 215, doi:10.3389/fmicb.2019.00215 (2019).

13 Kell, D. B. *et al.* Metabolic footprinting and systems biology: the medium is the message. *Nat Rev Microbiol* **3**, 557-565, doi:10.1038/nrmicro1177 (2005).

14 Dittmar, T., Koch B., Hertkorn, N., and Kattner, G. A simple and efficient method for the solid-phase extraction of dissolved organic matter (SPE-DOM) from seawater. *Limnol Oceanogr Methods* **6**, 230-235 (2008).

15 Amin, S. A. *et al.* Interaction and signalling between a cosmopolitan phytoplankton and associated bacteria. *Nature* **522**, 98-101, doi:10.1038/nature14488 (2015).

16 Johnson, W. M., Kido Soule, M. C., and Kujawinski, E. B. Extraction efficiency and quantification of dissolved metabolites in targeted marine metabolomics. *Limnol Oceanogr Methods* **15**, 417-428, doi:https://doi.org/10.1002/lom3.10181 (2017).

17 Widner, B., Kido Soule, M. C., Ferrer-González, F. X., Moran, M. A., and Kujawinski, E. B. Quantification of amine- and alcohol-containing metabolites in saline samples using pre-extraction benzoyl chloride derivatization and ultrahigh performance liquid

chromatography tandem mass spectrometry (UHPLC MS/MS). *Anal Chem* **93**, 4809-4817, doi:10.1021/acs.analchem.0c03769 (2021).

18 Lam, B., and Simpson A. J. Direct (1)H NMR spectroscopy of dissolved organic matter in natural waters. *Analyst* **133**, 263-269 (2008).

19 Keeler, J. *Understanding NMR Spectroscopy*. (Wiley & Sons, 2005).

20 Durham, B. P. *et al.* Cryptic carbon and sulfur cycling between surface ocean plankton. *Proceed Natl Acad Sci USA* **112**, 453-457, doi:10.1073/pnas.1413137112 (2015).

21 Nelson, D. M., Tréguer, P., Brzezinski, M. A., Leynaert, A., and Quéguiner, B. Production and dissolution of biogenic silica in the ocean: Revised global estimates, comparison with regional data and relationship to biogenic sedimentation. *Global Biogeochem Cycles* **9**, 359-372, doi:https://doi.org/10.1029/95GB01070 (1995).

22 Luo, H., and Moran, M. A. Evolutionary ecology of the marine Roseobacter clade. *Microbiol Mol Biol Rev* **78**, 573-587, doi:10.1128/mmbr.00020-14 (2014).

23 Gregory, G. J., Boas, K. E., and Boyd, E. F. The organosulfur compound dimethylsulfoniopropionate (DMSP) is utilized as an osmoprotectant by Vibrio species. *Appl Environ Microbiol* **87**, e02235-20, doi:10.1128/aem.02235-20 (2020).

24 Hatakeyama, S., Okuda, M., and Akimoto, H. Formation of sulfur dioxide and methanesulfonic acid in the photooxidation of dimethyl sulfide in the air. *Geophys Res Letts* **9**, 583-586, doi:https://doi.org/10.1029/GL009i005p00583 (1982).

25 Reisch, C., Moran, M., and Whitman, W. Bacterial Catabolism of Dimethylsulfoniopropionate (DMSP). *Frontiers Microbiol* **2,** 172, doi:10.3389/fmicb.2011.00172 (2011).

26 Malin, G. in *Biological and Environmental Chemistry of DMSP and Related Sulfonium Compounds* (eds Ronald P. Kiene, Pieter T. Visscher, Maureen D. Keller, and Gunter O. Kirst) 177-189 (Springer US, 1996).

27 Ferrer-González, F. X., Widner, B., Holderman, N. R., Glushka, J., Edison, A. S., Kujawinski, E. B., and Moran, M. A. Resource partitioning of phytoplankton metabolites that support bacterial heterotrophy. *ISME J* **15**, 762-773 (2021).

28 Judge, M. T. *et al.* Continuous in vivo metabolism by NMR. *Frontiers Mol Biosci* **6**, 26 doi:10.3389/fmolb.2019.00026 (2019).

29 Donat-P. Häder, V. E. V., and Helbling, E. W. Productivity of aquatic primary producers under global climate change. *Photochem Photobiol Sci* **13**, 1370-1392 (2014).

30 Pachauri, R. Climate Change 2014: Synthesis Report Contribution of Working Groups I, II and III to the Fifth Assessment Report of the Intergovernmental Panel on Climate Change. (IPCC, 2014).

31 Feely, R. A., Sabine, C. L., Lee, K., Berelson, W., Kleypas, J., Fabry, V. J., and Millero, F. J. The impact of anthropogenic CO2 on the CaCO3 system in the Oceans. *Science* **305**, 362-366 (2004).

32 Lassen, M. K., Nielsen, K. D., Richardson, K., Garde, K., and Schlüter, L. The effects of temperature increases on a temperate phytoplankton community - A mesocosm climate change scenario. *J Exp Marine Biol Ecol* **383**, 79-88 (2010).

33 Passow, U., and Carlson, C. A. The biological pump in a high CO2 world. *Marine Ecol Progress Series* **470**, 249-272 (2012).

34 Rajadurai, M., Poornima, E. H., Narasimhan, S. V., Rao, V. N. R., and Venugopalan, V. P. Phytoplankton growth under temperature stress: laboratory studies using two diatoms from a tropical coastal power station site. *J Thermal Biol* **30**, 299-305 (2005).

35 Boyce, D. G., Lewis, M. R., and Worm, B. Global phytoplankton decline over the past century. *Nature* **466**, 591-596 (2010).

36 Emerson, S., and Hedges, J. *Chemical oceanography and the marine carbon cycle*. (Cambridge Unviersity Press, 2008).

37 Kaur, A., Hernandez-Fernaud, J. R., del Mar Aguilo-Ferretjans, M., Wellington, E. M., and Christie-Oleza, J. A. 100 Days of marine Synechococcus–Ruegeria pomeroyi interaction: A detailed analysis of the exoproteome. *Environ Microbiol* **20**, 785-799 (2018).

38 Moran, M. A. *et al.* Deciphering ocean carbon in a changing world. *Proc Natl Acad Sci USA* **113**, 3143-3151, doi:doi:10.1073/pnas.1514645113 (2016).

39 Thornton, D. C. O. Dissolved organic matter (DOM) release by phytoplankton in the contemporary and future ocean. *Eur J Phycol* **49**, 20-46, doi:10.1080/09670262.2013.875596 (2014).

40 Moran, M. The global ocean microbiome. *Science* **350**, doi:10.1126/science.aac8455. (2015).

41 Durham, B. P. *et al.* Cryptic carbon and sulfur cycling between surface ocean plankton. *Proc Natl Acad Sci USA* **112**, 453-457, doi:10.1073/pnas.1413137112 (2015).

42 Armbrust, E. V. *et al.* The genome of the diatom Thalassiosira pseudonana: ecology, evolution, and metabolism. *Science* **306**, 79-86, doi:10.1126/science.1101156 (2004).

43 Christie-Oleza, J. A., Sousoni, D., Lloyd, M., Armengaud, J., and Scanlan, D. J. Nutrient recycling facilitates long-term stability of marine microbial phototroph-heterotroph interactions. *Nat Microbiol* **2**, 17100, doi:10.1038/nmicrobiol.2017.100 (2017).

44 Kazamia, E., Helliwell, K. E., Purton, S., and Smith, A. G. How mutualisms arise in phytoplankton communities: building eco-evolutionary principles for aquatic microbes. *Ecology Letts* **19**, 810-822 (2016).

45 Mayer, J. *et al.* 2,3-Dihydroxypropane-1-sulfonate degraded by Cupriavidus pinatubonensis JMP134: Purification of dihydroxypropanesulfonate 3-dehydrogenase. *Microbiology* **156**, 1556-1564, doi:https://doi.org/10.1099/mic.0.037580-0 (2010).

46 Gaubert, J., Greff, S., Thomas, O. P., and Payri, C. E. Metabolomic variability of four macroalgal species of the genus Lopophora using diverse approaches. *Phytochemistry* **162**, 165-172 (2019).

47 Hertkorn, N., Harir, M., Koch, B. P., Michalke, B. and Schmitt-Kopplin, P. High-field NMR spectroscopy and FTICR mass spectrometry: Powerful discovery tools for the molecular level characterization of marine dissolved organic matter. *Biogeosciences* **10**, 1583–1624 (2013).

48 Lechtenfeld, O. J., Hertkorn, N., Shen, Y., Witt, M., and Benner, R. Marine sequestration of carbon in bacterial metabolites. *Nat Commun* **6**, 6711, doi:10.1038/ncomms7711 (2015).

49 Rehman, Z. U, Jeong, S., Tabatabai, S. A. A., Emwas, A.-H., and Leiknes, T. Advanced characterization of dissolved organic matter released by bloom-forming marine algae. *Desalination and Water Treatment* **69**, 1-11 (2017).

50 Landa, M. *et al.* Sulfur metabolites that facilitate oceanic phytoplankton-bacteria carbon flux. *ISME J* **13**, 2536-2550, doi:10.1038/s41396-019-0455-3 (2019).

51 Clendinen, C. S. *et al.* An overview of methods using 13C for improved compound identification in metabolomics and natural products. *Frontiers Plant Sci* **6,** 611, doi:10.3389/fpls.2015.00611 (2015).

52 Petrova, I., Xu, S., Joesten, W. C., Ni, S., and Kennedy, M. A. Influence of drying method on NMR-based metabolic profiling of human cell lines. *Metabolites* **9**, 256, doi:10.3390/metabo9110256 (2019).

53 Molinski, T. F. NMR of natural products at the 'nanomole-scale'. *Natural Product Reports* **27**, 321-329 (2010).

54 Shimba, N. *et al.* Optimization of 13C direct detection NMR methods. *J Biomol NMR* **30**, 175-179, doi:10.1023/b:Jnmr.0000048855.35771.11 (2004).

55 Fang, M. *et al.* Thermal degradation of small molecules: a global metabolomic investigation. *Anal Chem* **87**, 10935-10941 (2015).

56 Molnar, A. *et al.* Lyophilization and homogenization of biological samples improves reproducibility and reduces standard deviation in molecular biology techniques. *Amino Acids* **53**, 917-928, doi:10.1007/s00726-021-02994-w (2021).

57 Zelentsova, E. A., Yanshole, V. V., and Tsentalovich, Y. P. A novel method of sample homogenization with the use of a microtome-cryostat apparatus. *RSC Advances* **9**, 37809-37817, doi:10.1039/C9RA06808B (2019).

58 Richards, S. A., and Hollerton, J. C. in *Essential Practical NMR for Organic Chemistry* 13-16 (Wiley, 2011).

59 Ramaswamy, V., Hooker, J. W., Withers, R. S., Nast, R. E., Brey, W. W., Edison, A. S. Development of a 13C-Optimized 1.5-mm High Temperature Superconducting NMR Probe. *J Magn Reson* **235**, 58-65, doi: 10.1016/j.jmr.2013.07.012 (2013).

60 Clark, T., Murray, J. S., Lane, P., and Politzer, P. Why are dimethyl sulfoxide and dimethyl sulfone such good solvents? *J Mol Model* **14**, 689-697, doi:10.1007/s00894-008-0279-y (2008).

61 Friedlingstein, P. *et al.* Global carbon budget 2020. *Earth System Sci Data* **12**, 3269-3340 (2020).

62 Häder, D.-P., and Gao, K. Interactions of anthropogenic stress factors on marine phytoplankton. *Frontiers Environ Sci* **3**, doi:10.3389/fenvs.2015.00014 (2015).

63 Hansell, D. A. Recalcitrant dissolved organic carbon fractions. *Ann Rev Mar Sci* **5**, 421-445, doi:10.1146/annurev-marine-120710-100757 (2013).

64 Azam, F. Microbial control of oceanic carbon flux: the plot thickens. *Science* **280**, 694+ (1998).

65 Simon, M., and Rosenstock, B. Different coupling of dissolved amino acid, protein, and carbohydrate turnover to heterotrophic picoplankton production in the Southern Ocean in austral summer and fall. *Limnol Oceanogr* **52**, 85-95 (2007).

66 Suttle, C., Chan, A., and Fuhrman, J. Dissolved free amino acids in the Sargasso Sea: Uptake and respiration rates, turnover times, and concentrations. *Marine Ecology-Progress Series* **70**, 189-199, doi:10.3354/meps070189 (1991).

67 Zubkov, M. V. *et al.* Rapid turnover of dissolved DMS and DMSP by defined bacterioplankton communities in the stratified euphotic zone of the North Sea. *Deep-Sea Research Part II-Topical Studies in Oceanography* **49**, 3017-3038 (2002).

68 Hertkorn, N. *et al.* Characterization of a major refractory component of marine organic matter. *Geochimica et Cosmochimica Acta* **70**, 2990-3010, doi:10.1016/j.gca.2006.03.021 (2006).

69 Koch, H. *et al.* Biphasic cellular adaptations and ecological implications of Alteromonas macleodii degrading a mixture of algal polysaccharides. *ISME J* **13**, 92-103, doi:10.1038/s41396-018-0252-4 (2019).

70 Ferguson, R. L., and Sunda, W. G. Utilization of amino acids by planktonic marine bacteria: Importance of clean technique and low substrate additions1,2. *Limnol Oceanogr* **29**, 258-274 (1984).

71 Fuhrman JA, F. R. Nanomolar concentrations and rapid turnover of dissolved free amino acids in seawater: agreement between chemical and microbiological measurements. *Mar Ecol Prog Ser* **33**, 237-242 (1986).

72 Hodson, R. E. *et al.* Microbial uptake of dissolved organic matter in Mcmurdo Sound, Antarctica. *Marine Biol* **61**, 89-94, doi:10.1007/BF00386648 (1981).

73 Fogg, G. E., Nalewajko, C., and Watt, W. D., Extracellular products of phytoplankton photosynthesis. *Proceedings of the Royal Society of Biological Sciences* **162**, 517-534, doi:10.1098/rspb.1965.0054

74 Mühlenbruch, M., Grossart, H. P., Eigemann, F., and Voss, M. Mini-review: Phytoplankton-derived polysaccharides in the marine environment and their interactions with heterotrophic bacteria. *Environ Microbiol* **20**, 2671-2685, doi:10.1111/1462-2920.14302 (2018).

75 Obernosterer, I., and Herndl, G. Phytoplankton extracellular release and bacterial growth: Dependence on the inorganic N:P ratio. *Marine Ecol Prog Ser* **116**, 247-257, doi:10.3354/meps116247 (1995).

76 Flynn, K. J., Clark, D. R., and Xue, Y. Modeling the release of dissolved organic matter by phytoplankton(1). *J Phycol* **44**, 1171-1187, doi:10.1111/j.1529-8817.2008.00562.x (2008).

77 Seymour, J. R., Simó, R., Ahmed, T., and Stocker, R. Chemoattraction to dimethylsulfoniopropionate throughout the marine microbial food web. *Science* **329**, 342-345, doi:10.1126/science.1188418 (2010).

78 Strom S, W. G., Slajer A, Lambert S, and Clough J. Chemical defense in the microplankton II: Inhibition of protist feeding by β-dimethylsulfoniopropionate (DMSP). *Limnol Oceanogr* **48**, 230-237 (2003).

79 Wolfe, G. V., Steinke, M., and Kirst, G. O. Grazing-activated chemical defence in a unicellular marine alga. *Nature* **387**, 894-897, doi:10.1038/43168 (1997).

80 Bidle, K. D. The molecular ecophysiology of programmed cell death in marine phytoplankton. *Ann Rev Mar Sci* **7**, 341-375, doi:10.1146/annurev-marine-010213-135014 (2015).

81 Caron, D. A., and Hutchins, D. A. The effects of changing climate on microzooplankton grazing and community structure: drivers, predictions and knowledge gaps. *J Plankton Res* **35**, 235-252, doi:10.1093/plankt/fbs091 (2012).

82 Fuhrman, J. A. Marine viruses and their biogeochemical and ecological effects. *Nature* **399**, 541-548, doi:10.1038/21119 (1999).

83 Landa, M., Burns, A. S., Roth, S. J., and Moran, M. A. Bacterial transcriptome remodeling during sequential co-culture with a marine dinoflagellate and diatom. *ISME J* **11**, 2677-2690, doi:10.1038/ismej.2017.117 (2017).

84 Newton, R. J. *et al.* Genome characteristics of a generalist marine bacterial lineage. *ISME J* **4**, 784-798, doi:10.1038/ismej.2009.150 (2010).

85 Avcı, B., Krüger, K., Fuchs, B. M., Teeling, H., and Amann, R. I. Polysaccharide niche partitioning of distinct Polaribacter clades during North Sea spring algal blooms. *ISME J* **14**, 1369-1383, doi:10.1038/s41396-020-0601-y (2020).

86 Kirchman, D. L. The ecology of Cytophaga-Flavobacteria in aquatic environments. *FEMS Microbiol Ecol* **39**, 91-100, doi:10.1111/j.1574-6941.2002.tb00910.x (2002).

87 Pedler, B. E., Aluwihare, L. I., and Azam, F. Single bacterial strain capable of significant contribution to carbon cycling in the surface ocean. *Proc Natl Acad Sci USA* **111**, 7202-7207, doi:doi:10.1073/pnas.1401887111 (2014).

88 Tang, K., Jiao, N., Liu, K., Zhang, Y., and Li, S. Distribution and functions of TonB-dependent transporters in marine bacteria and environments: implications for dissolved organic matter utilization. *PLoS One* **7**, e41204, doi:10.1371/journal.pone.0041204 (2012).

89 Alavi, M., Miller, T., Erlandson, K., Schneider, R., and Belas, R. Bacterial community associated with Pfiesteria-like dinoflagellate cultures. *Environ Microbiol* **3**, 380-396, doi:10.1046/j.1462-2920.2001.00207.x (2001).

90 Behringer, G. *et al.* Bacterial communities of diatoms display strong conservation across strains and time. *Front Microbiol* **9**, 659, doi:10.3389/fmicb.2018.00659 (2018).

91 Green, D. H., Llewellyn, L. E., Negri, A. P., Blackburn, S. I., and Bolch, C. J. S. Phylogenetic and functional diversity of the cultivable bacterial community associated with

the paralytic shellfish poisoning dinoflagellate Gymnodinium catenatum. *FEMS Microbiol Ecol* **47**, 345-357, doi:10.1016/s0168-6496(03)00298-8 (2004).

92 Hold, G. L. *et al.* Characterisation of bacterial communities associated with toxic and non-toxic dinoflagellates: Alexandrium spp. and Scrippsiella trochoidea. *FEMS Microbiol Ecol* **37**, 161-173, doi:10.1111/j.1574-6941.2001.tb00864.x (2001).

93 Guillard, R. R. L., and Hargraves, P. E. Stichochrysis immobilis is a diatom, not a chrysophyte. *Phycologia* **32**, 234-236, doi:10.2216/i0031-8884-32-3-234.1 (1993).

94 Love, M. I., Huber, W., and Anders, S. Moderated estimation of fold change and dispersion for RNA-seq data with DESeq2. *Genome Biol* **15**, 550, doi:10.1186/s13059-014-0550-8 (2014).

95 Zhang, H. *et al.* dbCAN2: A meta server for automated carbohydrate-active enzyme annotation. *Nucleic Acids Res* **46**, W95-w101, doi:10.1093/nar/gky418 (2018).

96 Widner, B., Soule, M., Ferrer González, F., Moran, M., and Kujawinski, E. *Superior and Novel Detection of Small, Polar Metabolites in Saline Samples Using Pre-Extraction Benzoyl Chloride Derivatization and Ultra-High Performance Liquid Chromatography Tandem Mass Spectrometry (UHPLC MS/MS)*. (2020).

97 Oehlke, J., Brudel, M., and Blasig, I. E. Benzoylation of sugars, polyols and amino acids in biological fluids for high-performance liquid chromatographic analysis. *J Chromatogr B Biomed Appl* **655**, 105-111, doi:10.1016/0378-4347(94)00067-0 (1994).

98 Wong, J. M. *et al.* Benzoyl chloride derivatization with liquid chromatography-mass spectrometry for targeted metabolomics of neurochemicals in biological samples. *J Chromatogr A* **1446**, 78-90, doi:10.1016/j.chroma.2016.04.006 (2016).

99 Kido Soule, M. C., Longnecker, K., Johnson, W. M., and Kujawinski, E. B. Environmental metabolomics: analytical strategies. *Marine Chem* **177**, 374-387 (2015).

100 Pino, L. K. *et al.* The Skyline ecosystem: Informatics for quantitative mass spectrometry proteomics. *Mass Spectrom Rev* **39**, 229-244, doi:10.1002/mas.21540 (2020).

101 Henderson, C. M., Shulman, N. J., MacLean, B., MacCoss, M. J., and Hoofnagle, A. N. Skyline performs as well as vendor software in the quantitative analysis of serum 25-hydroxy vitamin D and vitamin D binding globulin. *Clin Chem* **64**, 408-410, doi:10.1373/clinchem.2017.282293 (2018).

102 Howard, E. C. *et al.* Bacterial taxa that limit sulfur flux from the ocean. *Science* **314**, 649-652, doi:10.1126/science.1130657 (2006).

103 Todd, J. D., Curson, A. R., Sullivan, M. J., Kirkwood, M., and Johnston, A. W. The Ruegeria pomeroyi acuI gene has a role in DMSP catabolism and resembles yhdH of E. coli and other bacteria in conferring resistance to acrylate. *PLoS One* **7**, e35947, doi:10.1371/journal.pone.0035947 (2012).

104 Grondin, J. M., Tamura, K., Déjean, G., Abbott, D. W., and Brumer, H. Polysaccharide utilization loci: Fueling microbial communities. *J Bacteriol* **199**, doi:10.1128/jb.00860-16 (2017).

105 Boulanger, A. *et al.* Identification and regulation of the N-acetylglucosamine utilization pathway of the plant pathogenic bacterium Xanthomonas campestris pv. campestris. *J Bacteriol* **192**, 1487-1497, doi:10.1128/jb.01418-09 (2010).

106 Eisenbeis, S., Lohmiller, S., Valdebenito, M., Leicht, S., and Braun, V. NagA-dependent uptake of N-acetyl-glucosamine and N-acetyl-chitin oligosaccharides across the outer

membrane of Caulobacter crescentus. *J Bacteriol* **190**, 5230-5238, doi:10.1128/jb.00194-08 (2008).

107 Brinkkötter, A., Shakeri-Garakani, A., and Lengeler, J. W. Two class II D-tagatose-bisphosphate aldolases from enteric bacteria. *Arch Microbiol* **177**, 410-419, doi:10.1007/s00203-002-0406-6 (2002).

108 Leyn, S. A., Gao, F., Yang, C., and Rodionov, D. A. N-acetylgalactosamine utilization pathway and regulon in proteobacteria: genomic reconstruction and experimental characterization in Shewanella. *J Biol Chem* **287**, 28047-28056, doi:10.1074/jbc.M112.382333 (2012).

109 Rodionov, D. A. *et al.* Genomic encyclopedia of sugar utilization pathways in the Shewanella genus. *BMC Genomics* **11**, 494, doi:10.1186/1471-2164-11-494 (2010).

110 Lombard, V., Golaconda Ramulu, H., Drula, E., Coutinho, P. M., and Henrissat, B. The carbohydrate-active enzymes database (CAZy) in 2013. *Nucleic Acids Res* **42**, D490-495, doi:10.1093/nar/gkt1178 (2014).

111 Beattie, A., Hirst, E. L., and Percival, E. Studies on the metabolism of the Chrysophyceae. Comparative structural investigations on leucosin (chrysolaminarin) separated from diatoms and laminarin from the brown algae. *Biochem J* **79**, 531-537, doi:10.1042/bj0790531 (1961).

112 Størseth, T., Hansen, K., Reitan, K., and Skjermo, J. Structural characterization of β-D-(1→3)-glucans from different growth phases of the marine diatoms Chaetoceros mülleri and Thalassiosira weissflogii. *Carbohydrate Res* **340**, 1159-1164, doi:10.1016/j.carres.2004.12.036 (2005).

113 Becker, S. *et al.* Laminarin is a major molecule in the marine carbon cycle. *Proc Natl Acad Sci USA* **117**, 6599-6607, doi:10.1073/pnas.1917001117 (2020).

114 Unfried, F. *et al.* Adaptive mechanisms that provide competitive advantages to marine bacteroidetes during microalgal blooms. *ISME J* **12**, 2894-2906, doi:10.1038/s41396-018-0243-5 (2018).

115 Martens, E. C. *et al.* Recognition and degradation of plant cell wall polysaccharides by two human gut symbionts. *PLoS Biol* **9**, e1001221, doi:10.1371/journal.pbio.1001221 (2011).

116 Gügi, B. *et al.* Diatom-specific oligosaccharide and polysaccharide structures help to unravel biosynthetic capabilities in diatoms. *Mar Drugs* **13**, 5993-6018, doi:10.3390/md13095993 (2015).

117 Barbeyron, T. *et al.* Habitat and taxon as driving forces of carbohydrate catabolism in marine heterotrophic bacteria: Example of the model algae-associated bacterium Zobellia galactanivorans Dsij. *Environ Microbiol* **18**, 4610-4627, doi:10.1111/1462-2920.13584 (2016).

118 Kabisch, A. *et al.* Functional characterization of polysaccharide utilization loci in the marine Bacteroidetes 'Gramella forsetii' KT0803. ISME J **8**, 1492-1502, doi:10.1038/ismej.2014.4 (2014).

119 Mann, A. J. *et al.* The genome of the alga-associated marine flavobacterium Formosa agariphila KMM 3901T reveals a broad potential for degradation of algal polysaccharides. *Appl Environ Microbiol* **79**, 6813-6822, doi:10.1128/aem.01937-13 (2013).

120 Datta, M. S., Sliwerska, E., Gore, J., Polz, M. F., and Cordero, O. X. Microbial interactions lead to rapid micro-scale successions on model marine particles. *Nat Commun* **7**, 11965, doi:10.1038/ncomms11965 (2016).

121 Goldford, J. E. *et al.* Emergent simplicity in microbial community assembly. *Science* **361**, 469-474, doi:10.1126/science.aat1168 (2018).

122 Azam, F., Fenchel, T., Field, J. G., Gray, J. S., Meyer-Reil, L. A., and Thingstad, F. The ecological role of water-column microbes in the sea. *Mar Ecol Prog Ser* **10**, 257-263 (1983).

123 Cole, J., Findlay, S., and Pace, M. Bacterial production in fresh and saltwater ecosystems – a cross-system overview. *Marine Ecol Prog Ser* **43**, 1-10, doi:10.3354/meps043001 (1988).

124 Kujawinski, E. B. The impact of microbial metabolism on marine dissolved organic matter. *Ann Rev Mar Sci* **3**, 567-599, doi:10.1146/annurev-marine-120308-081003 (2011).

125 Larsbrink, J. *et al.* A polysaccharide utilization locus from Flavobacterium johnsoniae enables conversion of recalcitrant chitin. *Biotechnol Biofuels* **9**, 260, doi:10.1186/s13068-016-0674-z (2016).

126 Mathieu S, T.-L. M., Poulet L, Drouillard S, Vincentelli R, Henrissat B. Ancient acquisition of "alginate utilization loci" by human gut microbiota. *Sci Rep* **8**, 8075 (2018).

127 Azizan, A. *et al.* Metabolite profiling of the microalgal diatom chaetoceros calcitrans and correlation with antioxidant and nitric oxide inhibitory activities via ^{1}H NMR-based metabolomics. *Mar Drugs* **16**, 154, doi:10.3390/md16050154 (2018).

128 Hellebust, J. A. Excretion of some organic compounds by marine phytoplankton1. *Limnol Oceanogr* **10**, 192-206 (1965).

129 Boroujerdi, A. F. *et al.* Identification of isethionic acid and other small molecule metabolites of Fragilariopsis cylindrus with nuclear magnetic resonance. *Anal Bioanal Chem* **404**, 777-784, doi:10.1007/s00216-012-6169-2 (2012).

130 Iglesias, M. J. *et al.* NMR characterization and evaluation of antibacterial and antiobiofilm activity of organic extracts from stationary phase batch cultures of five marine microalgae (Dunaliella sp., D. salina, Chaetoceros calcitrans, C. gracilis and Tisochrysis lutea). *Phytochemistry* **164**, 192-205, doi:10.1016/j.phytochem.2019.05.001 (2019).

131 Jeong, K.-S. *et al.* Application of nuclear magnetic resonance for analyzing metabolic characteristics of winter diatom blooms. *J Plankton Res* **42**, 31-39, doi:10.1093/plankt/fbz069 (2020).

132 Scholz, B., and Liebezeit, G. Compatible solutes in three marine intertidal microphytobenthic Wadden Sea diatoms exposed to different salinities. *Eur J Phycol* **47**, doi:10.1080/09670262.2012.720714 (2012).

133 Miller, T. R., Hnilicka, K., Dziedzic, A., Desplats, P., and Belas, R. Chemotaxis of Silicibacter sp. strain TM1040 toward dinoflagellate products. *Appl Environ Microbiol* **70**, 4692-4701, doi:10.1128/aem.70.8.4692-4701.2004 (2004).

134 Rocap, G. *et al.* Genome divergence in two Prochlorococcus ecotypes reflects oceanic niche differentiation. *Nature* **424**, 1042-1047, doi:10.1038/nature01947 (2003).

135 Basan, M. *et al.* Overflow metabolism in Escherichia coli results from efficient proteome allocation. *Nature* **528**, 99-104, doi:10.1038/nature15765 (2015).

136 Kinkel, L. L., Schlatter, D. C., Xiao, K., and Baines, A. D. Sympatric inhibition and niche differentiation suggest alternative coevolutionary trajectories among Streptomycetes. *Isme j* **8**, 249-256, doi:10.1038/ismej.2013.175 (2014).

137 Kirchman, D. L. Phytoplankton death in the sea. *Nature* **398**, 293-294 (1999).

138 Durham, B. P. *et al.* Recognition cascade and metabolite transfer in a marine bacteria-phytoplankton model system. *Environ Microbiol* **19**, 3500-3513, doi:10.1111/1462-2920.13834 (2017).

139 Enke, T. N. *et al.* Modular assembly of polysaccharide-degrading marine microbial communities. *Curr Biol* **29**, 1528-1535.e1526, doi:10.1016/j.cub.2019.03.047 (2019).

140 Ferraris, R. P., and Diamond, J. M. Specific regulation of intestinal nutrient transporters by their dietary substrates. *Annu Rev Physiol* **51**, 125-141, doi:10.1146/annurev.ph.51.030189.001013 (1989).

141 McCarren, J. *et al.* Microbial community transcriptomes reveal microbes and metabolic pathways associated with dissolved organic matter turnover in the sea. *Proc Natl Acad Sci USA* **107**, 16420-16427, doi:10.1073/pnas.1010732107 (2010).

142 Poretsky, R. S., Sun, S., Mou, X., and Moran, M. A. Transporter genes expressed by coastal bacterioplankton in response to dissolved organic carbon. *Environ Microbiol* **12**, 616-627, doi:10.1111/j.1462-2920.2009.02102.x (2010).

143 Salzberg, S. L. Next-generation genome annotation: we still struggle to get it right. *Genome Biol* **20**, 92, doi:10.1186/s13059-019-1715-2 (2019).

144 Freilich, S. *et al.* Competitive and cooperative metabolic interactions in bacterial communities. *Nat Commun* **2**, 589, doi:10.1038/ncomms1597 (2011).

145 Fu, H., Uchimiya, M., Gore, J., and Moran, M. A. Ecological drivers of bacterial community assembly in synthetic phycospheres. *Proc Natl Acad Sci USA* **117**, 3656-3662, doi:10.1073/pnas.1917265117 (2020).

146 Zelezniak, A. *et al.* Metabolic dependencies drive species co-occurrence in diverse microbial communities. *Proc Natl Acad Sci USA* **112**, 6449-6454, doi:doi:10.1073/pnas.1421834112 (2015).

147 Benson, A. A., and Lee, R. F. . *Biochem J* **128**, 29p-30p, doi:10.1042/bj1280029pb (1972).

148 Busby, W. F. Sulfoporpanedial and cysteinolic acid in the diatom. *Biochim Biophys Acta* **121**, 160-161, doi:10.1016/0304-4165(66)90360-6 (1966).

149 Wishart, D. S. NMR metabolomics: A look ahead. *J Magn Reson* **306**, 155-161, doi:https://doi.org/10.1016/j.jmr.2019.07.013 (2019).

150 Wilson, D. M., and Burlingame, A. L. Deuterium and carbon-13 tracer studies of ethanol metabolism in the rat by 2H,1H-decoupled 13C nuclear magnetic resonance. *Biochem Biophys Res Commun* **56**, 828-835 (1974).

151 Andrew, E. R., Bradbury, A., and Eades, R. G. Nuclear magnetic resonance spectra from a crystal rotated at high speed. *Nature* **182**, 1659-1659, doi:10.1038/1821659a0 (1958).

152 Cheng, L. L. High-resolution magic angle spinning NMR for intact biological specimen analysis: Initial discovery, recent developments, and future directions. *NMR in Biomed* **36**, e4684, doi:https://doi.org/10.1002/nbm.4684 (2023).

153 Cheng, L. L. *et al.* Enhanced resolution of proton NMR spectra of malignant lymph nodes using magic-angle spinning. *Magn Reson Med* **36**, 653-658, doi:10.1002/mrm.1910360502 (1996).

154 Cheng, L. L. *et al.* Quantitative neuropathology by high resolution magic angle spinning proton magnetic resonance spectroscopy. *Proc Natl Acad Sci USA* **94**, 6408-6413, doi:doi:10.1073/pnas.94.12.6408 (1997).

155 Sitnikov, D. G., Monnin, C. S., and Vuckovic, D. Systematic assessment of seven solvent and solid-phase extraction methods for metabolomics analysis of human plasma by LC-MS. *Sci Rep* **6**, 38885, doi:10.1038/srep38885 (2016).

156 Tabatabaei Anaraki, M., Simpson, M. J., and Simpson, A. J. Reducing impacts of organism variability in metabolomics via time trajectory in vivo NMR. *Magn Reson Chem* **56**, 1117-1123, doi:10.1002/mrc.4759 (2018).

157 Hattori, A. *et al.* Cancer progression by reprogrammed BCAA metabolism in myeloid leukaemia. *Nature* **545**, 500-504, doi:10.1038/nature22314 (2017).

158 Edirisinghe, J. N. *et al.* Modeling central metabolism and energy biosynthesis across microbial life. *BMC Genomics* **17**, 568, doi:10.1186/s12864-016-2887-8 (2016).

159 Hassan, Q. *et al.* Improvements in lipid suppression for 1H NMR-based metabolomics: Applications to solution-state and HR-MAS NMR in natural and in vivo samples. *Magn Reson Chem* **57**, 69-81, doi:https://doi.org/10.1002/mrc.4814 (2019).

160 Maciejewski, M. W., Schuyler, A.D., Gryk, M.R., Moraru, I.I., Romero, P.R., Ulrich, E.L., Eghbalnia, H.R., Livny, M., Delaglio, F., and Hoch, J.C. NMRbox: A Resource for biomolecular NMR computation. *Biophys J* **112**, 1529-1534 (2017).